KEEPING BRITAIN TRADING

IMMINGHAM EASTERN RO-RO TERMINAL

3D Modelling of Revised Layout

Document 10.2.75

APFP Regulations 2009 – Regulation 5(2)(q)

PINS Reference – TR030007

January 2024

Document Information

Document Information	
Project	Immingham Eastern Ro-Ro Terminal
Document title	3D Modelling of Revised Layout
Commissioned by	Associated British Ports
Document ref	10.2.75
APFP Regs	5(2)(q)
Prepared by	ABP Project Team

Date	Version	Revision Details
12/2023	01	Deadline 7
01/2024	02	Deadline 8

hr wallingford

Immingham Eastern Ro-Ro Terminal

3D modelling of revised layout

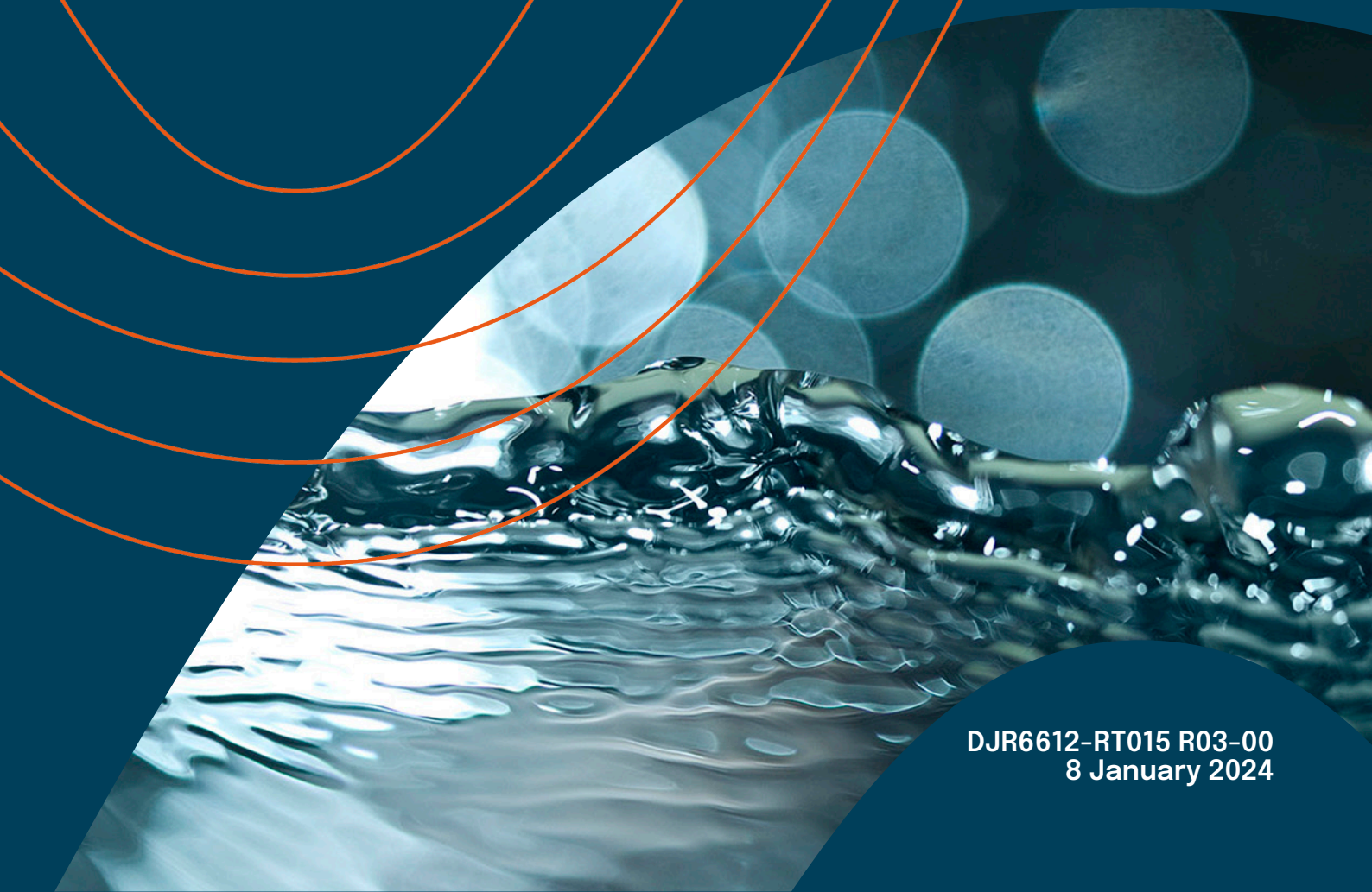

DJR6612-RT015 R03-00
8 January 2024

Document information

Document permissions	Confidential - client
Project number	DJR6612
Project name	Immingham Eastern Ro-Ro Terminal
Report title	3D modelling of revised layout
Report number	RT015
Release number	03-00
Report date	8 January 2024
Client	ABP
Client representative	Josh Bush
Project manager	Mike Parr
Project director	Mark McBride

Document history

Date	Release	Prepared	Approved	Authorised	Notes
8 Jan 2024	03-00	JVB	MPA	MPA	
21 Dec 2023	02-00	JVB	MPA	MPA	
11 Dec 2023	01-00	JVB	MPD	MPD	

Document authorisation

Prepared	Approved	Authorised
John Baugh	Mike Parr	Mike Parr

Contents

Appendices

Figures

1 Introduction

1.1 Background

Associated British Ports (ABP) Humber has applied for a Development Consent Order for the creation of a new Ro-Ro facility to the east of the Immingham dock, which will be known as the Immingham Eastern Ro-Ro Terminal (IERRT).

HR Wallingford have been supporting the project's marine design and impact studies by mooring and navigability analyses including hydrodynamic modelling of the project.

HR Wallingford provided a face to face brief regarding flows to interested parties on 14 December 2023. Following feedback from that this report was amended to include:

- A comparison with baseline conditions - Section 3.2;
- Flow conditions between IERRT and IOT - Section 3.3;
- Sensitivity to moored vessels at IERRT - Section 3.4.

1.2 Objective

A series of modelling a navigation studies have been completed for the IERRT project. As the project has proceeded the layout has developed scheme with the present revised scheme shown by Figure 1.1.

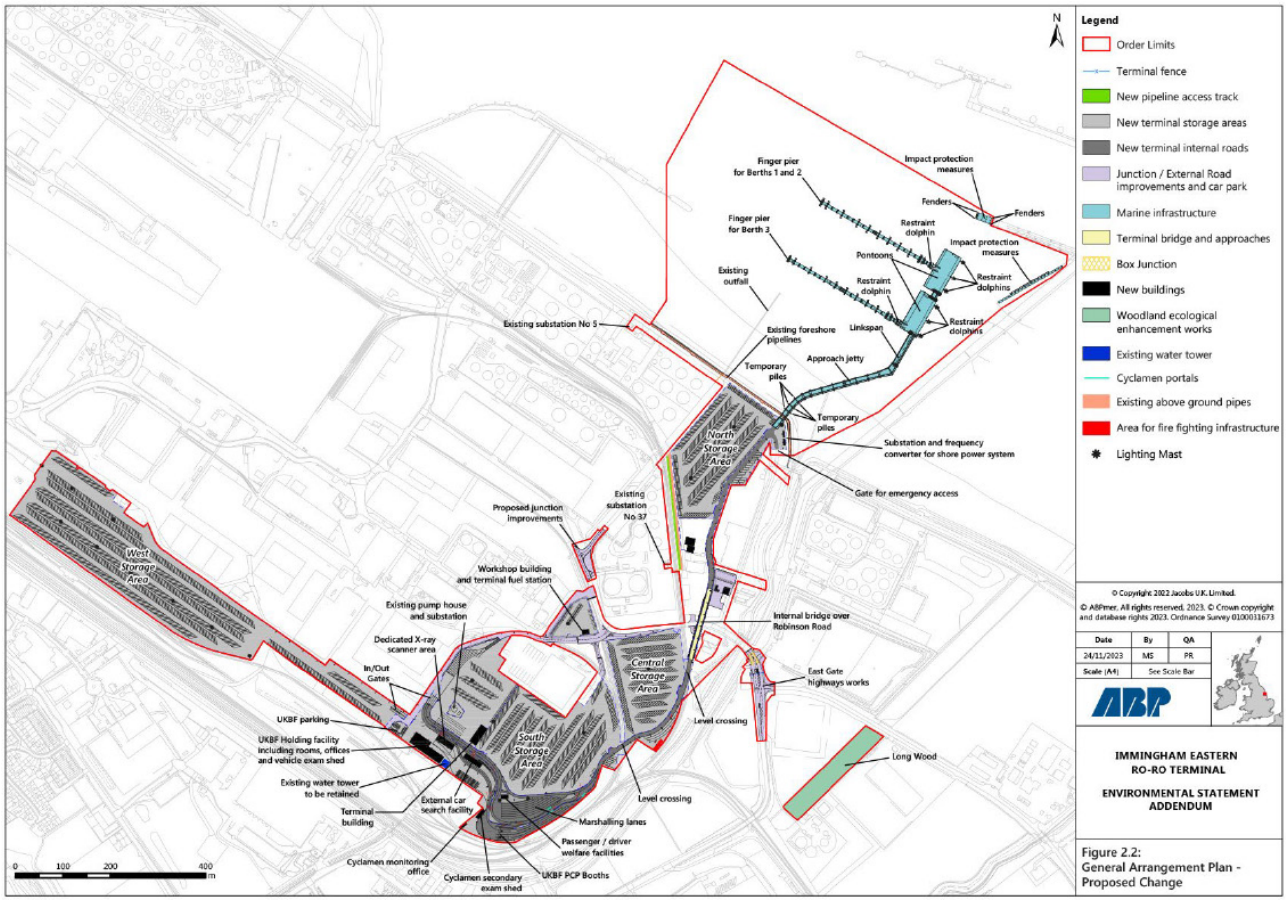

Figure 1.1: Immingham Eastern Ro-Ro Terminal - general arrangement of revised layout

Source: ABP (2023)

The revised layout to assess included larger Ro-Ro pontoons than that previously modelled and used in navigation simulation. All other parameters of the development, dredged area and depth are unchanged from that previously modelled and assessed.

The requirement for the modelling described in this report was to simulate the effect of the revised layout of the IERRT on local tidal flows and to provide currents and water depths for navigation simulation both for the existing and proposed cases. The area required for flow data to be extracted from the model and supplied to the navigation simulator is presented in Figure 1.2.

The hydrodynamic results for the revised scheme were also required to be compared to those previously modelled to confirm whether conclusions reached for the previous layout remain valid for the revised layout.

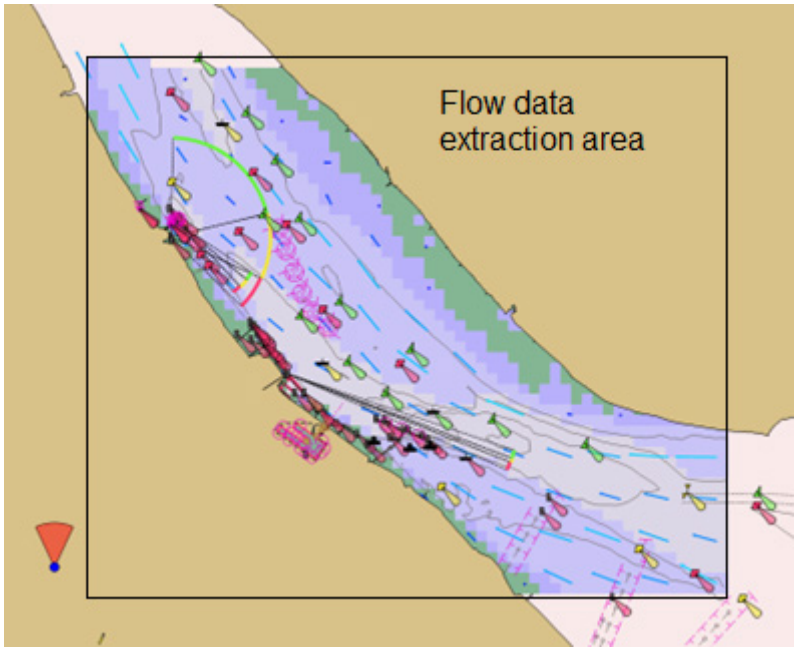

Figure 1.2: Area of flow data extraction for Navigation Simulator

2 Model basis

2.1 Choice of model

When considering the suitable modelling approach to achieve the objective the requirements are firstly, to model an area large enough to exclude any boundary effects for the flows within the area of data extraction for the navigation simulation, secondly to model through tide conditions over a series of tides and, thirdly detailed modelling at the site of the IERRT sufficient to resolve the principal effects of the structures on the flows. The need to model a suitably large area for a series of tides excluded application of Computational Fluid Dynamic (CFD) modelling.

The model applied to the project, TELEMAC-3D, solves the 3D Navier-Stokes flow equations making the hydrostatic pressure assumption (i.e. no significant vertical flow accelerations) using a finite element solution method on an unstructured triangular grid. This triangular grid allows the model mesh resolution to continually vary in space resulting in good representation of existing and proposed features. TELEMAC-3D is part of the TELEMAC system originated by the hydraulic research laboratory hosted by EDF.

The model used had its boundaries approximately 20 km away from the IERRT site. Both the landward and seaward boundary conditions were imposed water tidal levels which drove the currents in the study area.

The calibration exercise as summarised below showed that the observed flow direction changes at the end of the flood tide were likely to be driven by a longitudinal salinity gradient. Hence, schematized time varying salinity boundary conditions were also imposed at the open boundaries.

The model grid sizes ranged from approximately 250 m at the open boundaries to 10 m in the area around the IERRT site. The forms of all the structures – piled or floating – were included in the model mesh to provide an accurate representation of their effects on hydrodynamics.

The vertical mesh used a sigma approach where the model layers are located at a set proportion of the total water depth. 6 layers were used at the following proportions of the total water depth (D); 0D, 0.25D, 0.5D, 0.75D, 0.9D, 1.0D. The vertical layering is illustrated by the section shown in Figure 2.1.

2.2 Inclusion of the effect of piled structures

A field of piles can alter the flow which would otherwise pass through it due to the local turbulence and complex flow structures as the flow interacts with each pile. This effect is increased with the density of piles, for example if the piles are less than 10 pile diameters apart the effect of each pile can combine to result in a significantly enhanced effect on the passing flow. In modelling the project site with several piled structures and hundreds of individual piles including each pile in the model would result in an extremely large number of model nodes and impractically long model run times. A reasonable approach to include the influence of piles on the flow in the model is available in TELEMAC-3D by adding extra turbulent drag within each model cell within the piled region using the following equation:

$$F_{u,v} = -0.5 * N * D * C_D * U_{norm} \qquad \text{(Eq. 1)}$$

Where:

- $F_{u,v}$ = drag in the X and Y direction;
- N = total number of piles in the jetty;
- D = diameter of the piles (m);
- C_D = a drag coefficient related to the shape of the pile; for example circular piles have C_D = 1.0 and square piles have C_D = 2.0 (Mutlu Sumer and Fredsøe, 2006);
- U_{norm} = depth averaged current flow speed (m/s);
- F_u and F_v are then included implicitly within the hydrodynamic momentum equations used by the model within areas containing the piles.

2.3 Inclusion of the effect of floating structures

The blockage effect of the proposed pontoons on the passing flow was included in the model by applying additional air pressure to the free surface of the 3D hydrodynamic model, locally depressing the water surface to a level equivalent to the draft of each pontoon. A cross section showing the representation of the IERRT pontoon in the model is provided by Figure 2.1. As TELEMAC is a free surface model whilst the overall blockage of the pontoon is included and varies with the tide, representation of exactly vertical structures using this method is not possible as some the effect of the pontoon can extend in the area up to the next adjacent model node. The additional depression of the water surface around the edge of the representation of the pontoon is illustrated in Figure 2.1. This effect means that the blockage to flow associated with the pontoon is more than that in reality, however other local effects such as the local friction from the form of the pontoon and small scale local turbulence will also occur within in this area immediately around the pontoon.

TELEMAC-3D's use of the hydrostatic pressure assumption means that any large vertical accelerations close to the pontoon, up and downstream of the structure are not modelled. However, assuming a typical expansion rate of the flow around the pontoon of 1:10 any local

effects would be confined to within 50 m of the pontoon in the up and down stream directions. Neither of these assumptions would be expected to have any significant influence on flows perpendicular to the stream direction. Noting the assumptions described above the representation of the pontoon is considered appropriate for the purpose of predicting the effect of the project on nearby infrastructure.

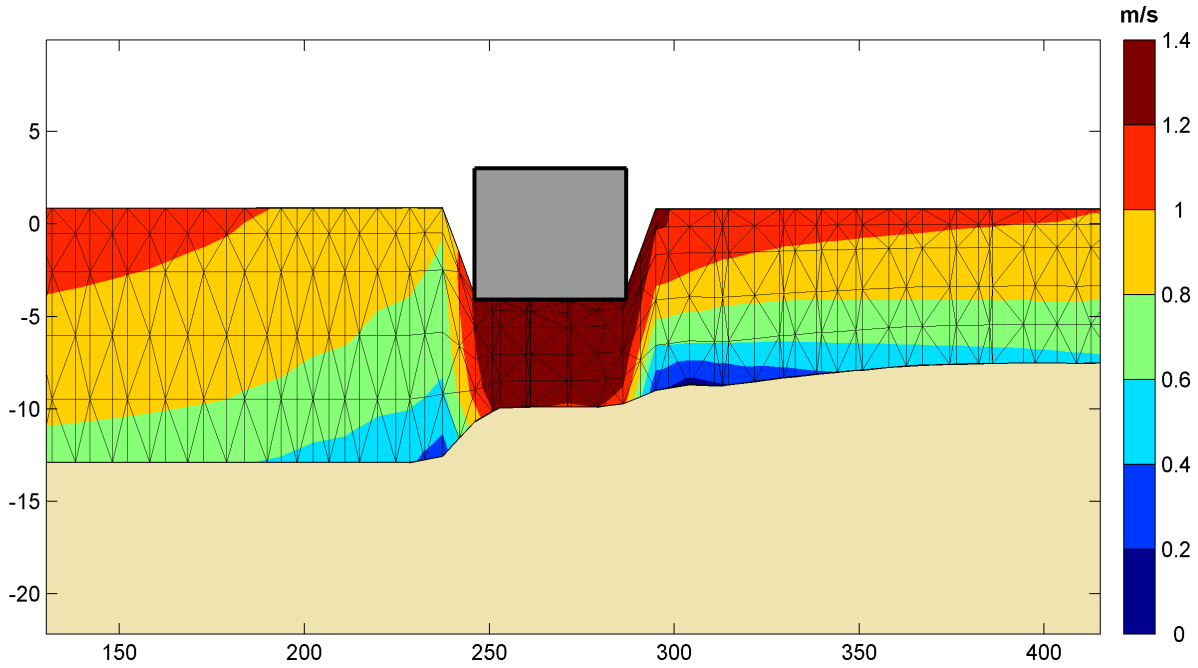

Figure 2.1: Example cross section showing model mesh and 3D representation of pontoon and current speed

2.4 Model calibration and validation

The applied TELEMAC-3D model has been extensively calibrated and validated against data collected at the IERRT site. HR Wallingford (2022) describes the data comparison. For completeness a summary of the calibration and validation results are included below.

2.4.1 Calibration

The original model validation was against a set of spring tides of tidal range close to a mean spring tide. The particular focus was to represent the variation in current direction towards high water. Figure 2.3 shows the original validation against a set of spring tides observed by a long term Acoustic Wave and Current Profile (AWAC) deployment in November 2019. The location of the AWAC data is shown in Figure 2.2.

The AWAC data collected at the site over an 18 month period provided an excellent presentation of the currents at the site covering both tide to tide and seasonally variability. Furthermore, data was available throughout the water column to aid understanding of vertical variability on flows as emerged to be the case at this site. This data source provides a much improved dataset for calibration of the model compared to, for example, tidal diamonds which only provide representative currents for mean spring and mean neap tides.

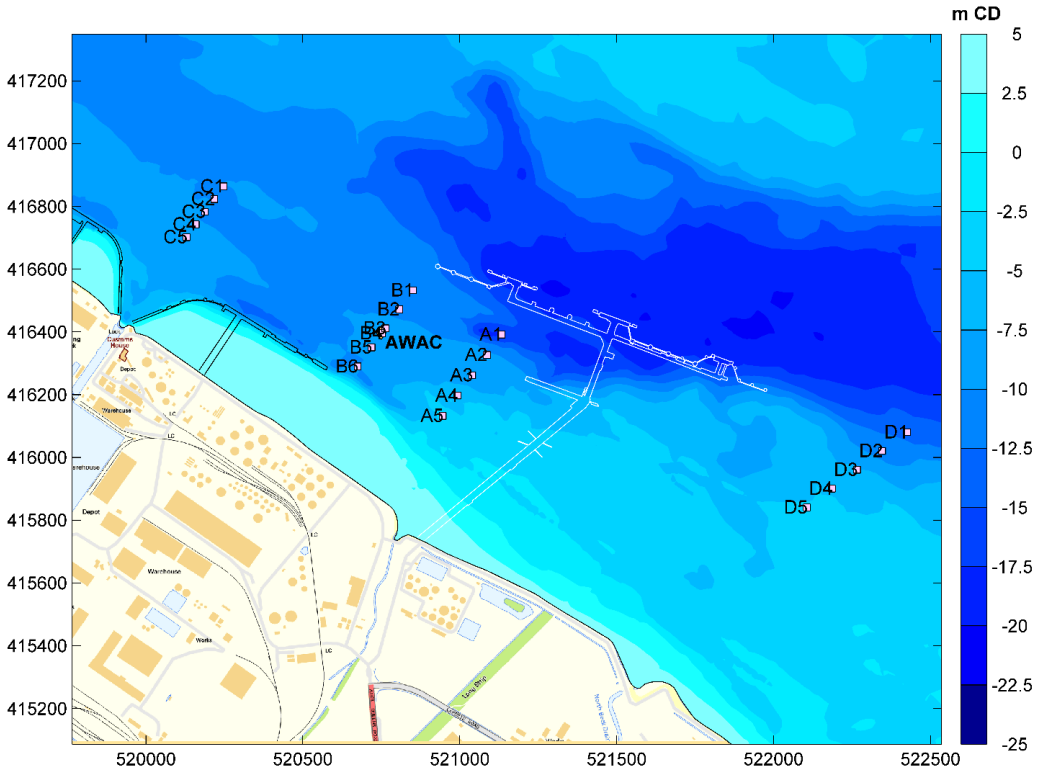

Figure 2.2: Locations of AWAC and ADCP survey data extraction points

Source: Background information includes data from Ordnance Survey © Crown Copyright 2022

To show the simulated currents in the upper part of the water column the model results shown in Figure 2.3 are the predicted near surface current and the predicted current at 0.75 and 0.9 times the water depth above the seabed, i.e. 25% and 10% of total water depth below the water surface.

The key phenomena of the AWAC data are well represented by the model with the dominance of ebb tide currents and the variation in flood tide currents between 295° in the early flood to 315° as the tide level approaches high water. During the ebb tide the current directions in both the model and observations are more consistent, being around 120°.

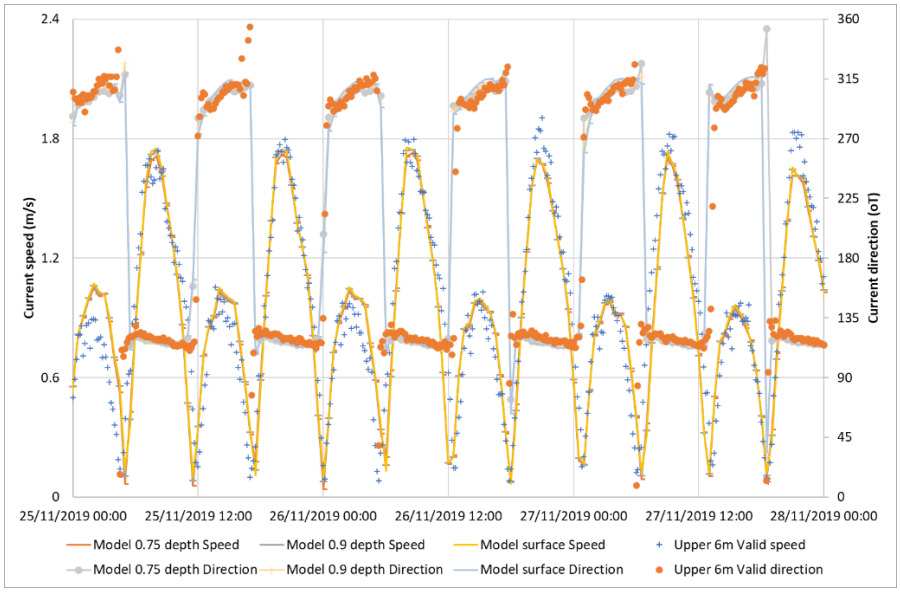

Figure 2.3: Comparison of simulated current speed with data from AWAC, 25-27 November 2019

2.4.2 Validation

As described by HR Wallingford (2022) a set of four vessel mounted Acoustic Dopler Current Profiler (ADCP) transects were performed in October 2022. The project team requested that the validated model be compared to the new data without rerunning the model for the specific tidal period of the ADCP transects. Hence, the model was validated against a period of the existing simulation of approximate mean spring tide conditions with tide ranges of the order of 6.2 m whereas the ADCP observations included tide ranges of 6.6 to 6.9 m. Some additional variance in the model comparison may occur by not modelling the conditions on the day of the ADCP survey.

Data was extracted at 21 points from the four ADCP transects. These were averaged over the total water depth and over the top 5, 6 and 7 m of the water column to allow observation of the current directional variability in the portion of the water column corresponding to various vessel drafts. The full set of comparisons are provided in HR Wallingford (2022).

The ebb tide comparison at Transect D is of particular interest to the inclusion of the piled structures using drag as it includes the area where currents would be expected to be influenced by the piled Immingham Oil Terminal (IOT) jetty.

Figure 2.4 to Figure 2.7 show the comparison of the modelled and observed currents at the relevant points along Transect D. Interestingly, both the data and model show a reduction in ebb tide currents at Point D2 compared to the neighbouring Points D1 and D3. This shows that the effect of the drag due to the piles on the IOT jetty can be seen at some distance from the structures and that the modelled approach to representing the piled IOT jetty is reasonable.

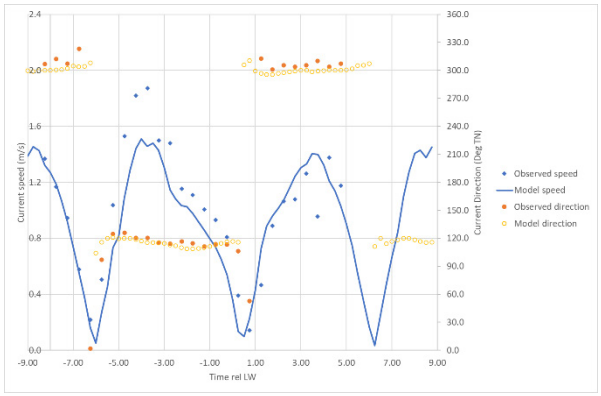

Figure 2.4: Comparison of simulated current speed and direction with data from ADCP point D1, 12/10/2022

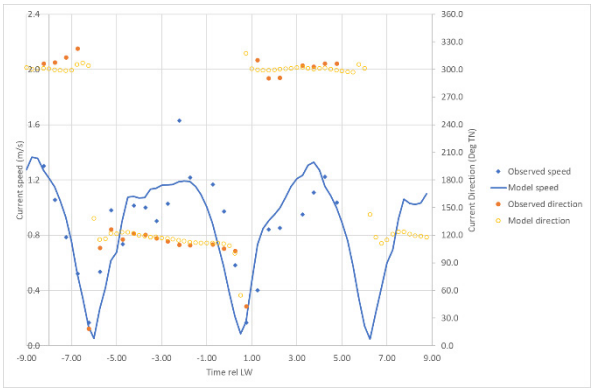

Figure 2.5: Comparison of simulated current speed and direction with data from ADCP point D2, 12/10/2022

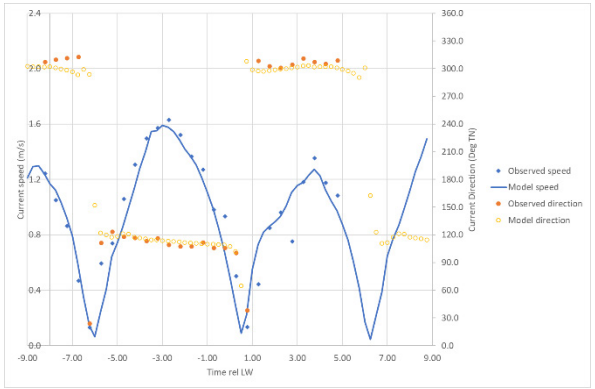

Figure 2.6: Comparison of simulated current speed and direction with data from ADCP point D3, 12/10/2022

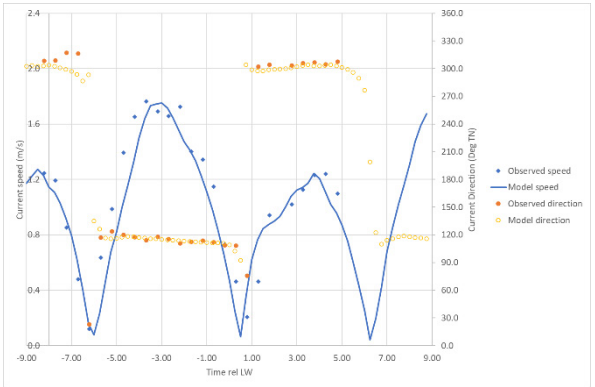

Figure 2.7: Comparison of simulated current speed and direction with data from ADCP point D4, 12/10/2022

3 Model results

3.1 Comparison of revised scheme with original scheme

To demonstrate any difference in hydrodynamics with the revised layout for the IERRT compared to that previously included in navigation simulations the same two tidal conditions as used previously were modelled with the new layout – a peak spring tide range and a mean spring tide range case. The tides chosen cover the conditions for larger tide ranges; the peak spring tide may occur monthly, mean spring (or larger) tides occur every two weeks.

Any changes to currents at lower range tides would be expected to be within the footprint of the changes modelled. Hourly plots showing the comparison of the results are included in Appendix A. All results are for the top 7 m of the water column as that was the data supplied to the navigation simulations. For reference the time of tide of the results plotted is indicated in the frame on the bottom left of the plot. Figure A.1 to Figure A.13 show the results for the peak spring tide and Figure A.14 to Figure A.26 show the results for the mean spring tide.

Inspection of the results presented in Appendix A confirmed the anticipated effect of the larger pontoon in the revised layout leading to a larger effect in reducing currents up and down stream of the pontoon and some associated speed increases immediately to the side of the pontoon. The area of speed increase greater than 0.05 m/s is confined to with 30 m of the edge of the pontoon between the pontoon and the IOT finger jetty. The area of speed reduction up and down stream is larger with changes greater than 0.2 m/s extending 500 m north west during the flood tide and 1000 m south east during the ebb. The differences in these areas is linked to the larger currents which occur on the ebb.

The results indicate no additional hydrodynamic effects from the revised layout at the IOT jetties at times of peak ebb or flood tide flow. In the immediate approaches to the IERRT berths currents are lower in the revised layout compared to the original case.

The results did show a period shortly after LW which had a transient, short period of increased footprint of change for both the peak and mean spring cases. Further investigation of these effects were completed by extracting time series results at the location of the highest speed increase shown close to the IOT finger jetty. The time series extraction point is shown in Figure 3.1.

Figure 3.2 (Peak Spring) and Figure 3.3 (Mean Spring) show the comparison of the time series current speed and direction and indicate the transient nature of the effect as the tide turns following low water. At all other times of tide negligible differences are seen.

The reason for this effect is illustrated by Figure 3.4 to Figure 3.6 which overlay the current patterns for the original layout (blue vectors) with current pattern for the revised layout (red vectors). As is typical for estuaries the tide turns first over the shallow edges of the estuary, being areas of increased bed friction. Then, slightly later the tide turns within the deeper channel. During this period an area of low flow propagates offshore. The blockage effect of the pontoons and the deeper dredged depths appear to alter the propagation of the turn in the tide very slightly which can make apparently larger changes appear, albeit on low currents. For example Figure 3.2 shows very low currents (less than 0.1 m/s) at LW+0.5 but for the revised layout the current is approximately 0. 3 m/s. It should be noted that this effect is much smaller for the second LW simulated (after hour 12 in Figure 3.2) confirming the transient nature of the effect.

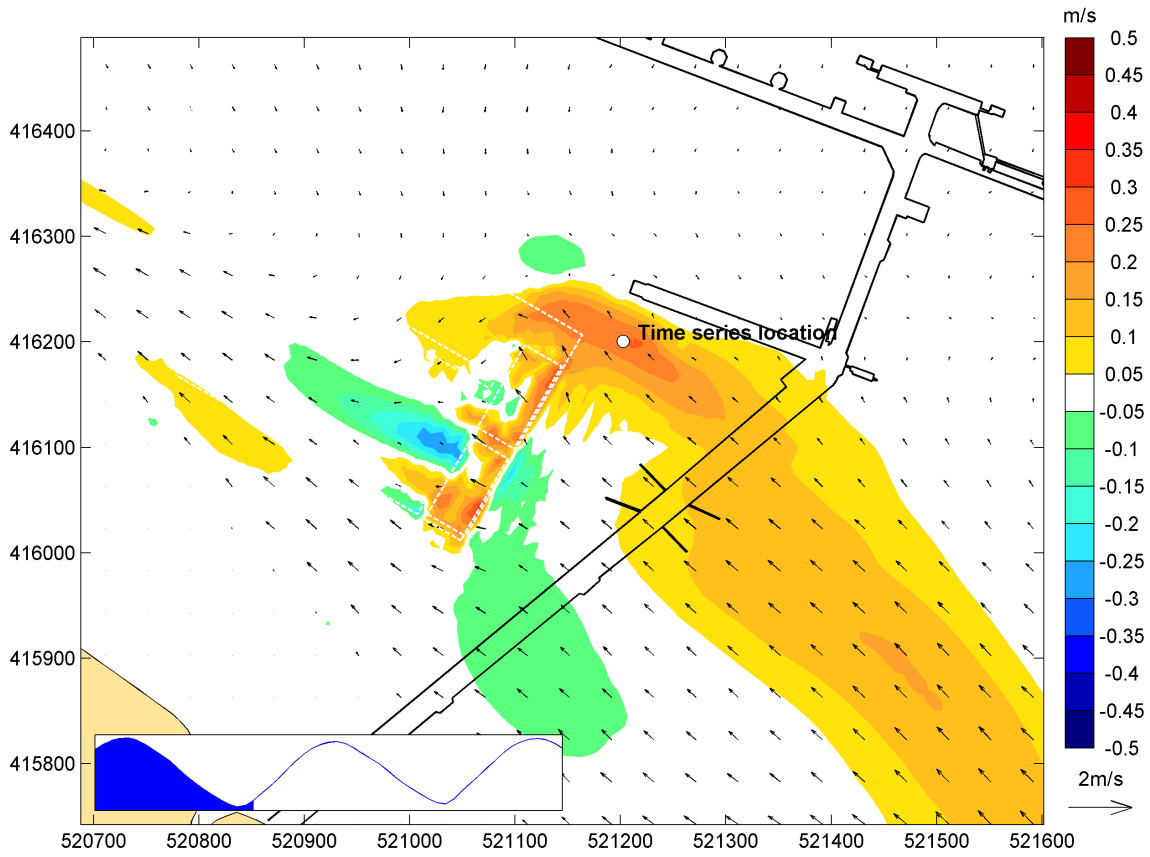

Figure 3.1: Difference in current speed between revised and original IERRT layout, LW+0.5 hour, peak spring tide, location of data extraction point shown

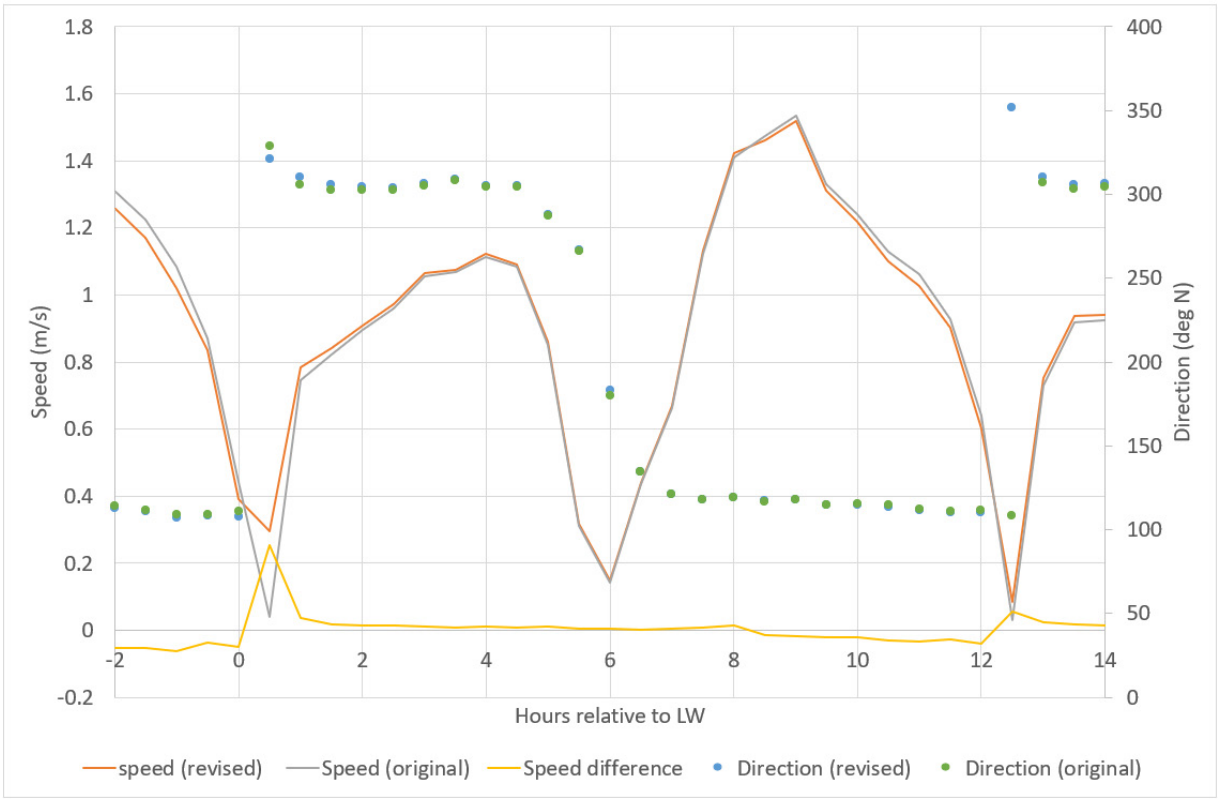

Figure 3.2: Time series current speed and direction for revised and original IERRT layout, peak spring tide

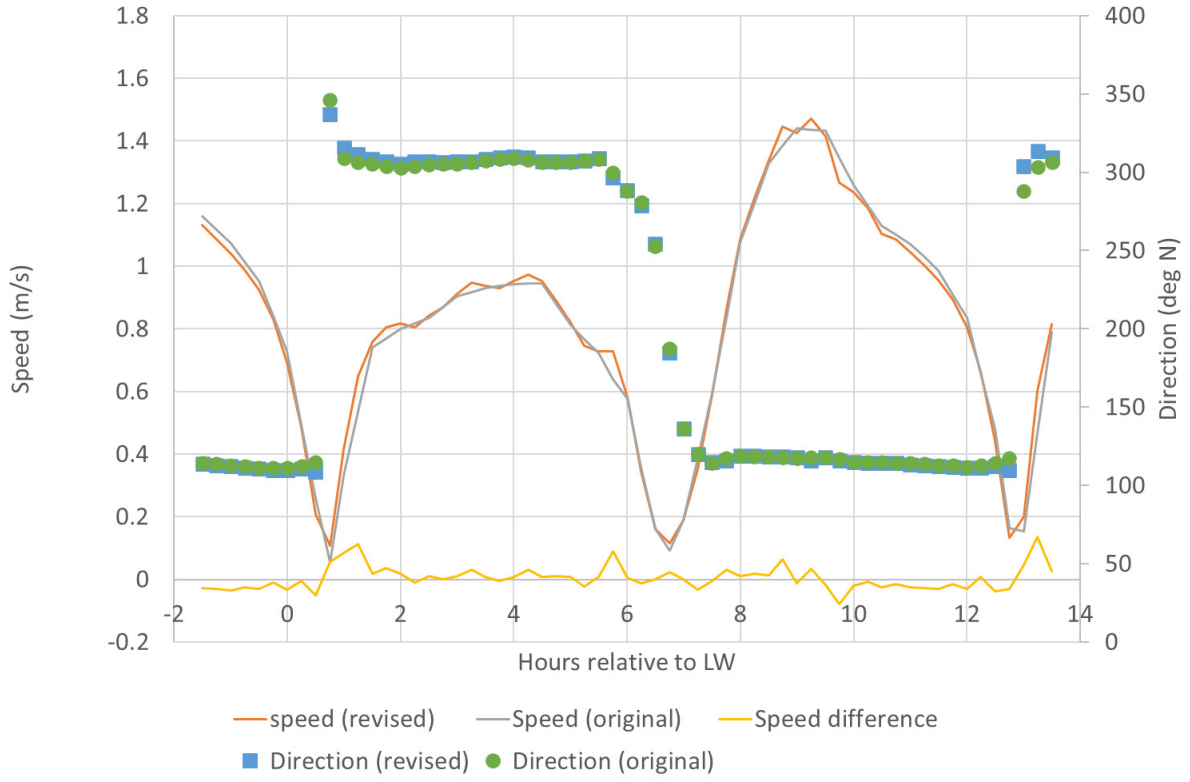

Figure 3.3: Time series current speed and direction for revised and original IERRT layout, mean spring tide

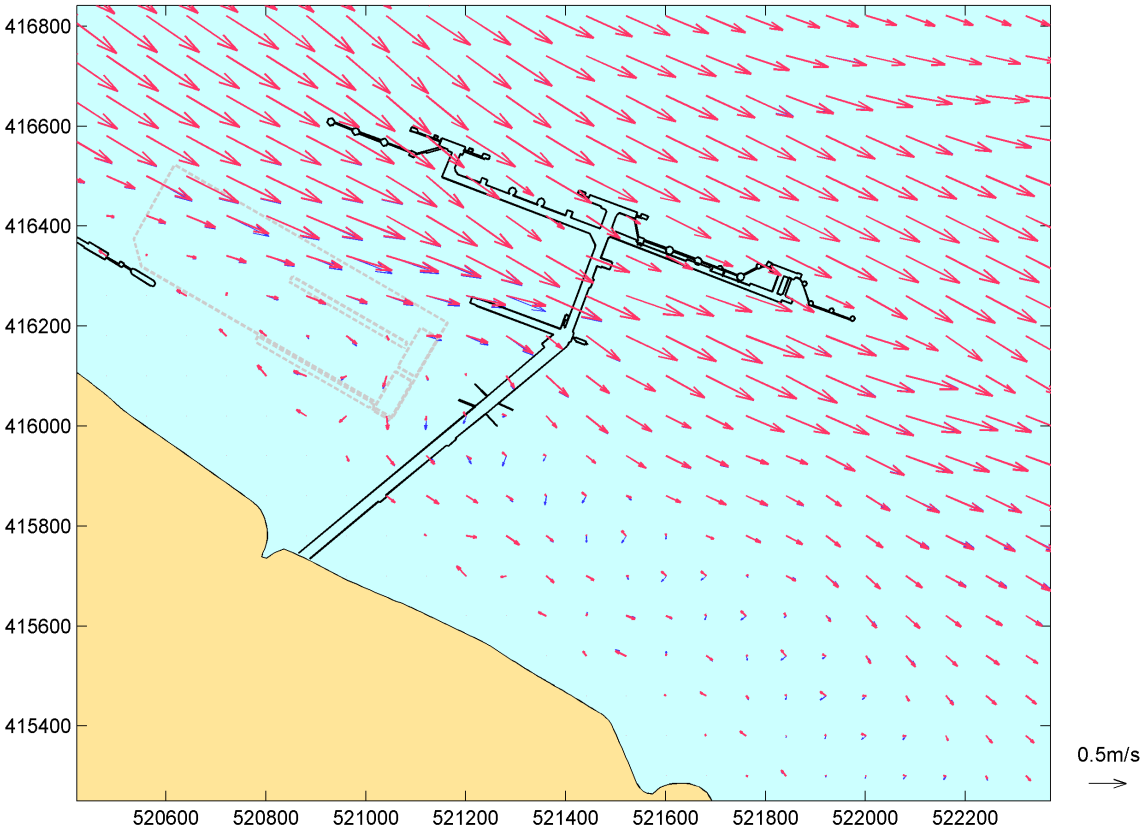

Figure 3.4: Comparison of peak spring current vectors at LW - original layout (blue), revised layout (red)

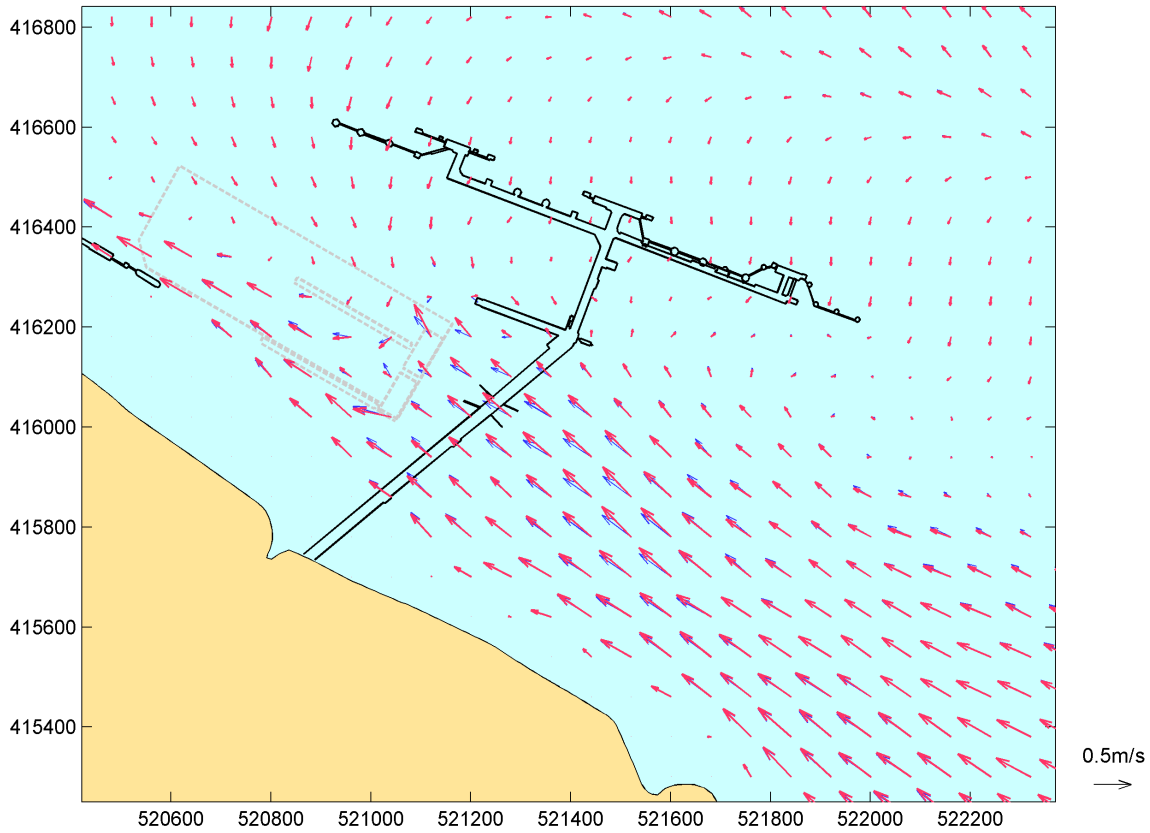

Figure 3.5: Comparison of peak spring current vectors at LW+0.5 hours - original layout (blue), revised layout (red)

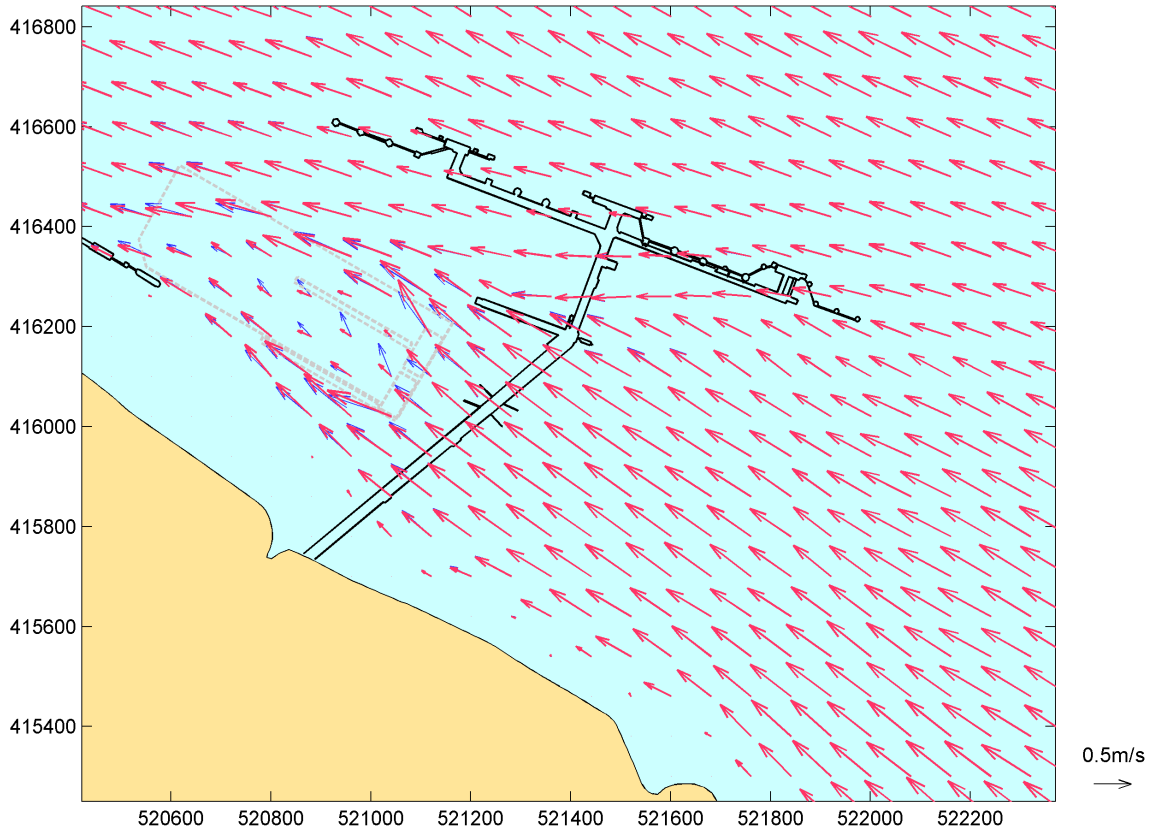

Figure 3.6: Comparison of peak spring current vectors at LW+1.0 hours - original layout (blue), revised layout (red)

3.2 Comparison with baseline conditions

The above results show the incremental effect of the revised IERRT pontoon. For nearby navigation the anticipated change in currents between the present day and those with the revised IERRT are also of importance. Examples of the change in current speed at times of approximate mid ebb and flood tides are provided for the peak spring tide simulation in Figure 3.7 and Figure 3.8. Equivalent results for mean spring tide case are shown in Figure 3.9 and Figure 3.10. Hourly results covering the whole of each tide are included in Appendix B. For these figures the minimum threshold for plotting changes is 0.1 m/s, which is more than the 0.05 m/s used for the comparison of the original and revised IERRT schemes. A threshold of 0.1 m/s (<0.25 kn) is a more typical choice to show changes to estuarine flows. The more refined choice of 0.05 was used to provide evidence for all the changes between the two IERRT schemes.

The main effects of the project are predicted to be current reductions to either side of the pontoon due to the blockage of the structure and local acceleration under the pontoon. Some transient patches of speed increase of the order of 0.1 m/s are seen at times to the side of the development during the flood tide and similar magnitude patches of speed decreases are seen occasionally to the sides of the development during the ebb tide.

The full set of comparison plots are provided in Appendix B.

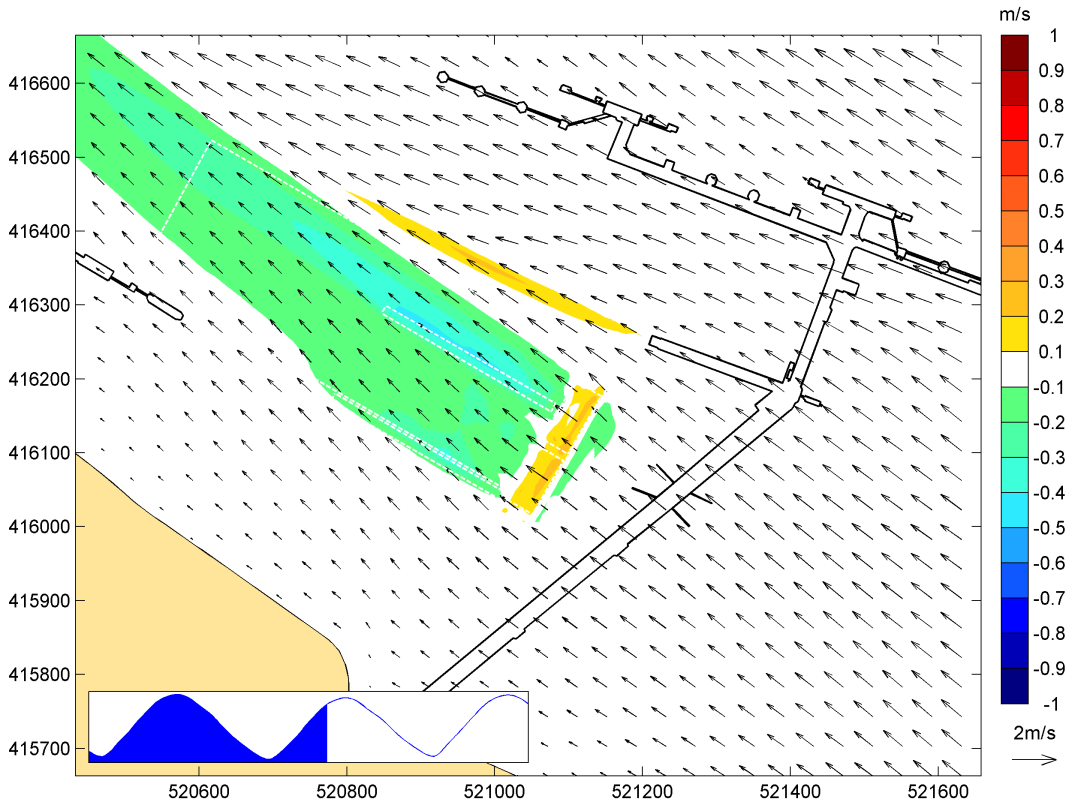

Figure 3.7: Difference in current speed between revised IERRT and baseline conditions, mid flood tide, peak spring tide

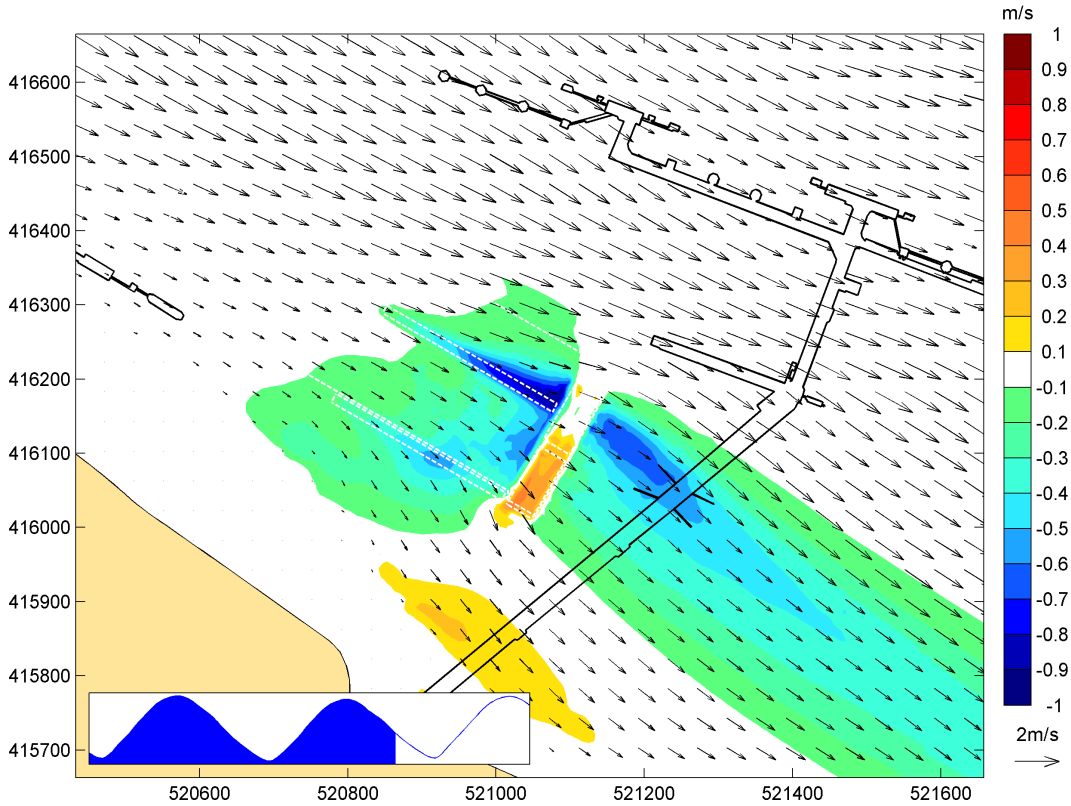

Figure 3.8: Difference in current speed between revised IERRT and baseline conditions, mid ebb tide, peak spring tide

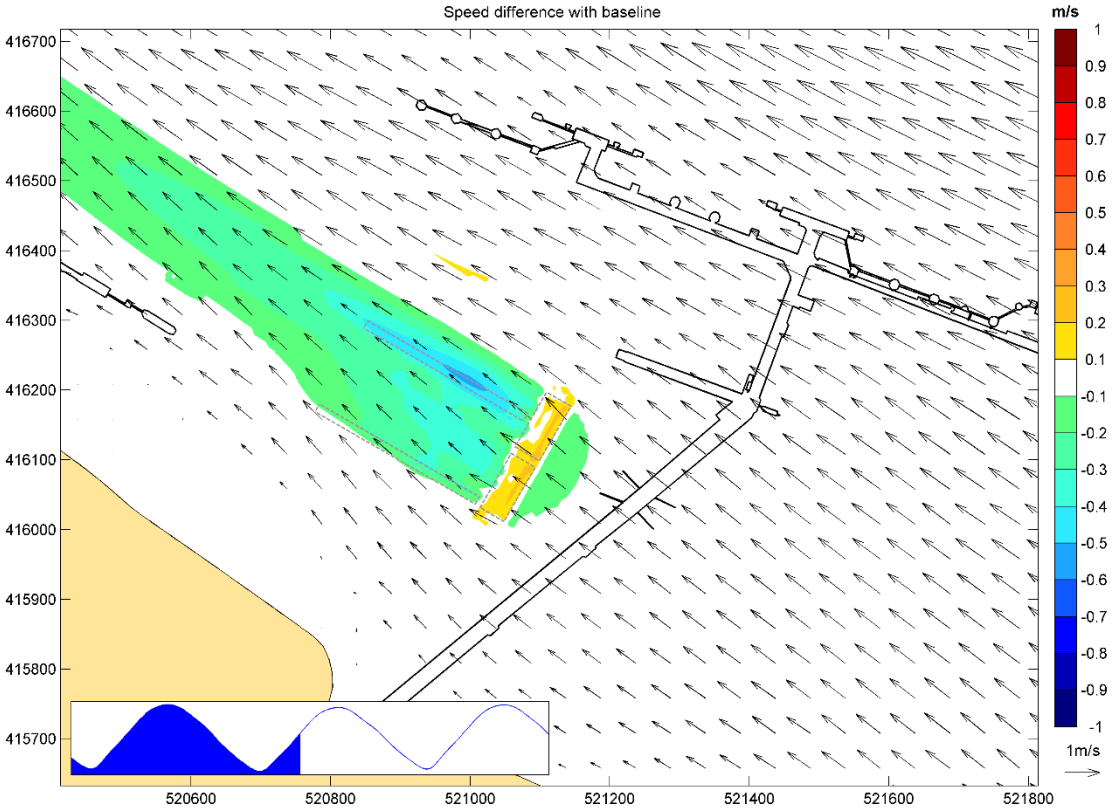

Figure 3.9: Difference in current speed between revised IERRT and baseline conditions, mid flood tide, mean spring tide

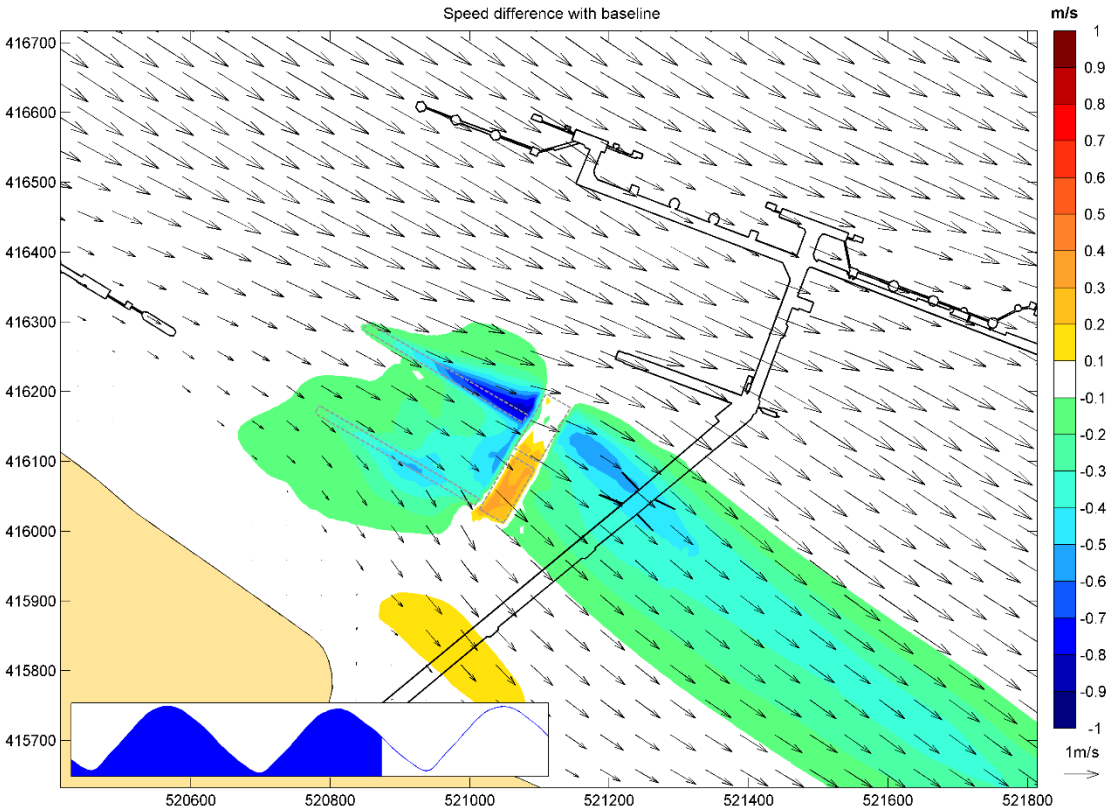

Figure 3.10: Difference in current speed between revised IERRT and baseline conditions, mid ebb tide, mean spring tide

3.3 Flow conditions between IERRT and IOT

The above results shows the current pattern with the revised IERRT in place interpolated onto a 30 m square grid. To remove any potential effect of the interpolation and to provide further details of the current pattern in the gap between IERRT and the IOT finger jetty current vectors of every model node were plotted provide additional details of the simulation results. The times of mid ebb and flood currents are plotted in Figure 3.11 and Figure 3.12; the hourly results are included in Appendix C.

These results confirm that whilst some deflection of the currents around the pontoon does occur, no large scale eddies which might influence vessels are seen. Smaller eddies, of a few metres diameter, may occur in the immediate vicinity of the pontoon structure as are seen for other marine structures at this site but these are considered too small to significantly effect navigation.

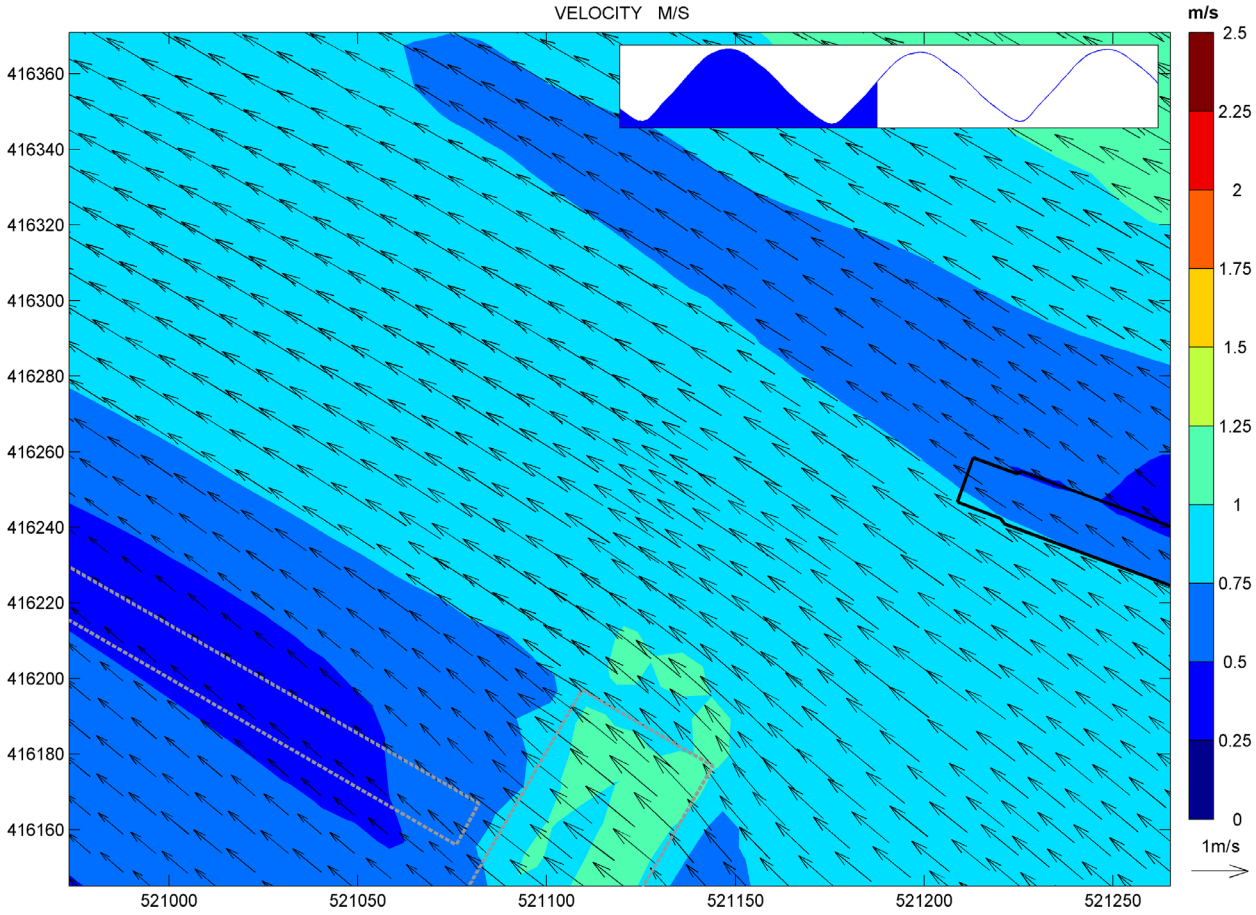

Figure 3.11: Distribution of current speed and direction between IERRT and IOT, mid flood tide, mean spring tide range

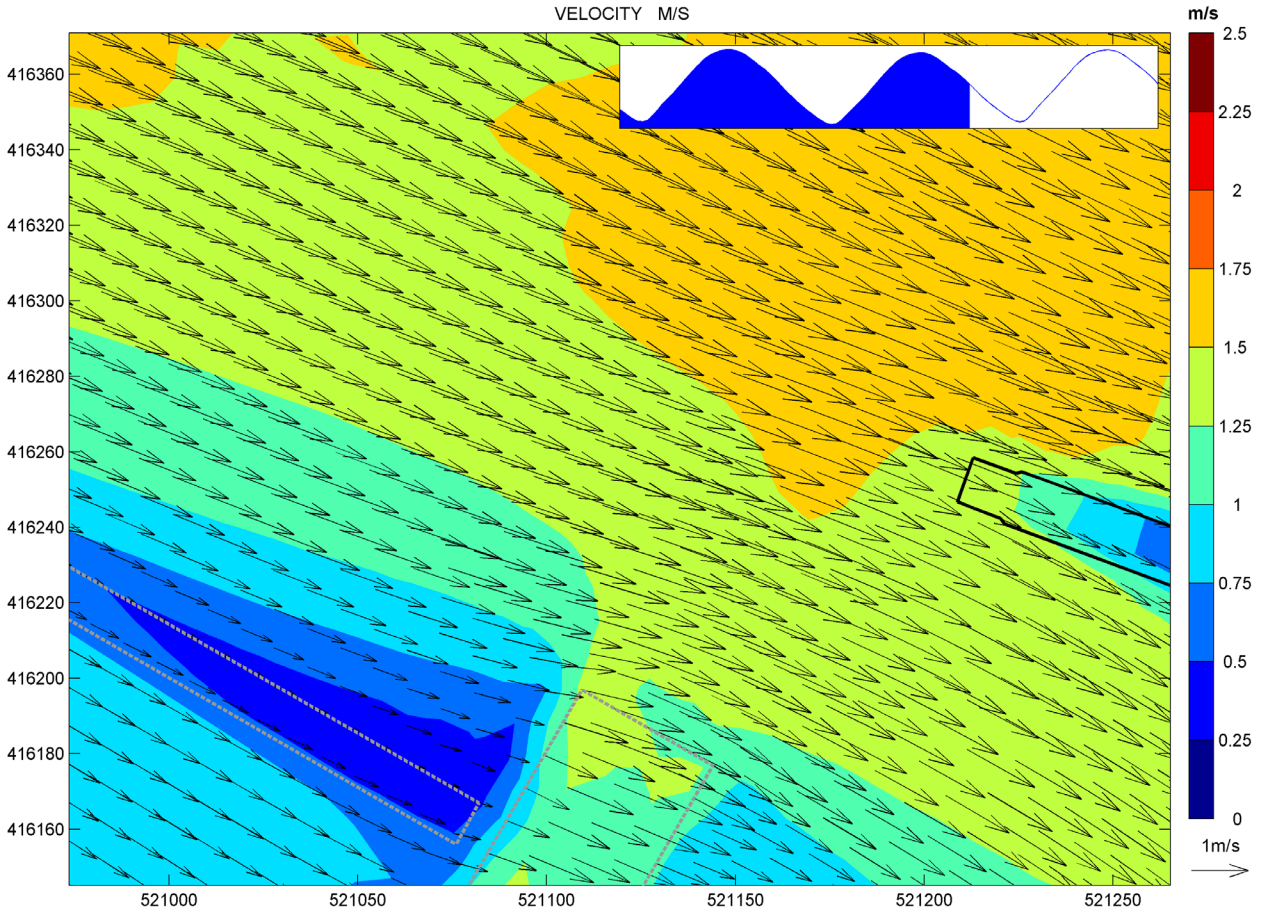

Figure 3.12: Distribution of current speed and direction between IERRT and IOT, mid ebb tide, mean spring tide range

3.4 Sensitivity to moored vessels at IERRT

All the modelling has included the permanent parts of the IERRT project, in particular the pontoon. It is noted that vessels which are to use the IERRT may have a greater draught than the pontoon. The situation is described in Figure 3.13 and Figure 3.14.

The spatial view indicates the relatively large width across the flow of the pontoon compared to the vessel, which will also be moored in the area of low currents associated with the blockage of the pontoon (see Appendix B). The likely proximity of the moored vessel to the pontoon is illustrated by Figure 3.14. Assuming a typical 1:10 expansion of the flow, the flood tide flow will not have recovered from the effect of the pontoon before reaching the vessel. That means any effect is likely to be only from the lower part of the vessel's hull. The additional blockage of the vessel will also be acting on the lower part of the water column where currents are lower.

Most likely the moored vessels will extend the flow effect of the project along the flow stream direction. No additional effect beyond that predicted for the pontoon is anticipated for the across stream direction.

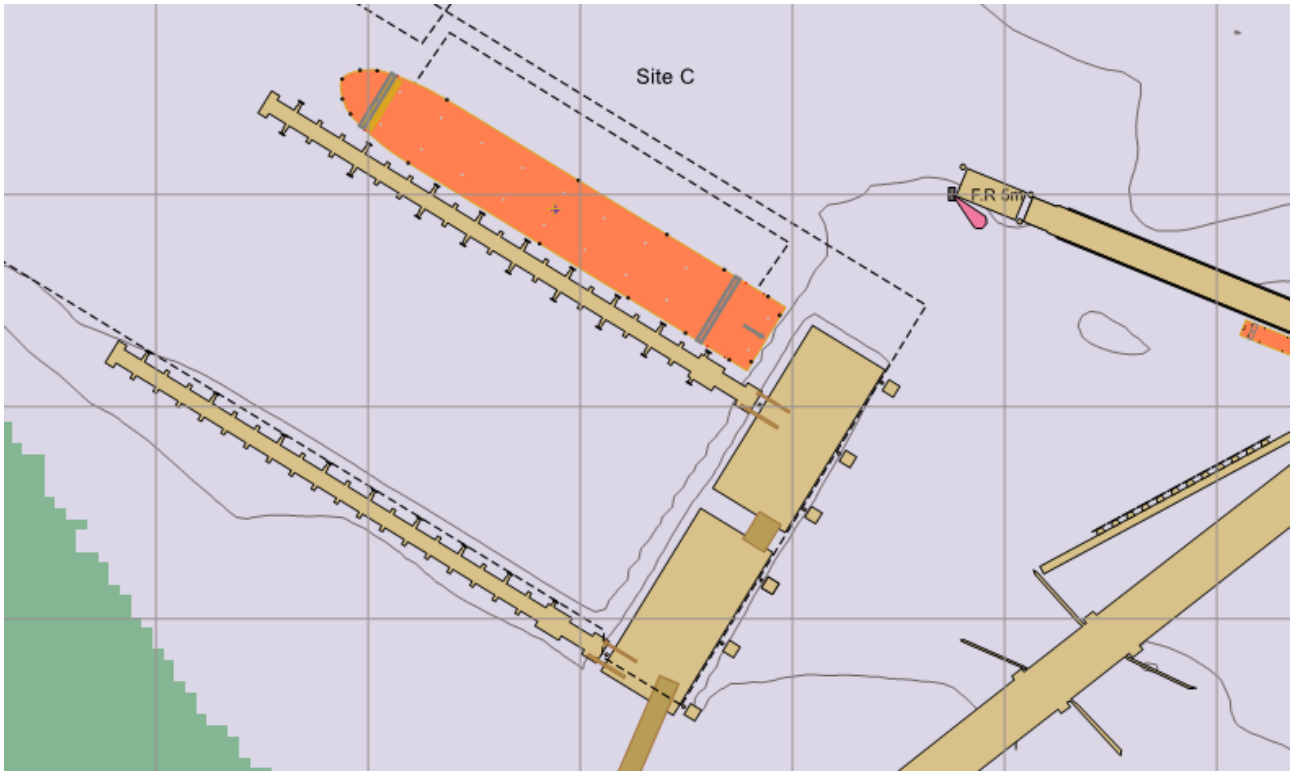

Figure 3.13: Spatial view of moored vessel at IERRT

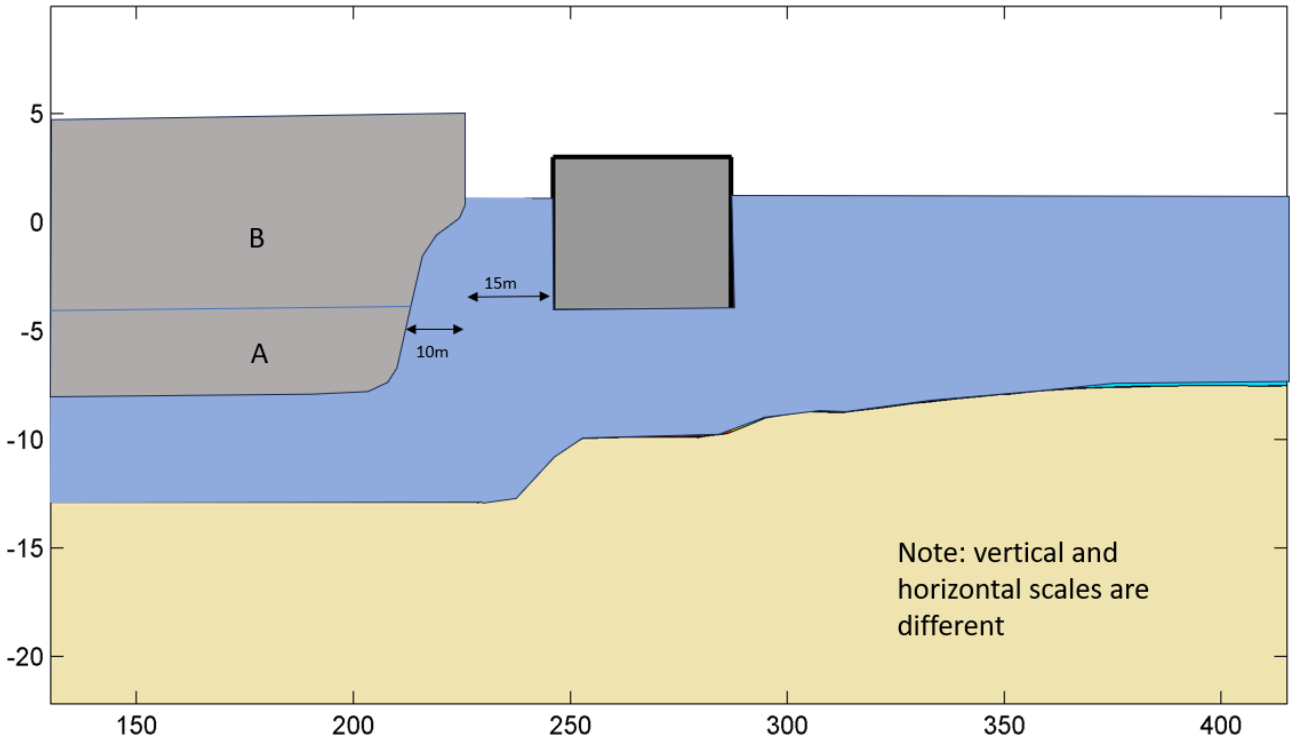

Figure 3.14: Schematic section of moored vessel and IERRT pontoon

4 Conclusions

A 3D modelling exercise of the revised IERRT has been completed to demonstrate any difference between its impacts on flows and those modelled for the original scheme. The difference between the hydrodynamics were extracted hourly throughout the tide for two tidal conditions and are included in Appendix A. Further plotting and assessment was undertaken for the period differences seen at the turn of the tide at low water. The conclusions of the work are:

- The revised IERRT layout does not change the assessment of the hydrodynamic effect of the IERRT for nearby maritime facilities. No changes in the effect of the IERRT on hydrodynamics are shown at IOT. The area of speed increase across the flow greater than 0.05 m/s is confined to the area close to the IERRT pontoon, within 30 m of the edge of the pontoon between the pontoon and the IOT finger jetty.
- The revised layout results in lower currents at the times of peak flow up and down stream of the IERRT as might be expected for the larger pontoon associated with the revised layout. The area of speed reduction with changes greater than 0. 2 m/s extends 500 m north west during the flood tide and 1000 m south east during the ebb. The differences in the spatial extent of these areas is linked to the larger currents which occur on the ebb tide.
- A short, period of higher differences between the revised and original layouts is seen on occasion as the tide turns at low water. This phenomenon appears linked to localised, transient changes to the timing and pattern of the turn of the tide. It should be noted that current magnitudes at these times remain low (<0.3 m/s) for both the original and revised layout. This effect is seen more for the large spring tide than the mean spring tide due to the generally higher currents for the large spring.

Presentation of the comparison of the currents with the revised IERRT with baseline (no project) conditions were also undertaken. They showed:

- Current reductions to either side of the pontoon due to the blockage of the structure and local acceleration under the pontoon. Some transient patches of speed increase of the order of 0.1 m/s are seen at times to the side of the development during the flood tide and similar magnitude patches of speed decreases are seen occasionally to the sides of the development during the ebb tide.
- No eddy features of a scale that might influence navigation.
- The predicted effects of the IERRT were considered to be dominated by the blockage to the flow of the pontoon. Any additional effect of vessels moored at IEERT was considered to be small compared to the pontoon due to the relatively small additional blockage to flow from the vessels and that this additional blockage is acting on the lower parts of the water column where currents are lower.

5 References

ABP (2023). Immingham Eastern Ro-Ro Terminal. Environmental Statement Addendum. Document 10.3.8.

HR Wallingford (2022). Project Sugar - ABP Humber - Immingham East Development, flow model comparison with October 2022 ADCP survey. Report DJR6612_RT007_R01-00.

Mutlu Sumer, B. and Fredsøe, J. (2006). Hydrodynamics Around Cylindrical Structures (New edition). World Scientific Publishing Co Pte Ltd, Singapore. ISBN 13: 978-9-81-270039-1.

Appendices

A Hourly comparison of currents for revised and original IERRT layouts

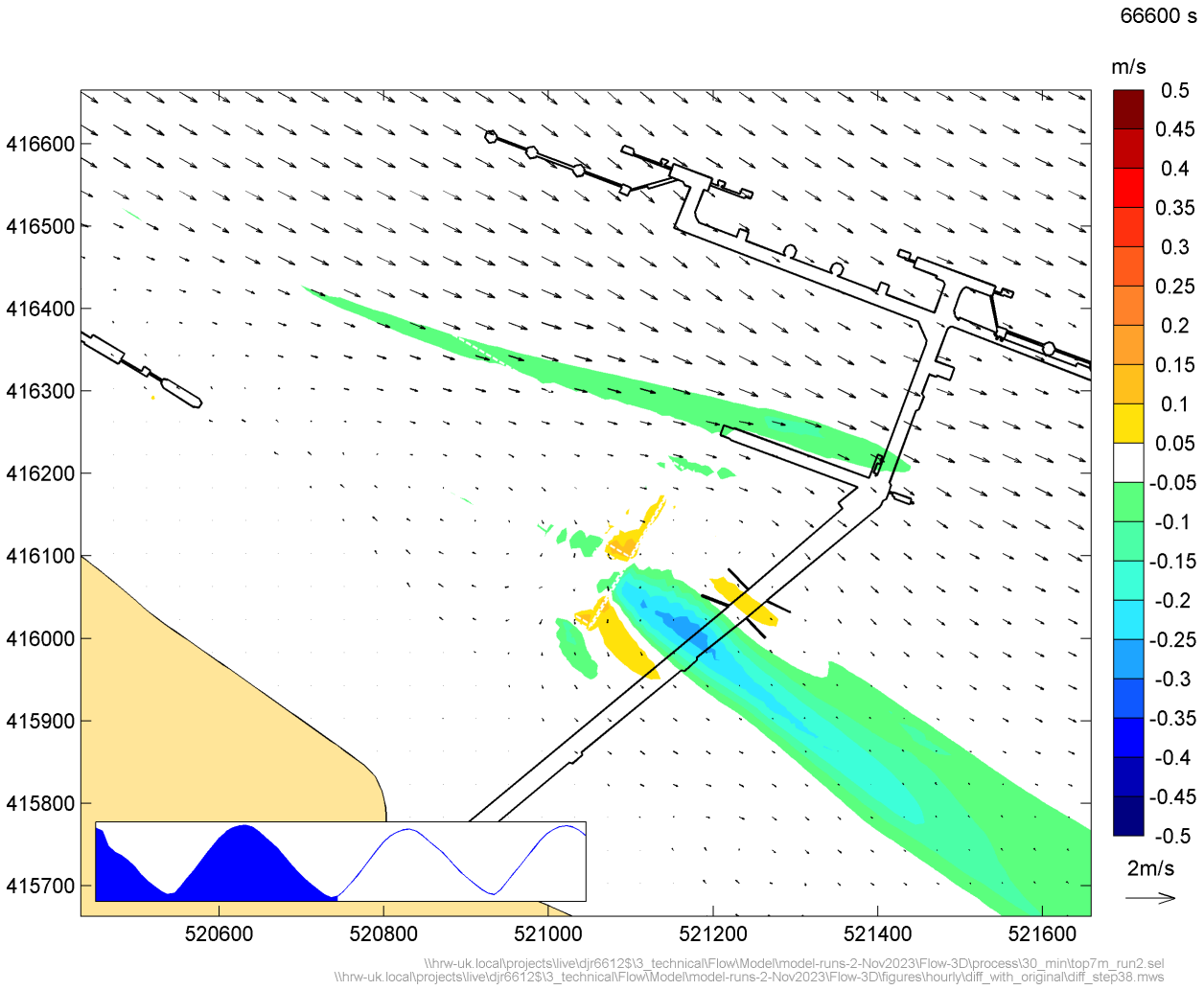

Figure A.1: Difference in current speed between revised and original IERRT layout, LW, peak spring tide

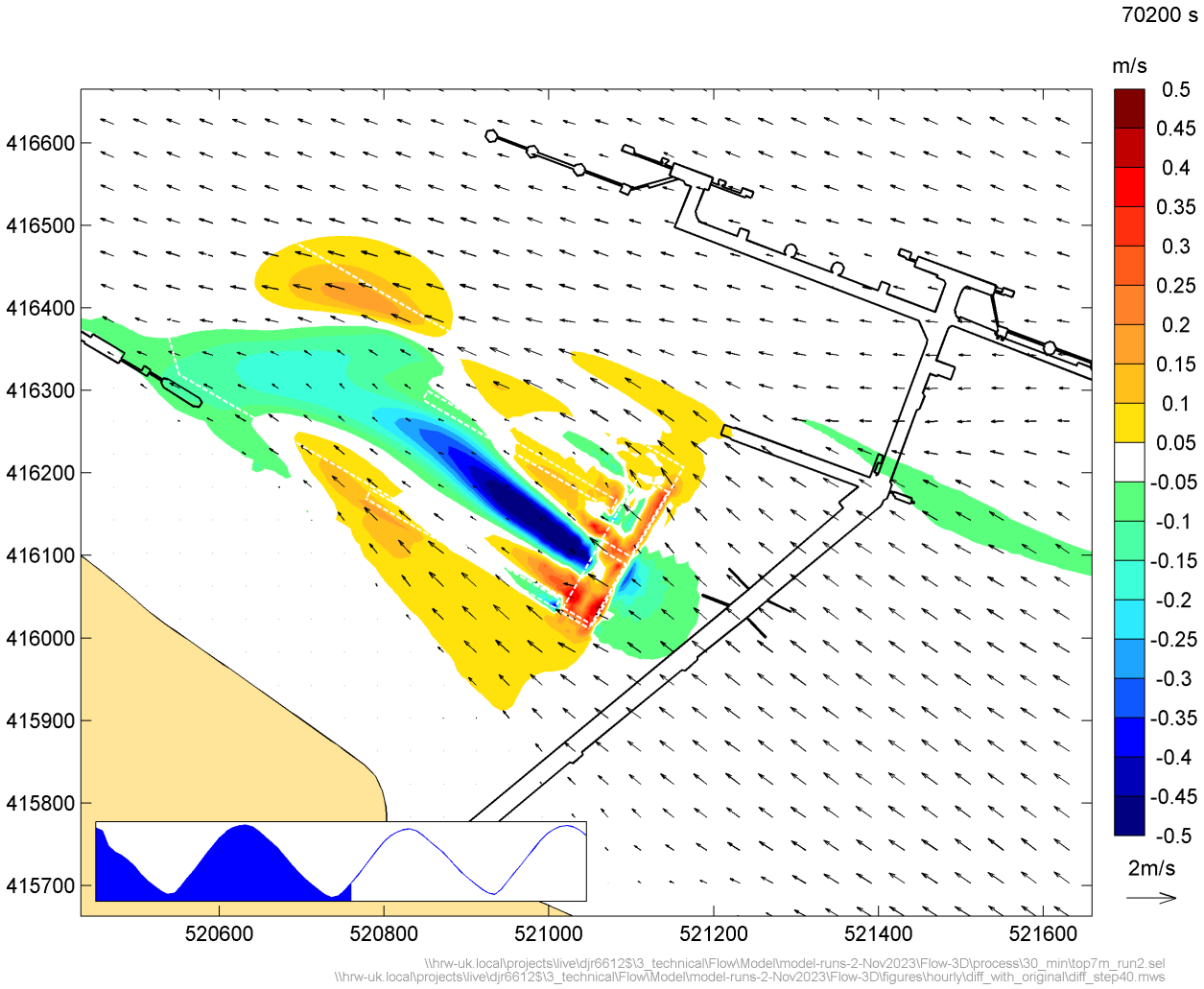

Figure A.2: Difference in current speed between revised and original IERRT layout, LW+1, peak spring tide

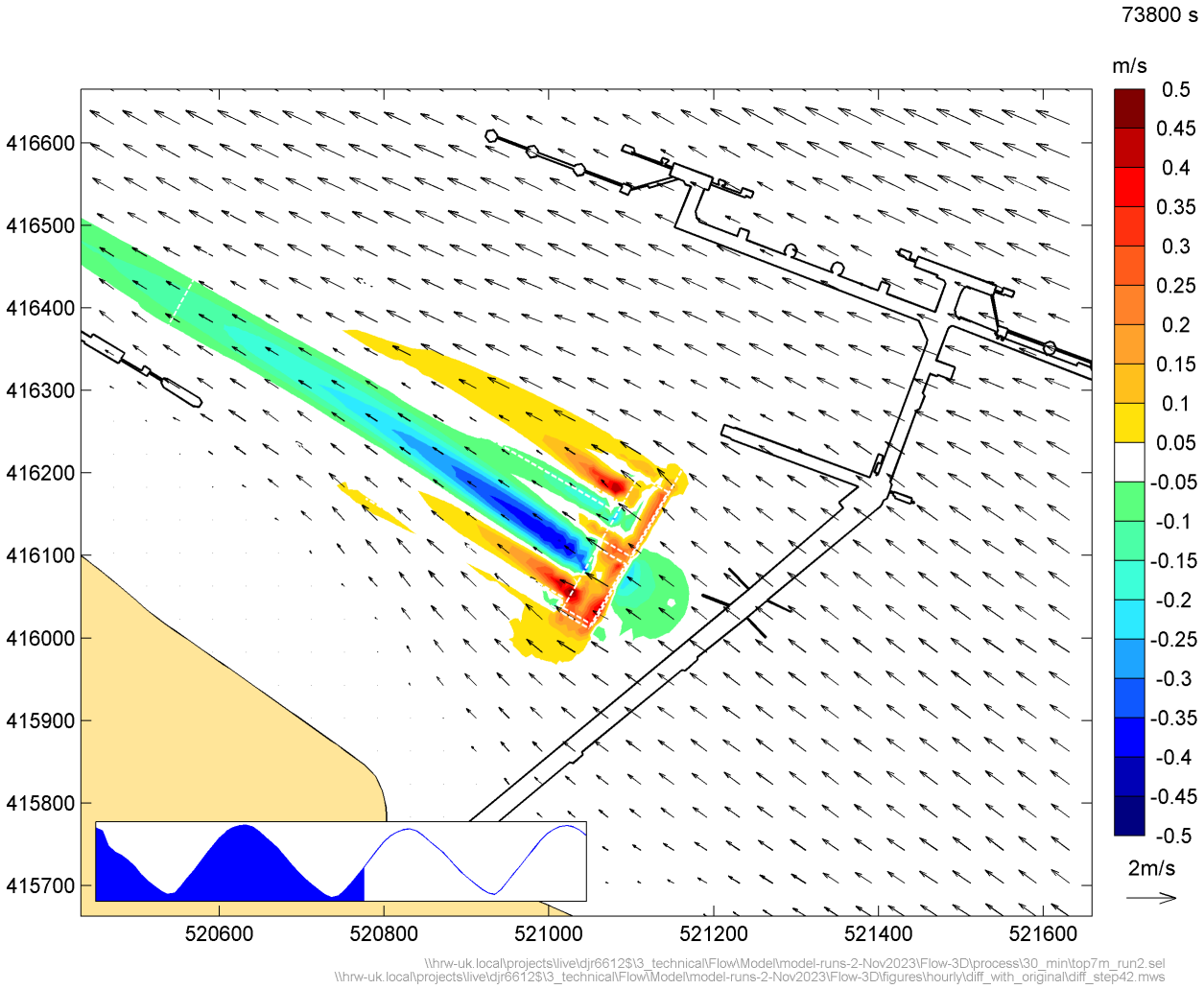

Figure A.3: Difference in current speed between revised and original IERRT layout, LW+2, peak spring tide

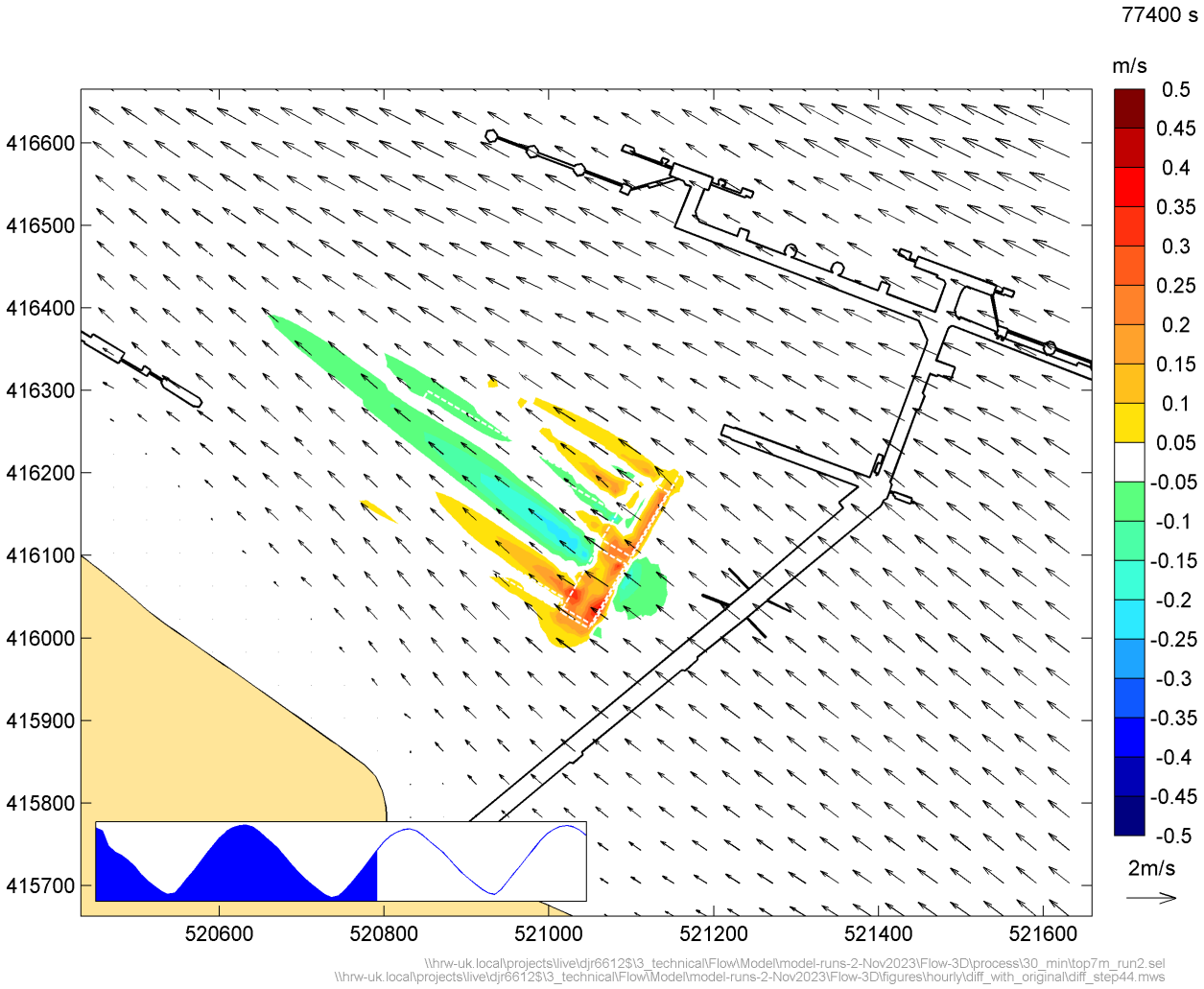

Figure A.4: Difference in current speed between revised and original IERRT layout, LW+3, peak spring tide

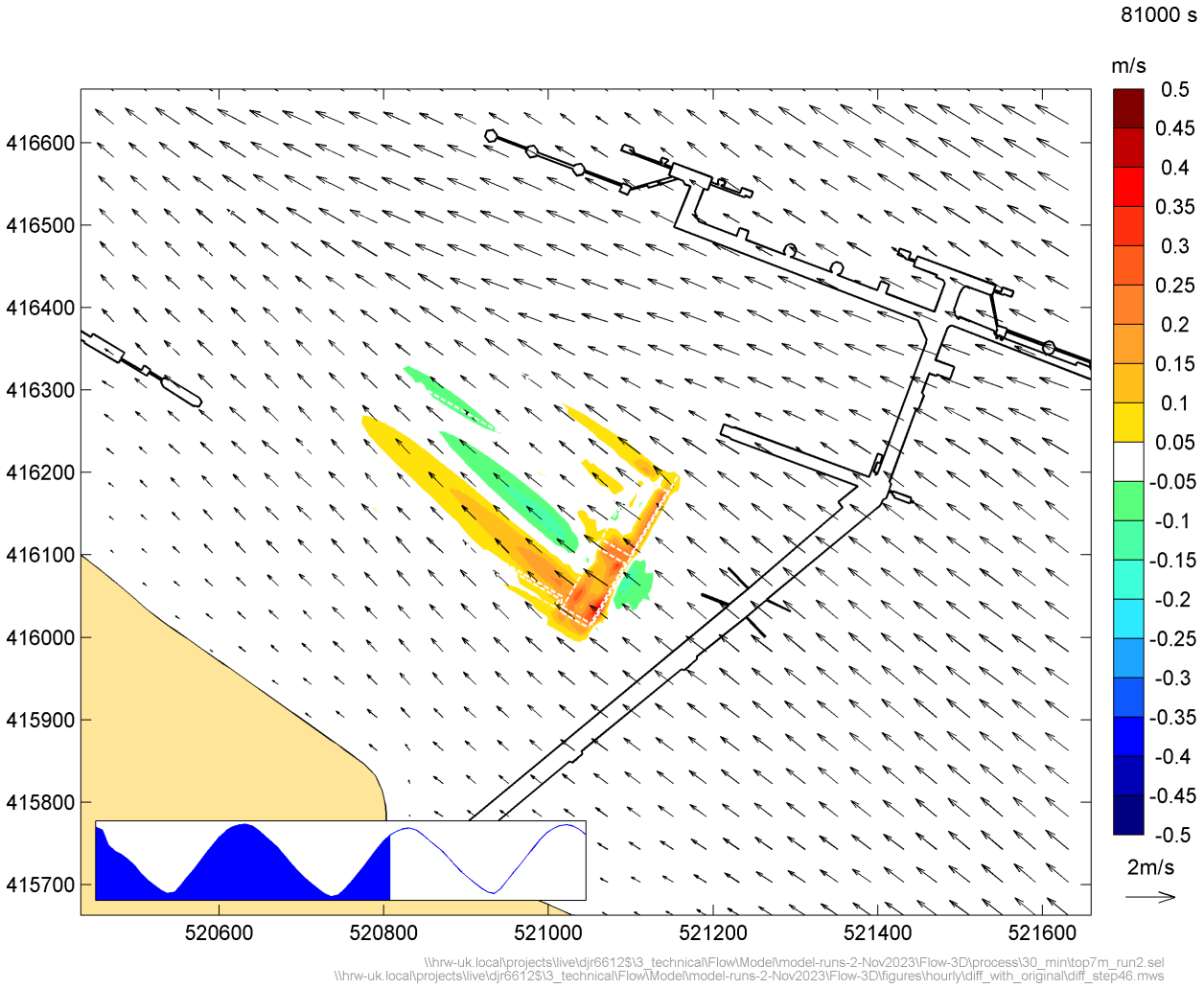

Figure A.5: Difference in current speed between revised and original IERRT layout, LW+4, peak spring tide

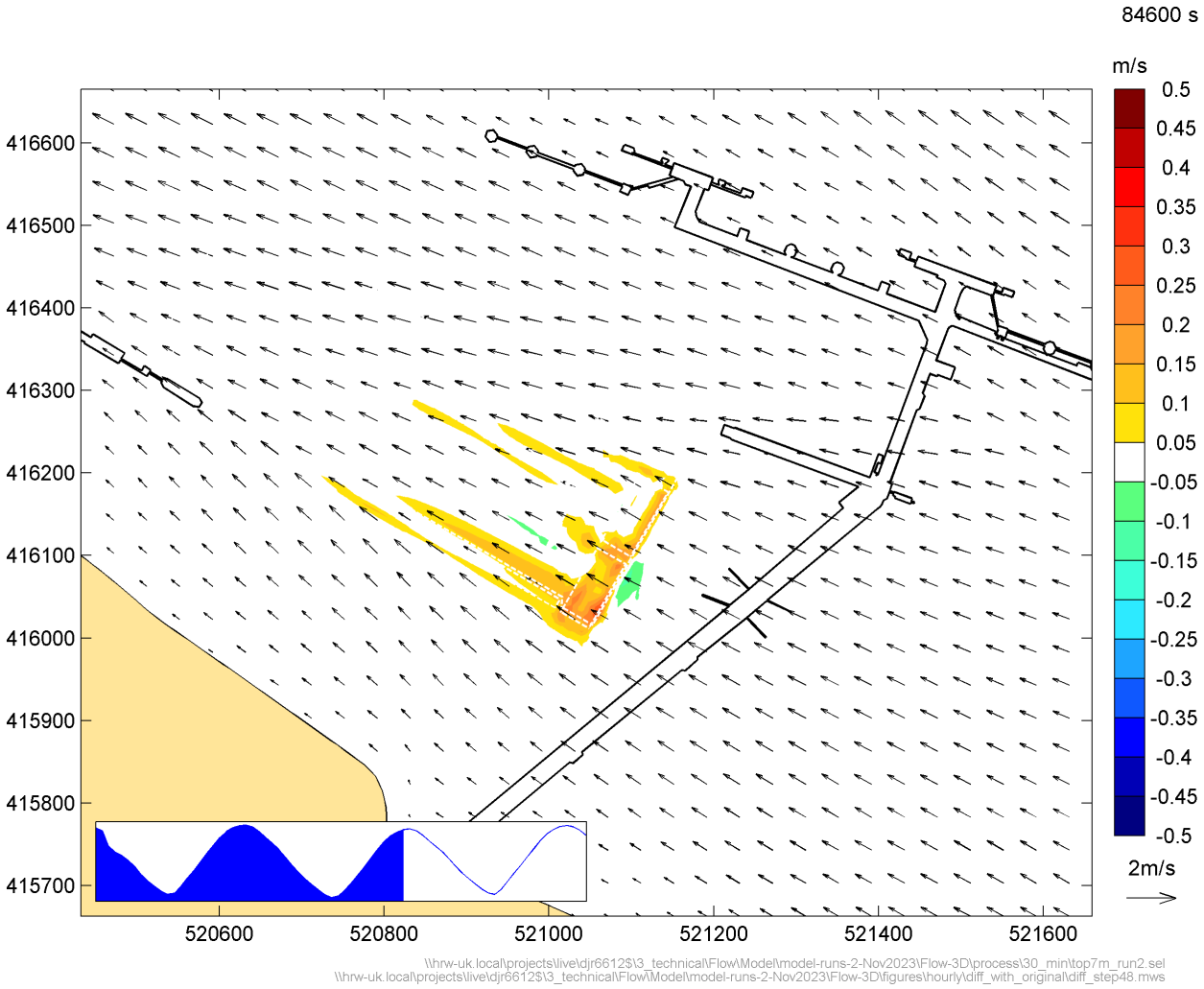

Figure A.6: Difference in current speed between revised and original IERRT layout, LW+5, peak spring tide

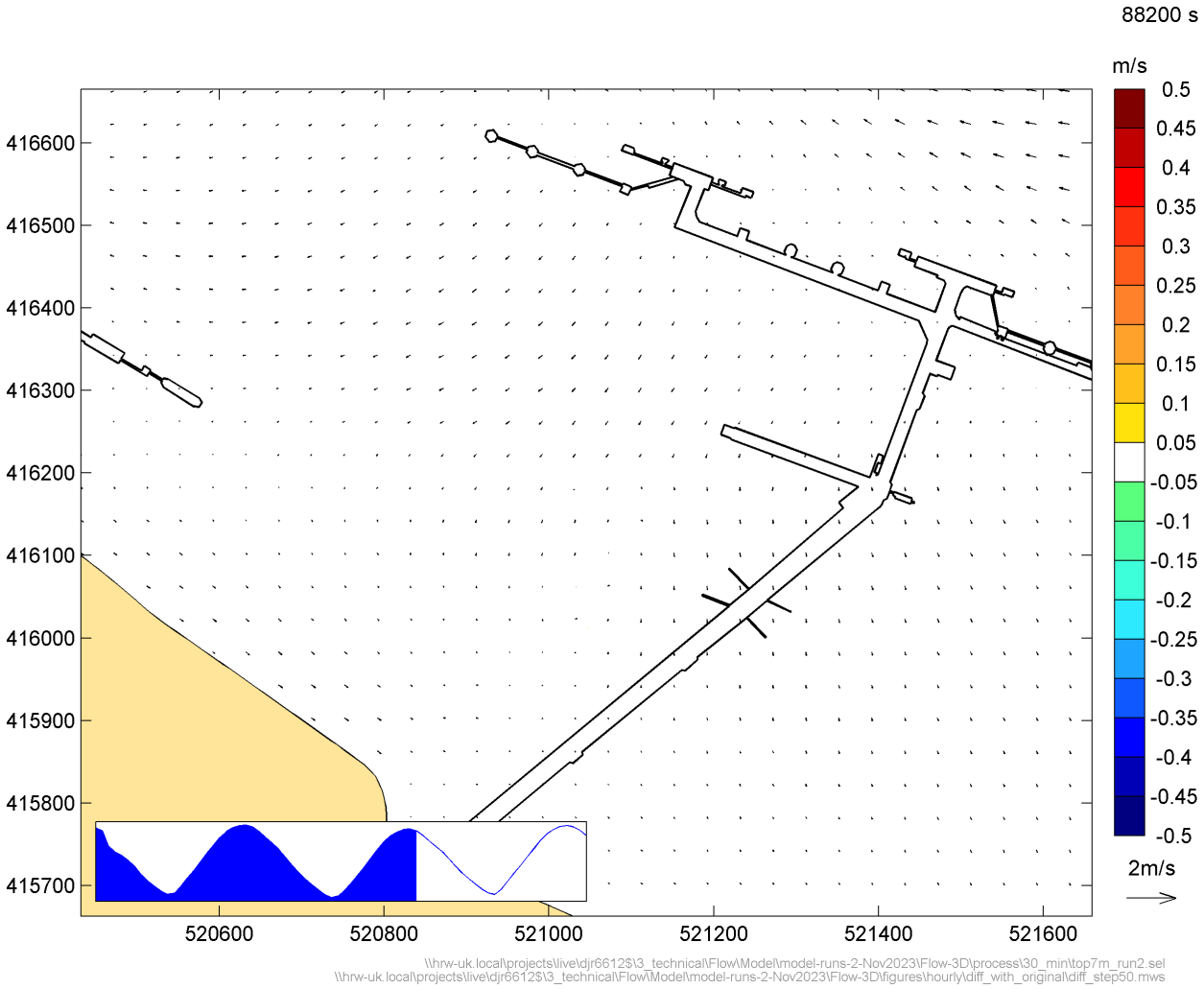

Figure A.7: Difference in current speed between revised and original IERRT layout, LW+6, peak spring tide

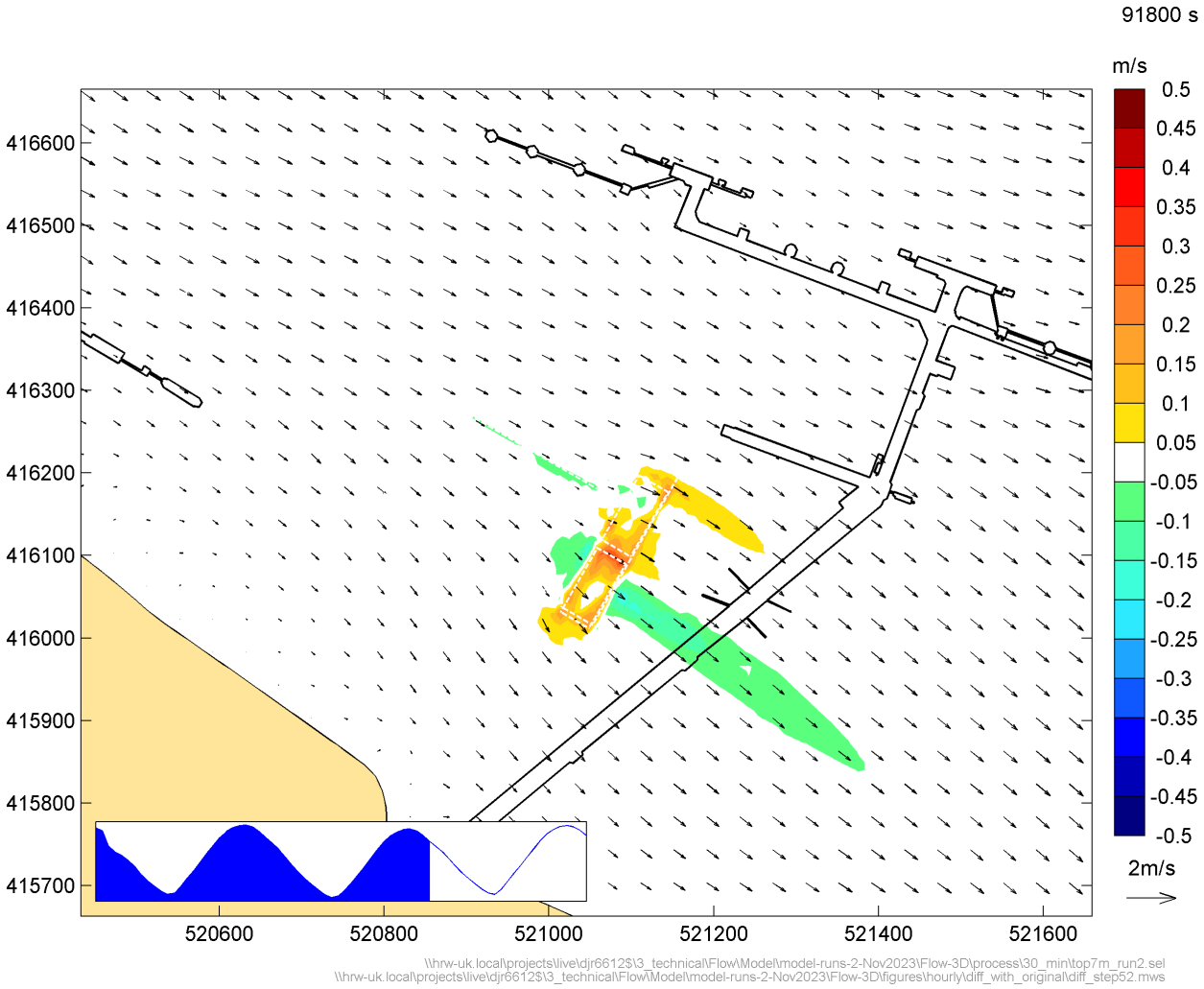

Figure A.8: Difference in current speed between revised and original IERRT layout, LW+7, peak spring tide

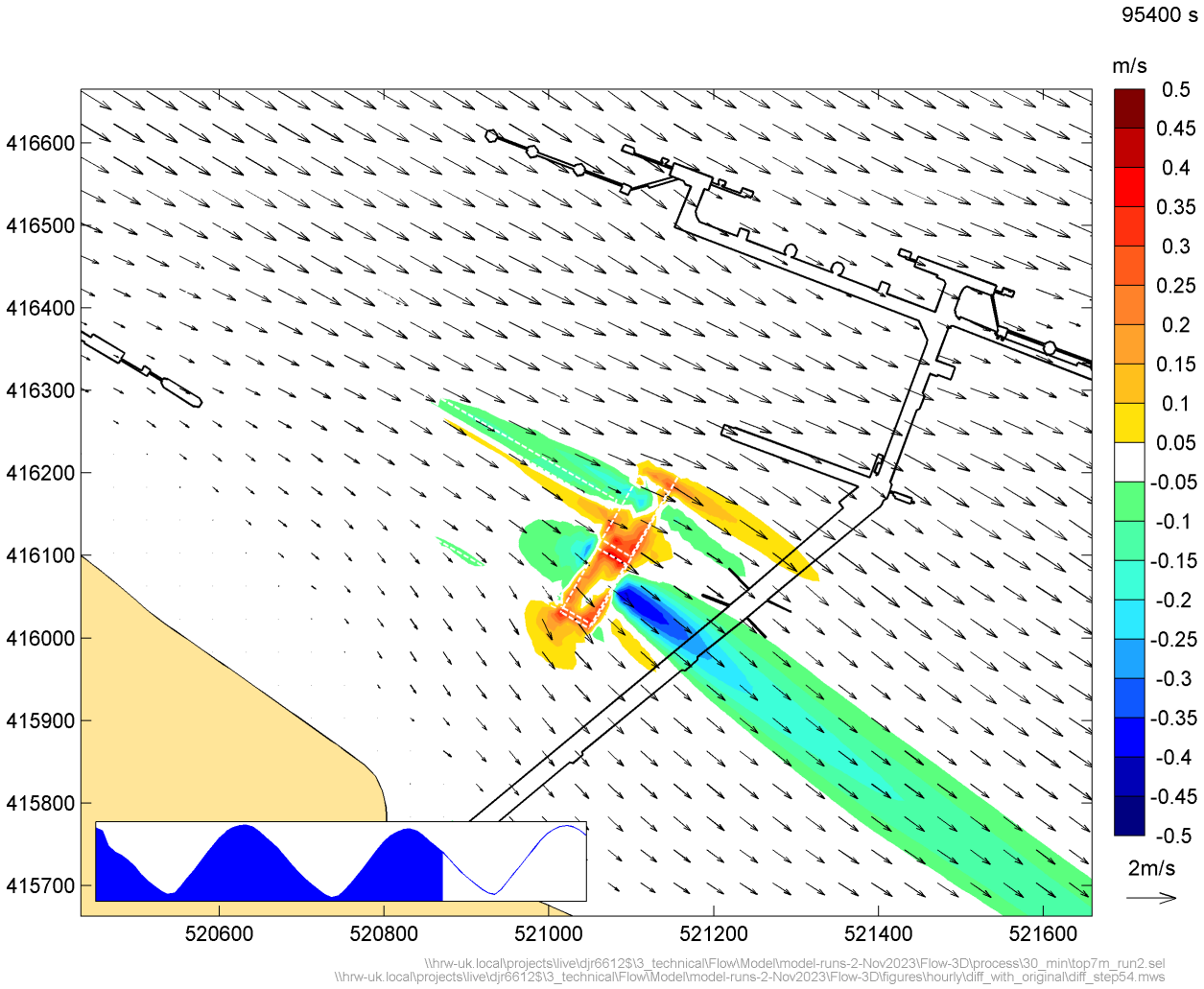

Figure A.9: Difference in current speed between revised and original IERRT layout, LW+8, peak spring tide

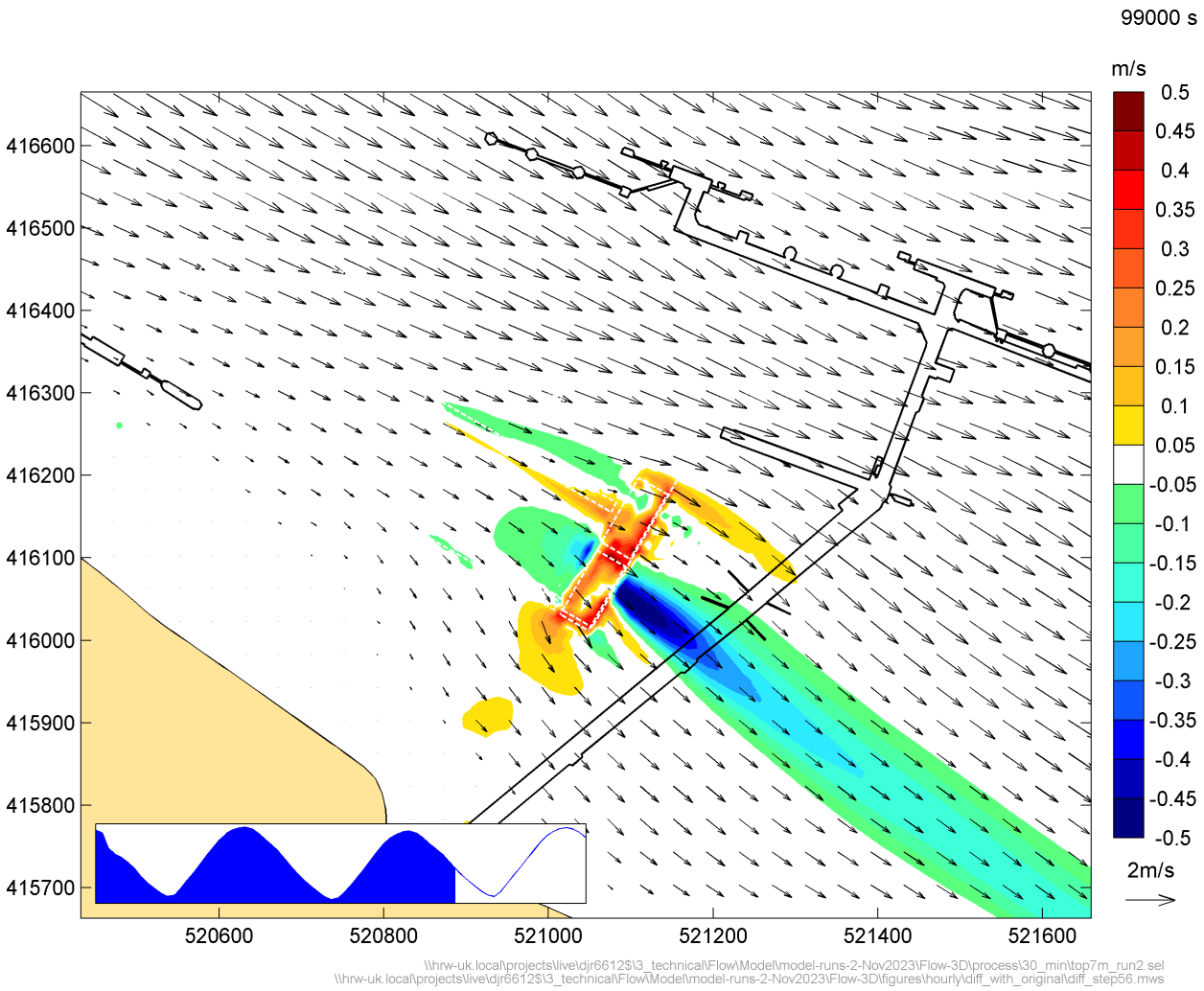

Figure A.10: Difference in current speed between revised and original IERRT layout, LW+9, peak spring tide

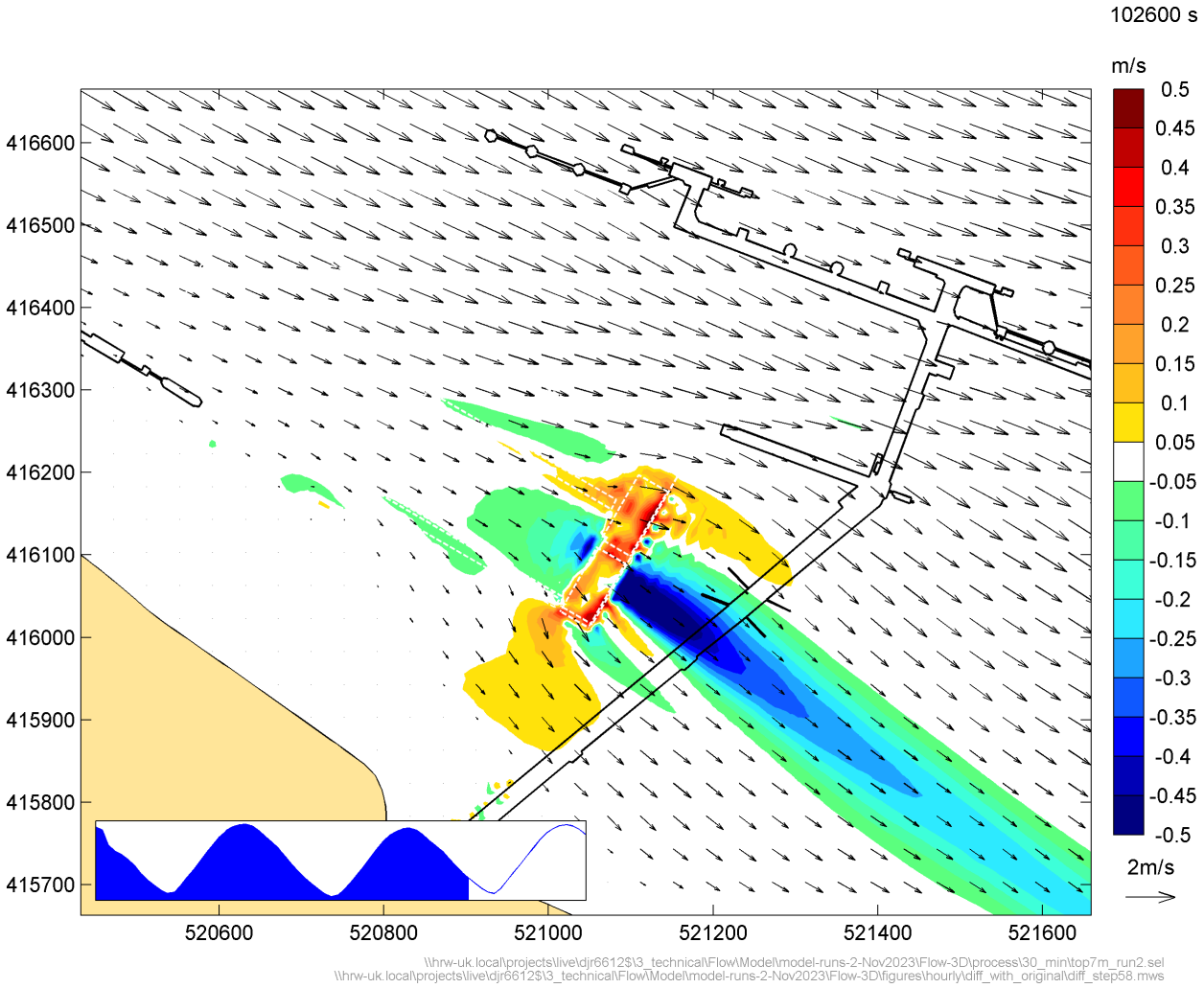

Figure A.11: Difference in current speed between revised and original IERRT layout, LW+10, peak spring tide

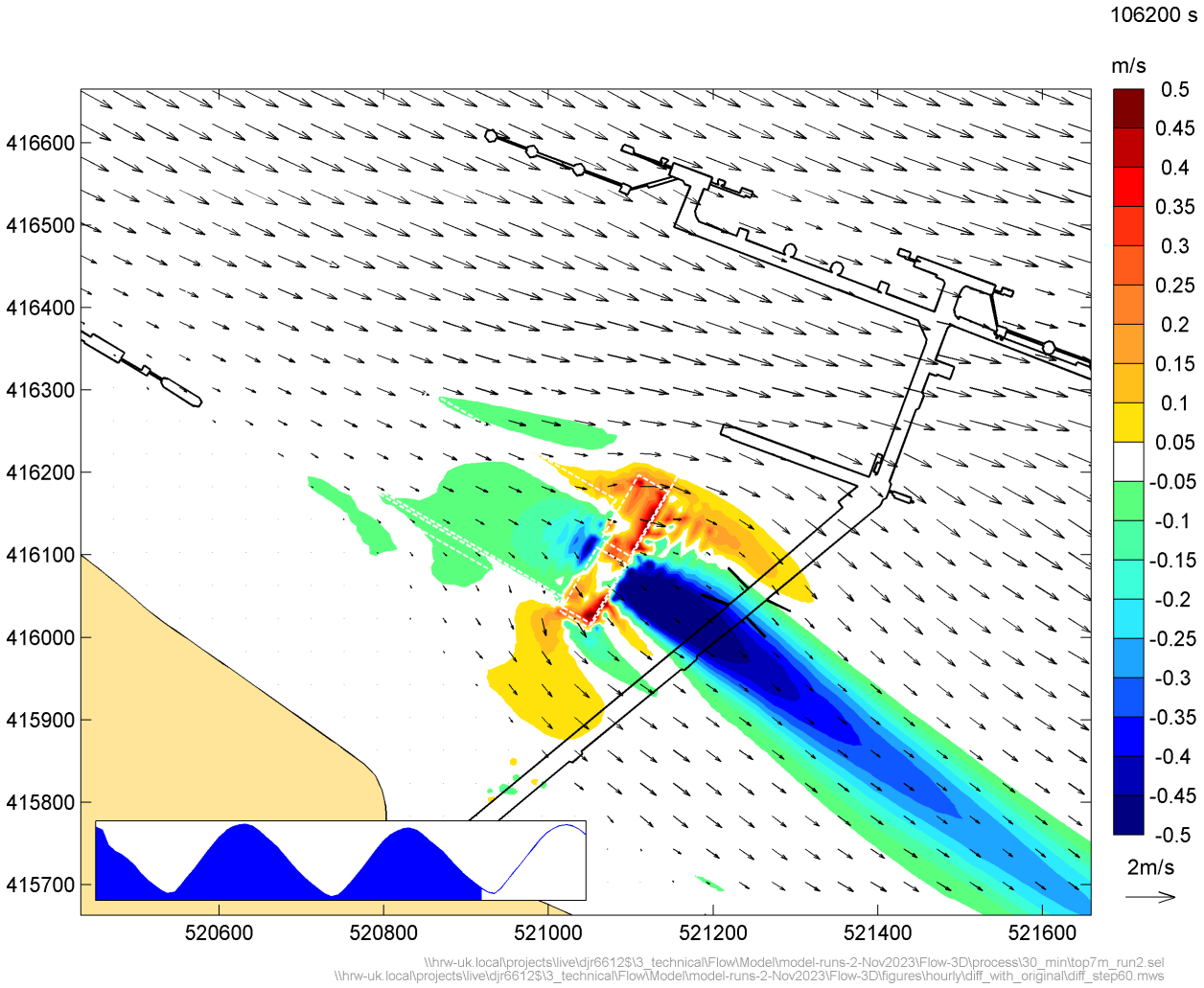

Figure A.12: Difference in current speed between revised and original IERRT layout, LW+11, peak spring tide

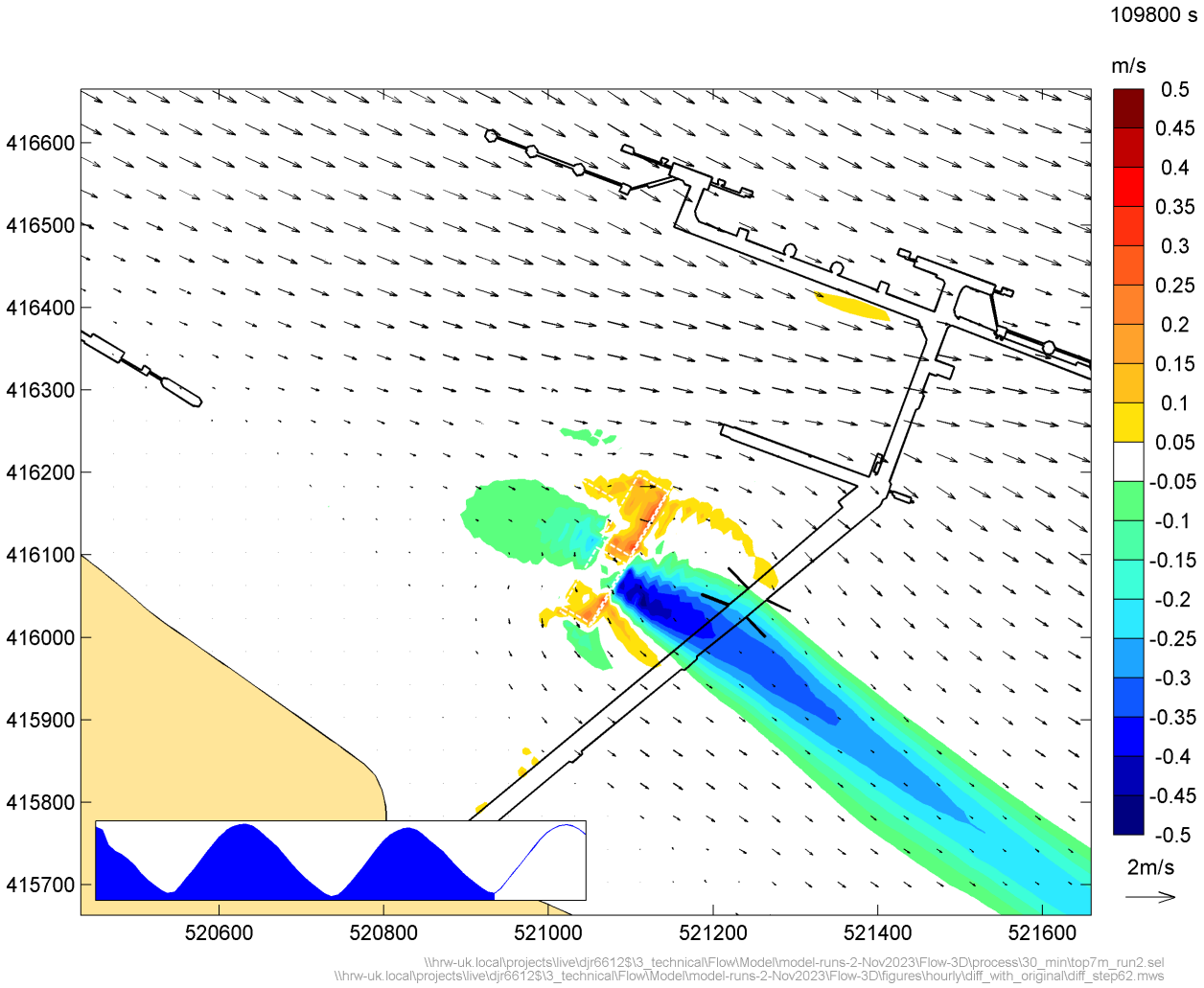

Figure A.13: Difference in current speed between revised and original IERRT layout, LW+12, peak spring tide

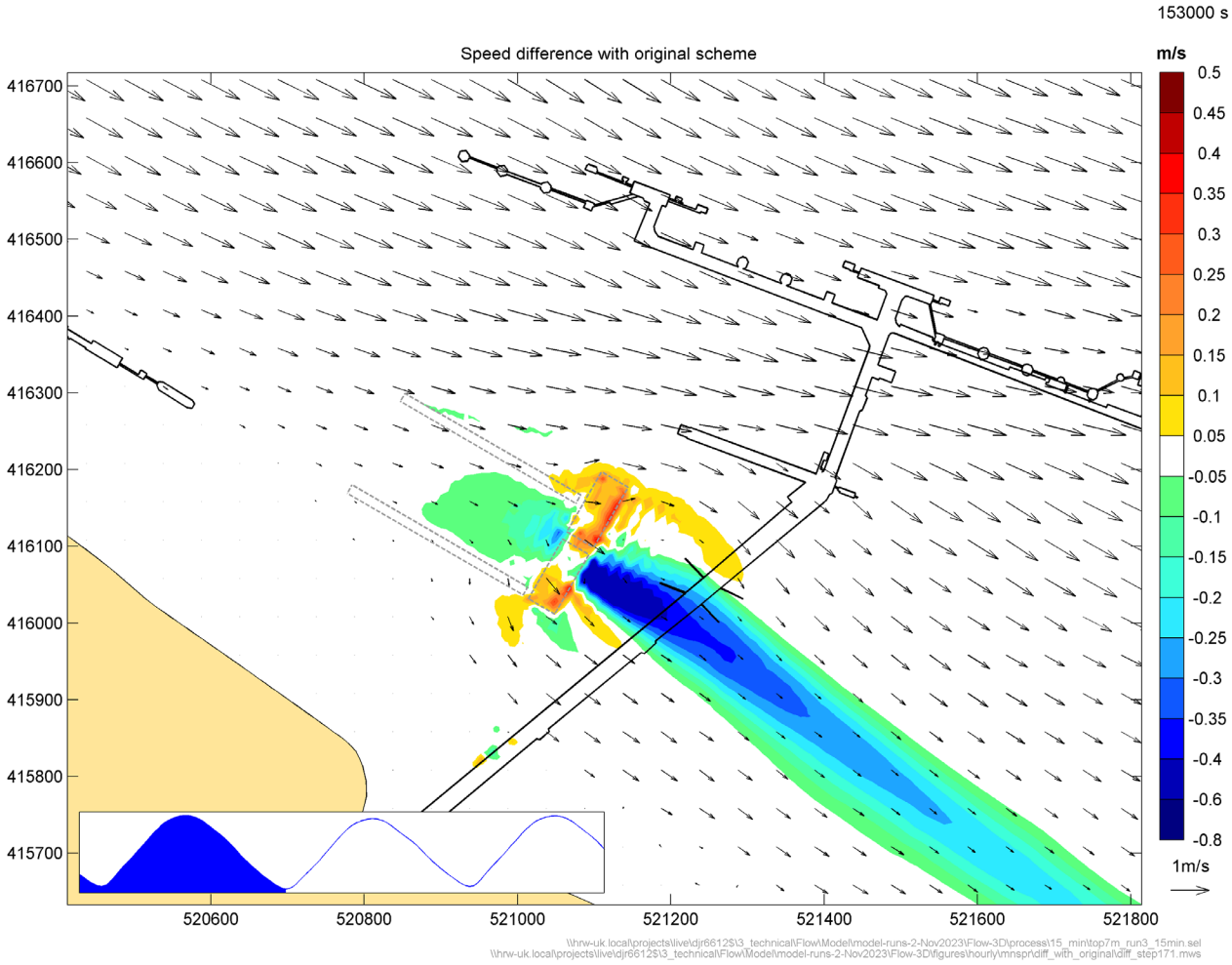

Figure A.14: Difference in current speed between revised and original IERRT layout, LW, mean spring tide

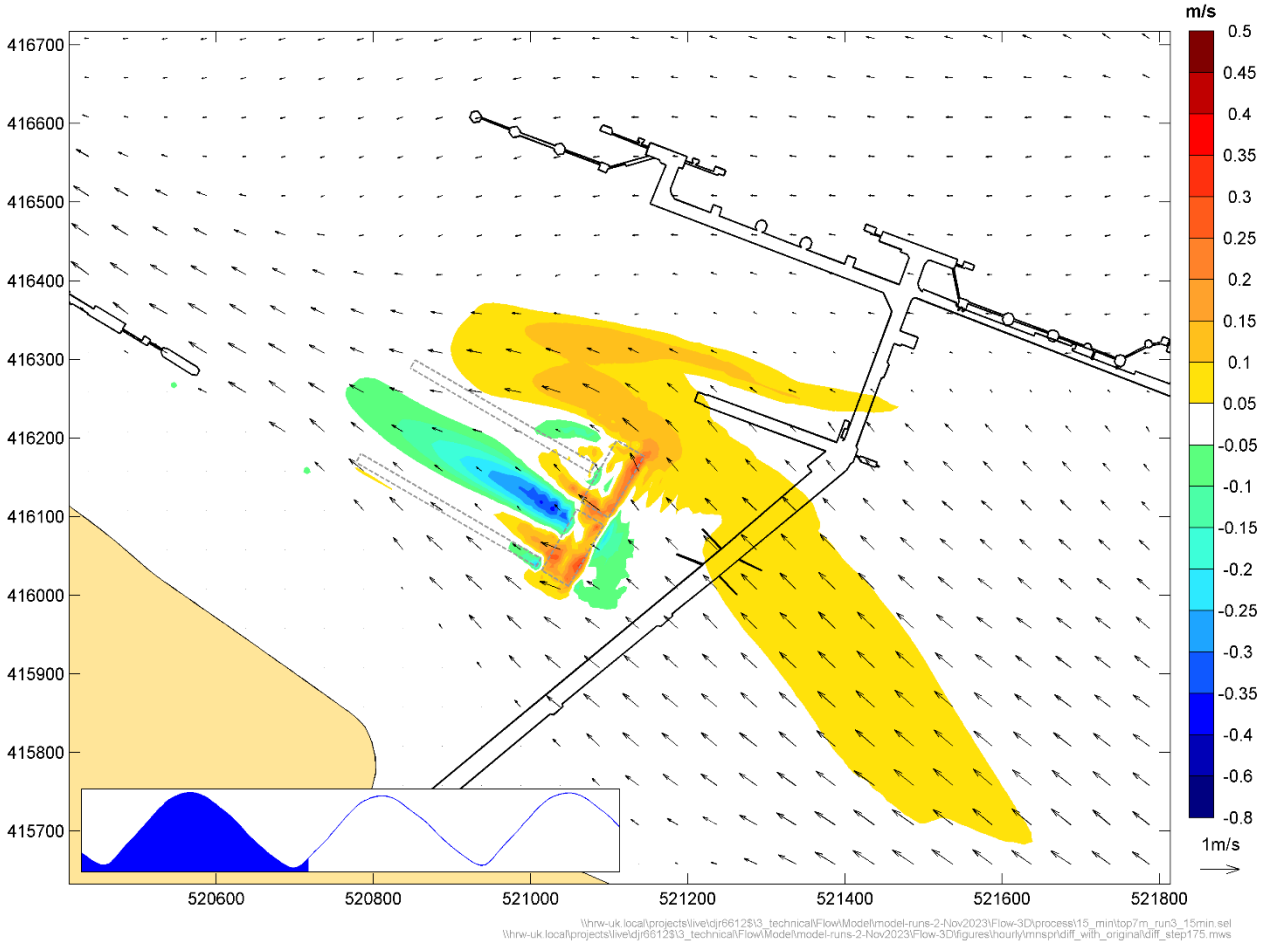

Figure A.15: Difference in current speed between revised and original IERRT layout, LW+1, mean spring tide

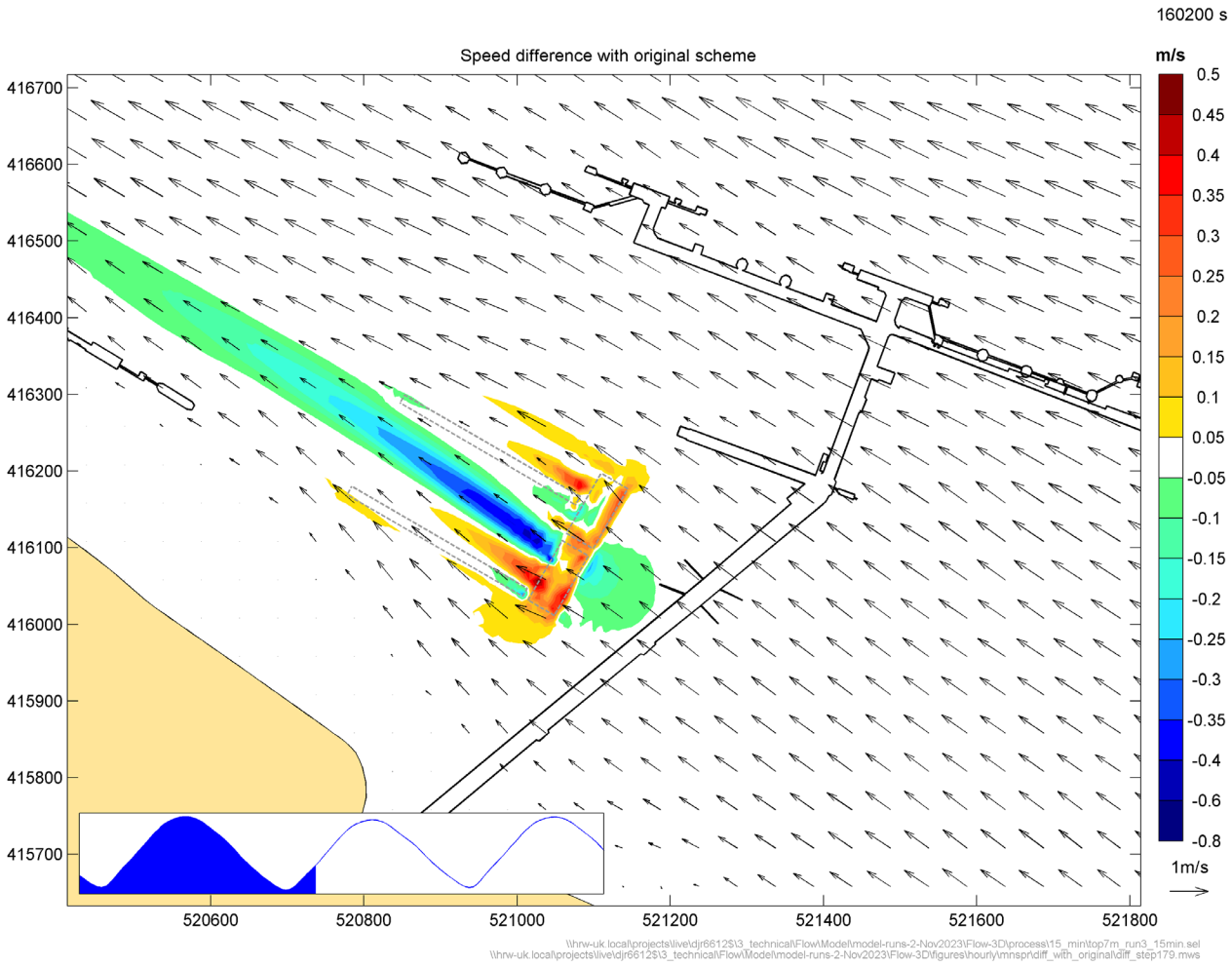

Figure A.16: Difference in current speed between revised and original IERRT layout, LW+2, mean spring tide

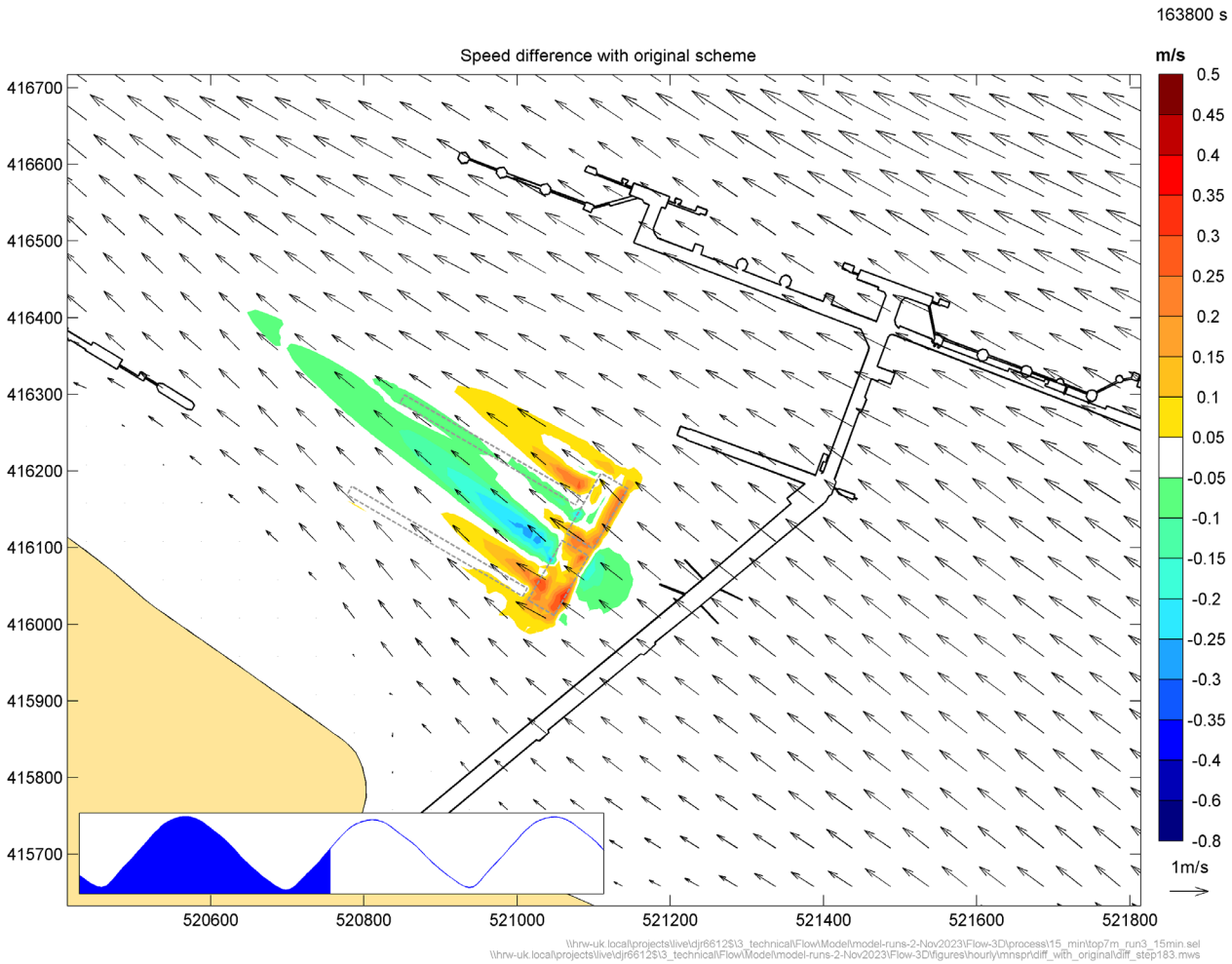

Figure A.17: Difference in current speed between revised and original IERRT layout, LW+3, mean spring tide

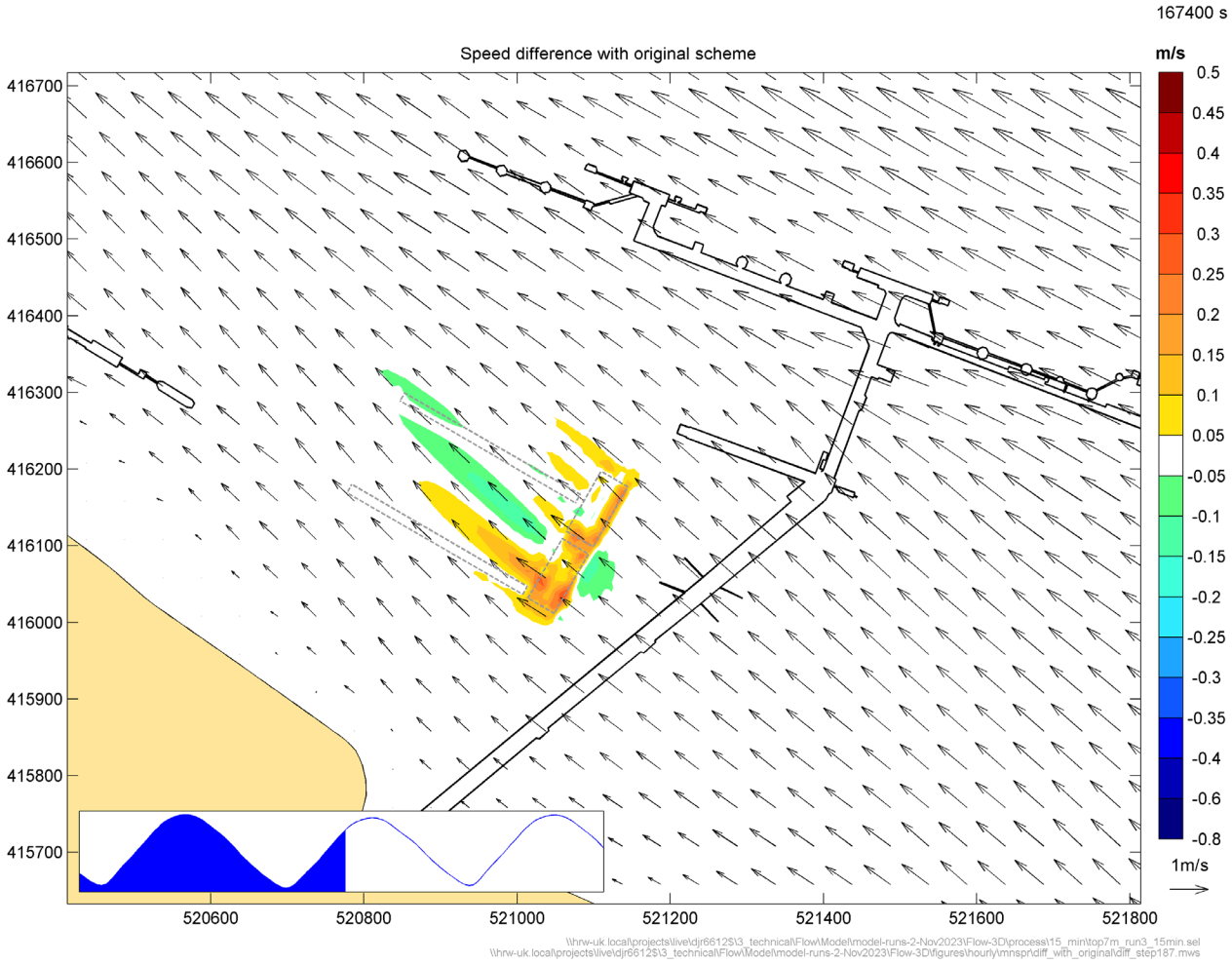

Figure A.18: Difference in current speed between revised and original IERRT layout, LW+4, mean spring tide

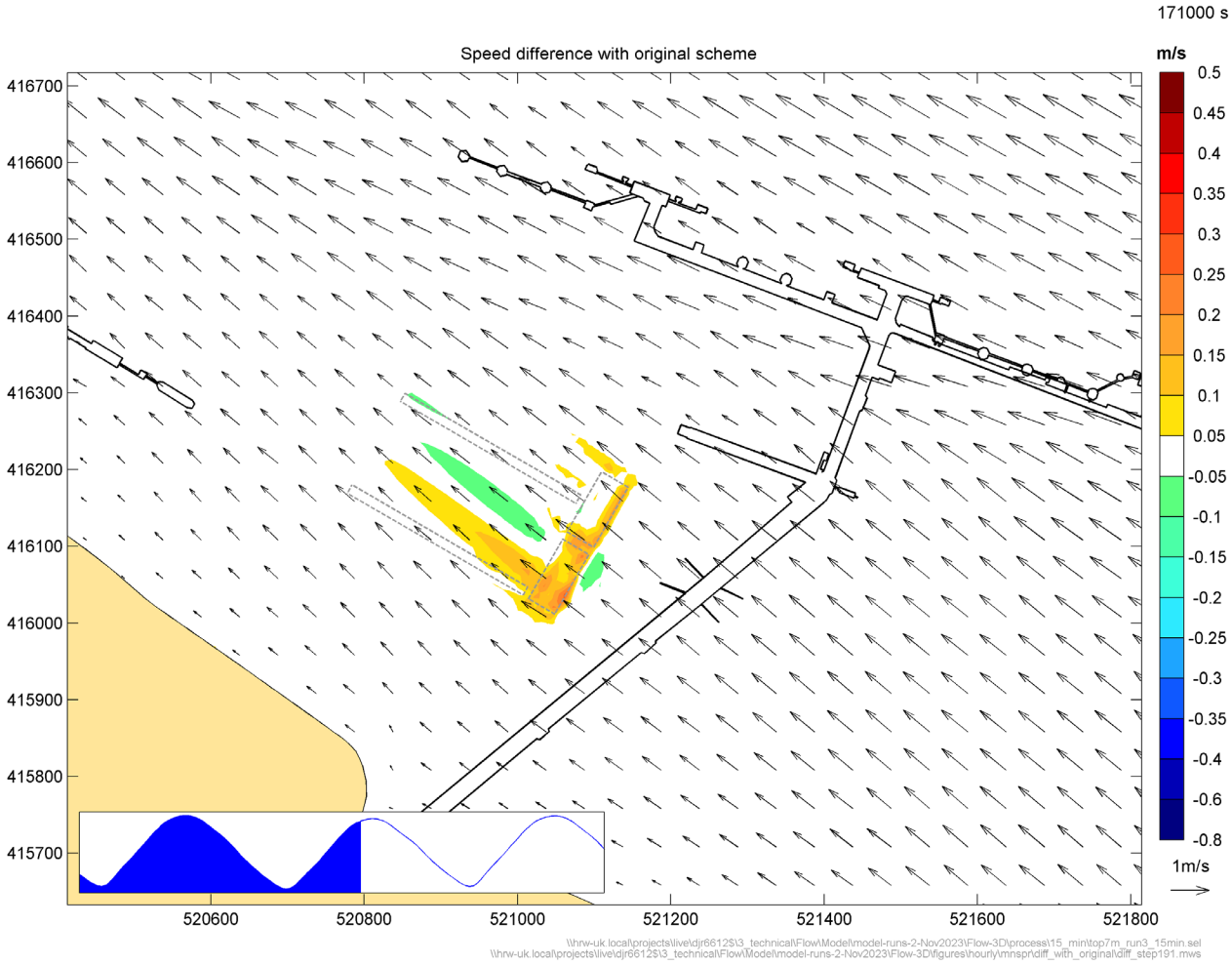

Figure A.19: Difference in current speed between revised and original IERRT layout, LW+5, mean spring tide

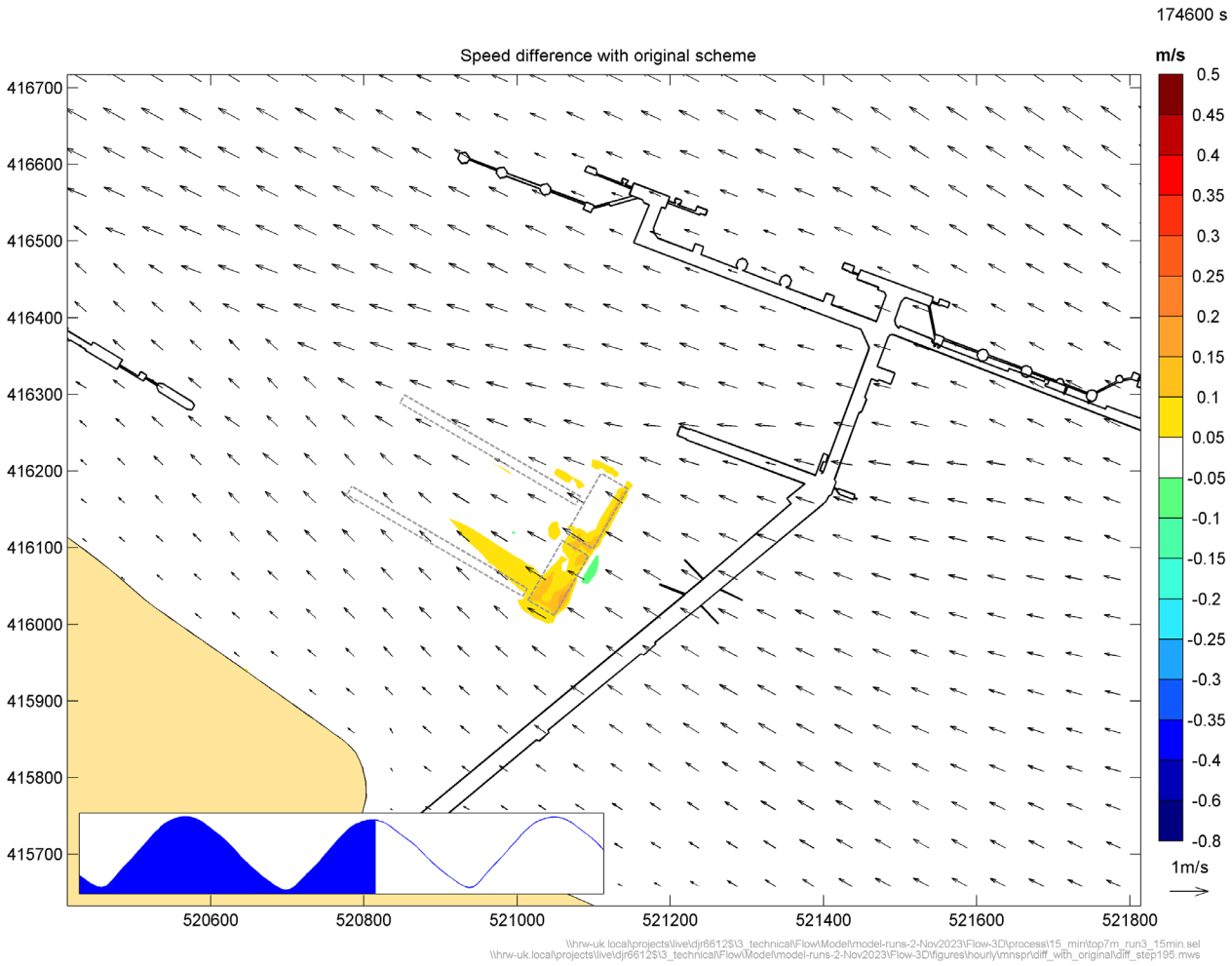

Figure A.20: Difference in current speed between revised and original IERRT layout, LW+6, mean spring tide

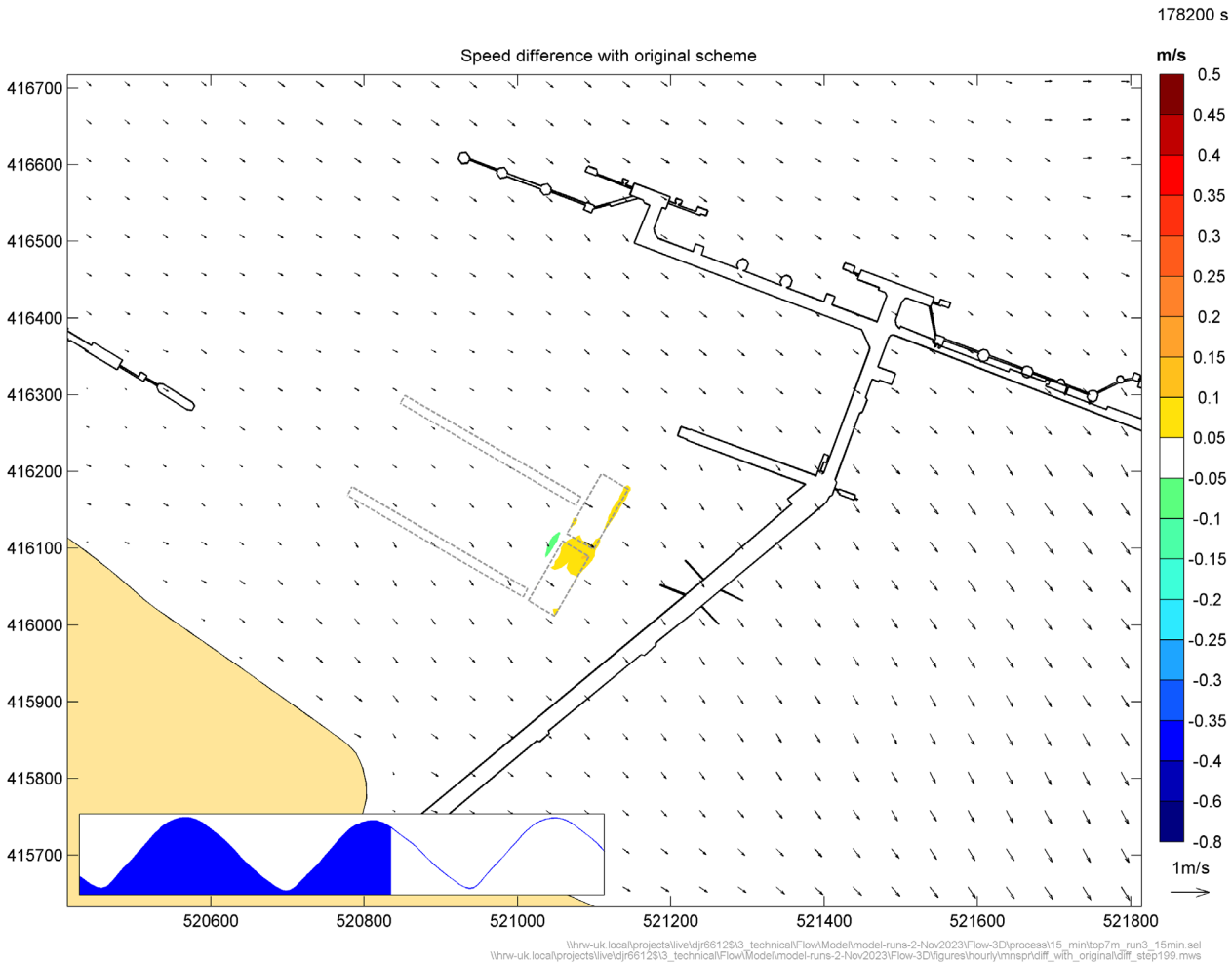

Figure A.21: Difference in current speed between revised and original IERRT layout, LW+7, mean spring tide

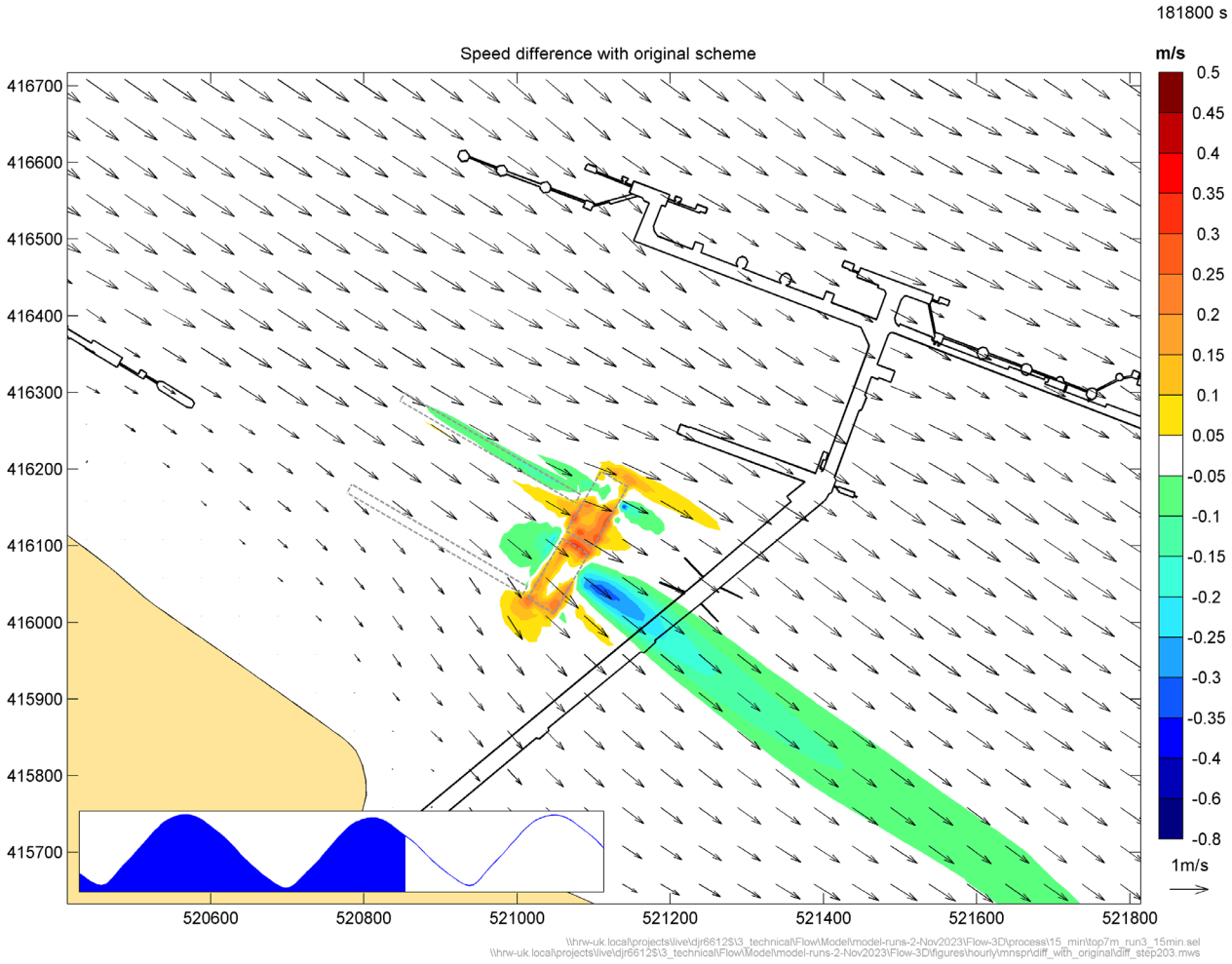

Figure A.22: Difference in current speed between revised and original IERRT layout, LW+8, mean spring tide

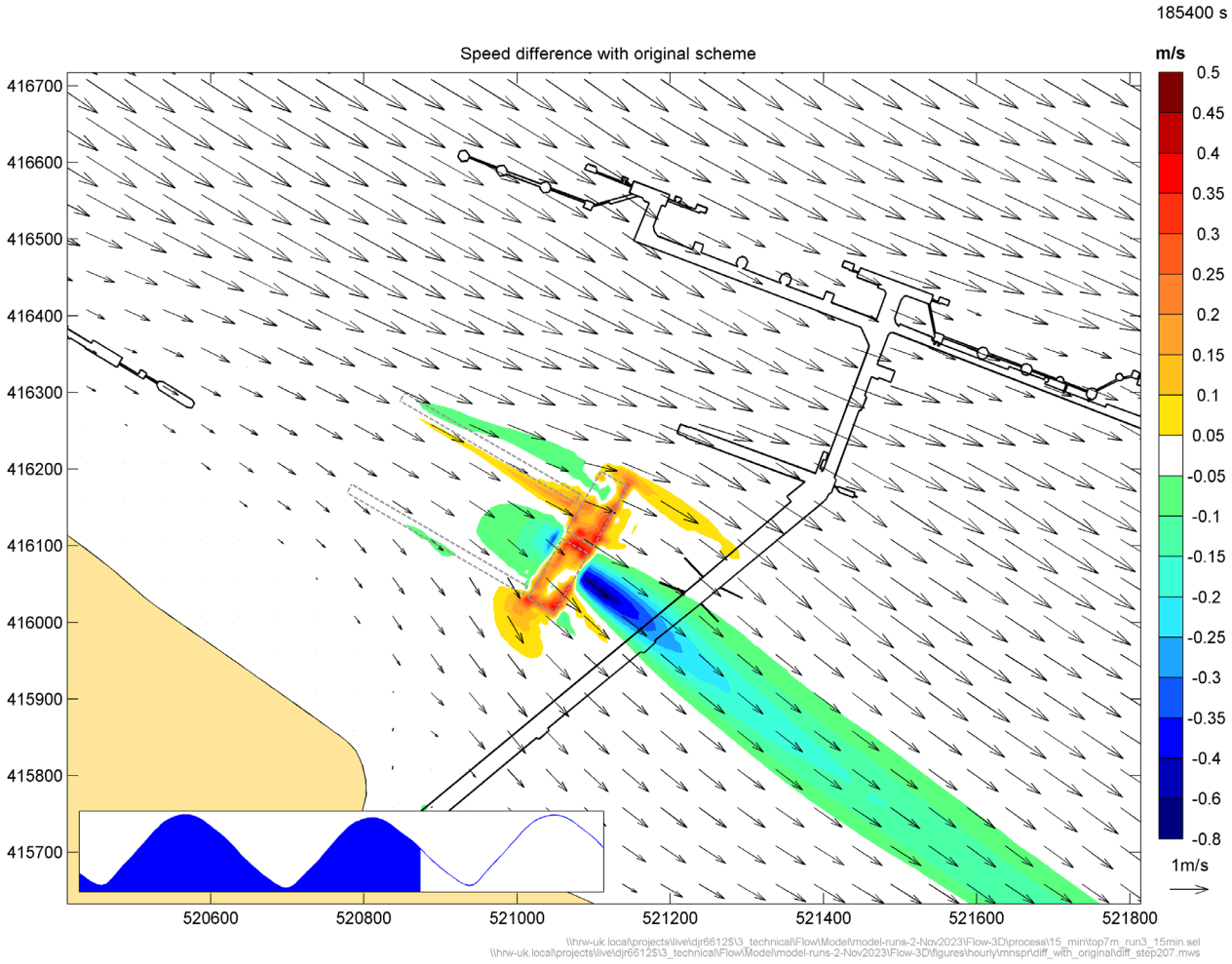

Figure A.23: Difference in current speed between revised and original IERRT layout, LW+9, mean spring tide

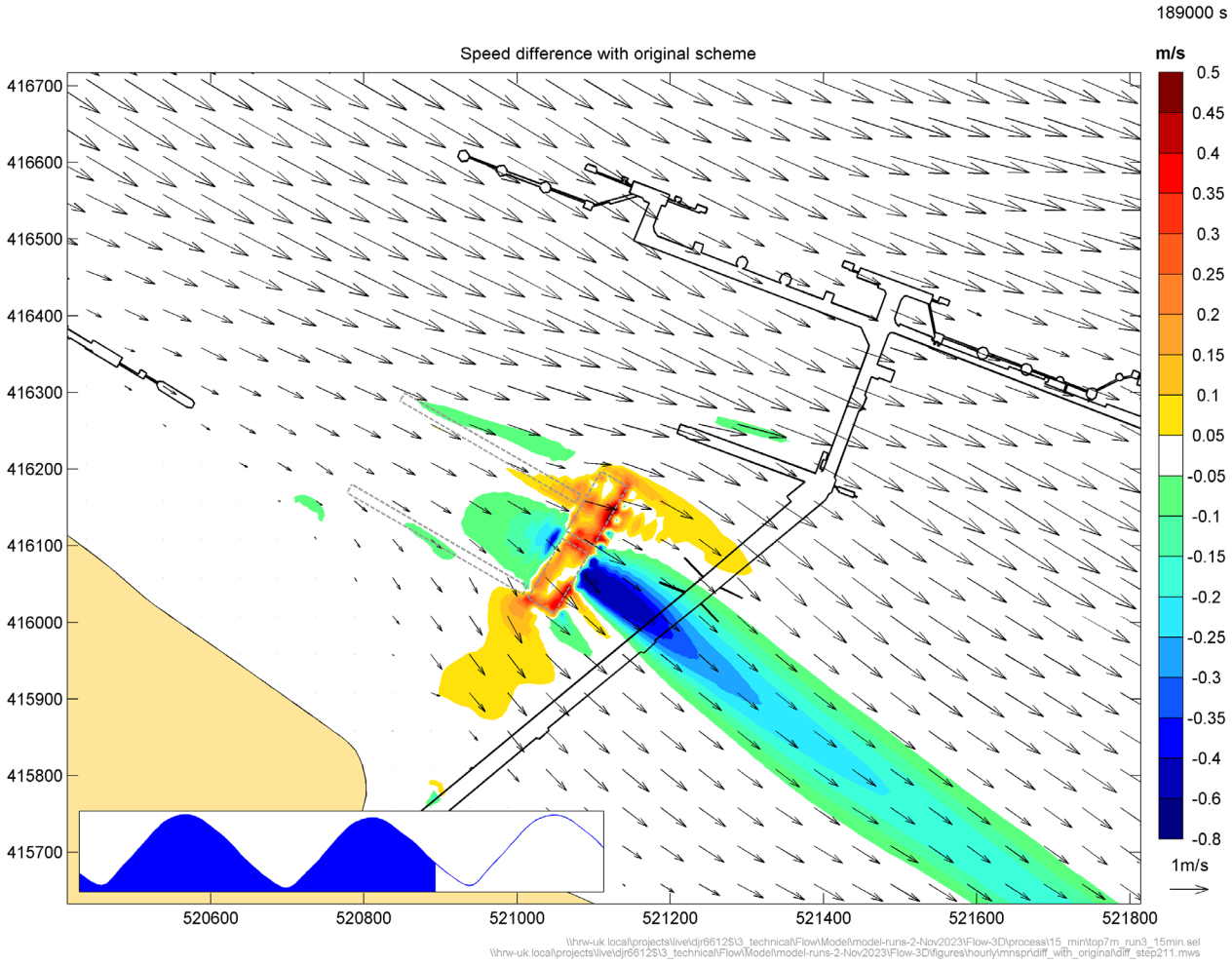

Figure A.24: Difference in current speed between revised and original IERRT layout, LW+10, mean spring tide

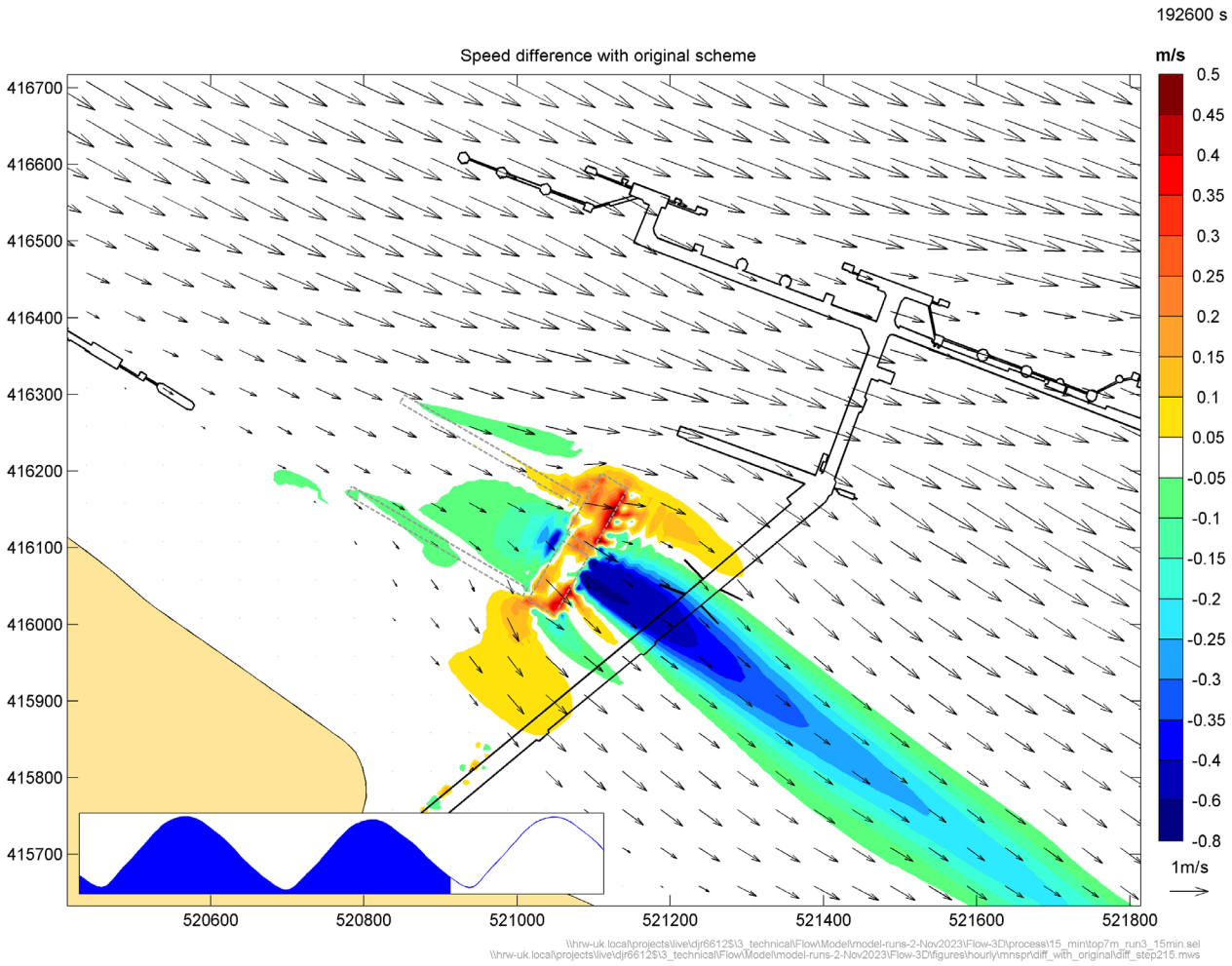

Figure A.25: Difference in current speed between revised and original IERRT layout, LW+11, mean spring tide

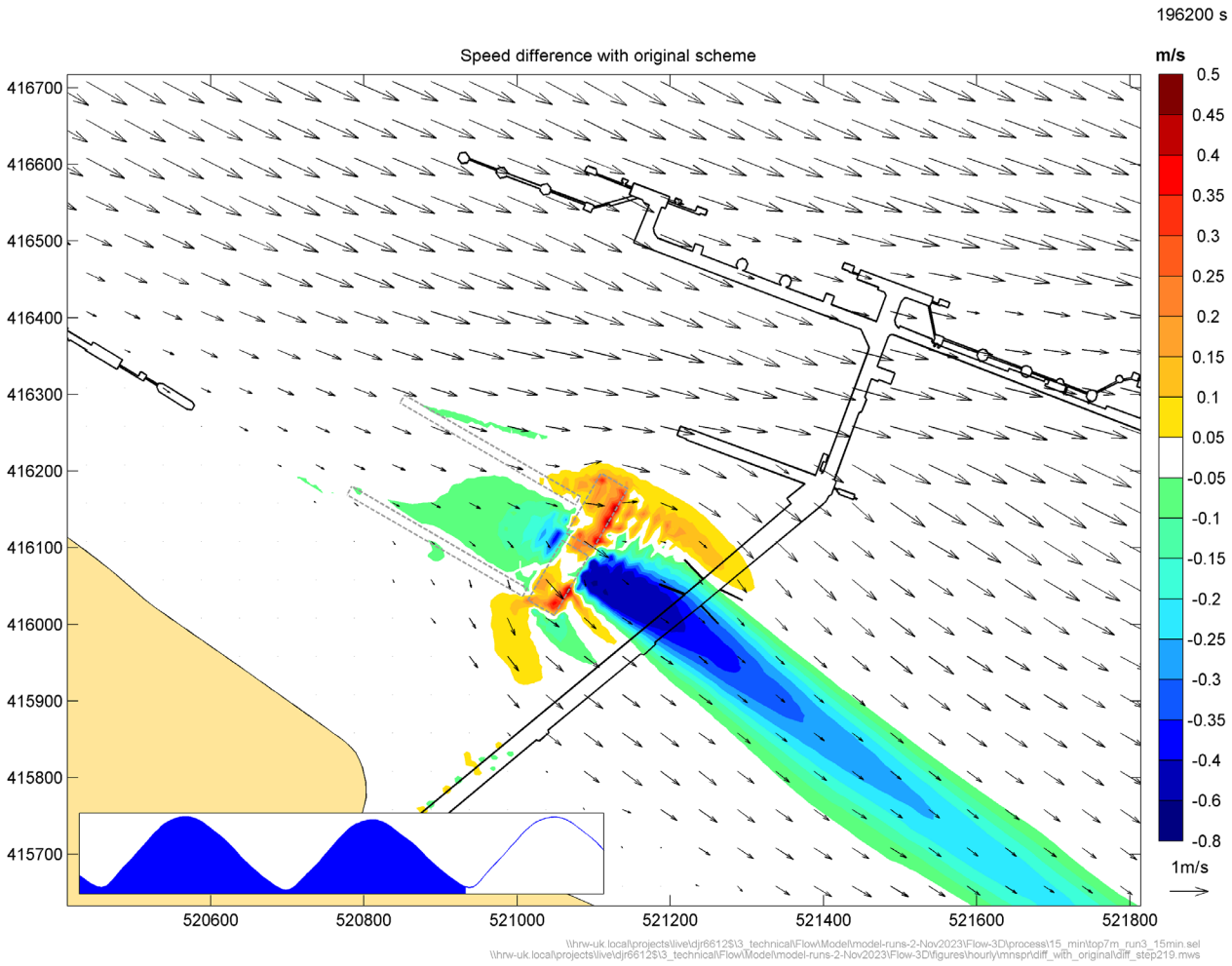

Figure A.26: Difference in current speed between revised and original IERRT layout, LW+12, mean spring tide

B Hourly comparison of currents for revised and original IERRT layouts

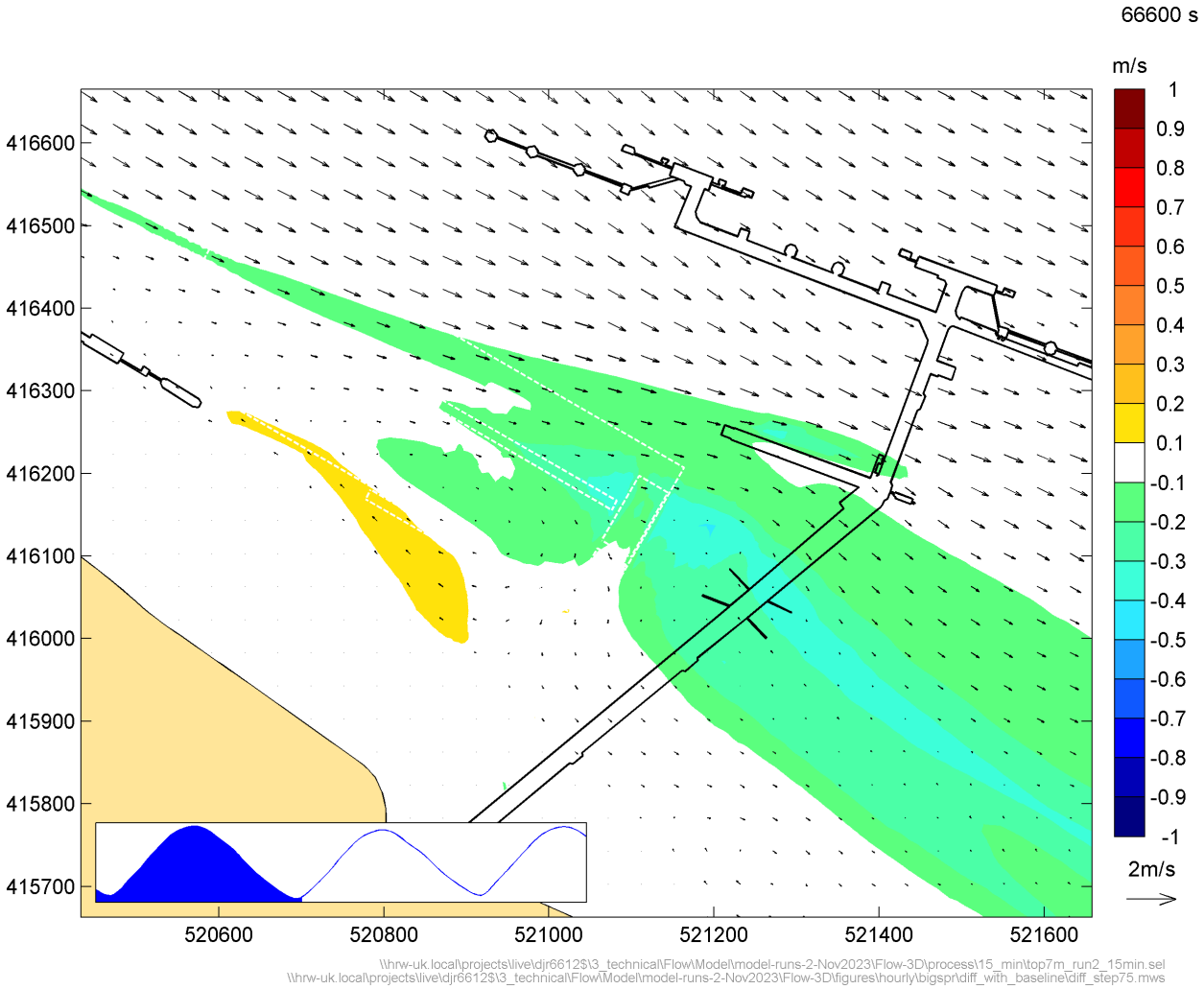

Figure B.1: Difference in current speed between revised IERRT and baseline conditions, LW+0, peak spring tide

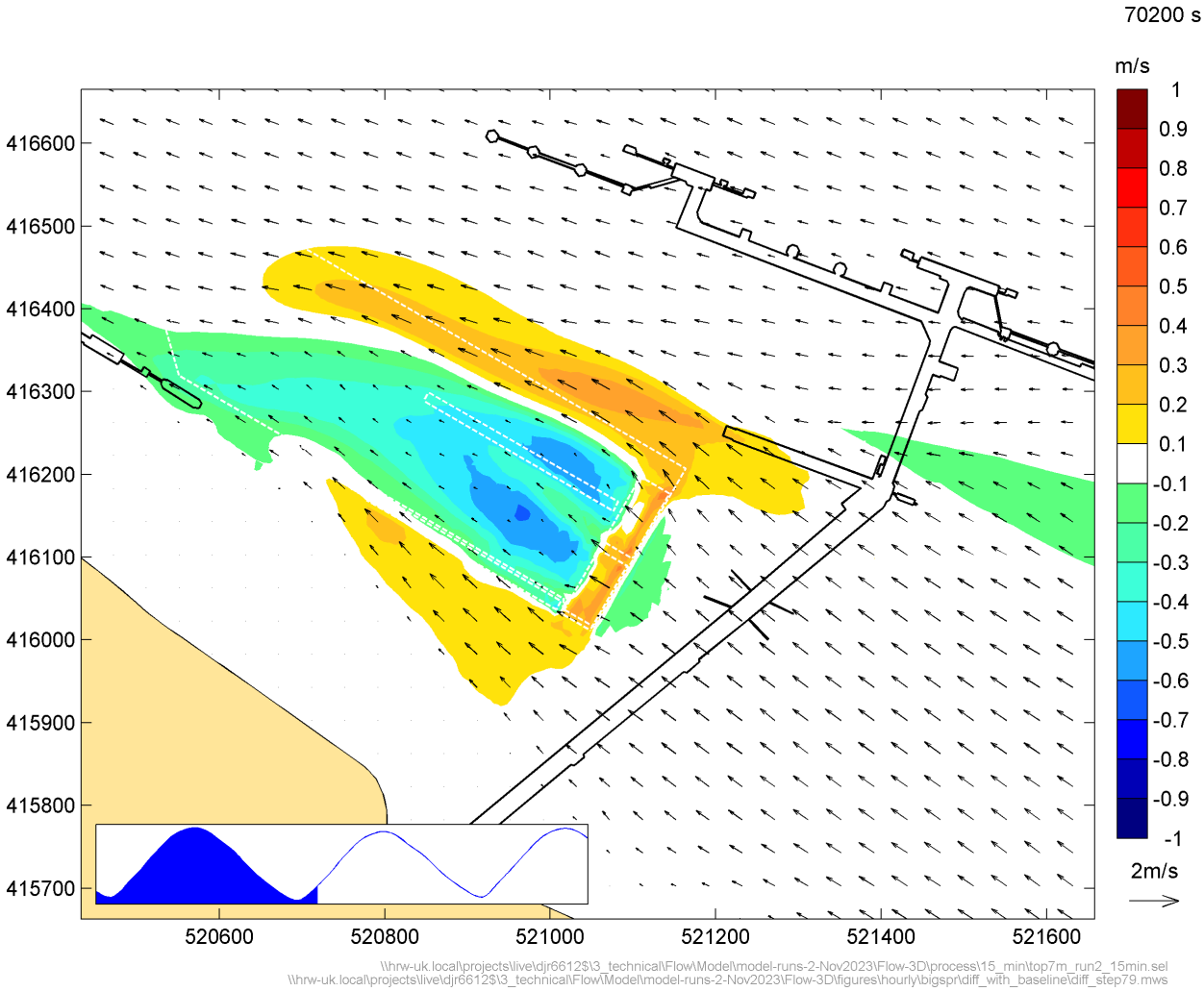

Figure B.2: Difference in current speed between revised IERRT and baseline conditions, LW+1, peak spring tide

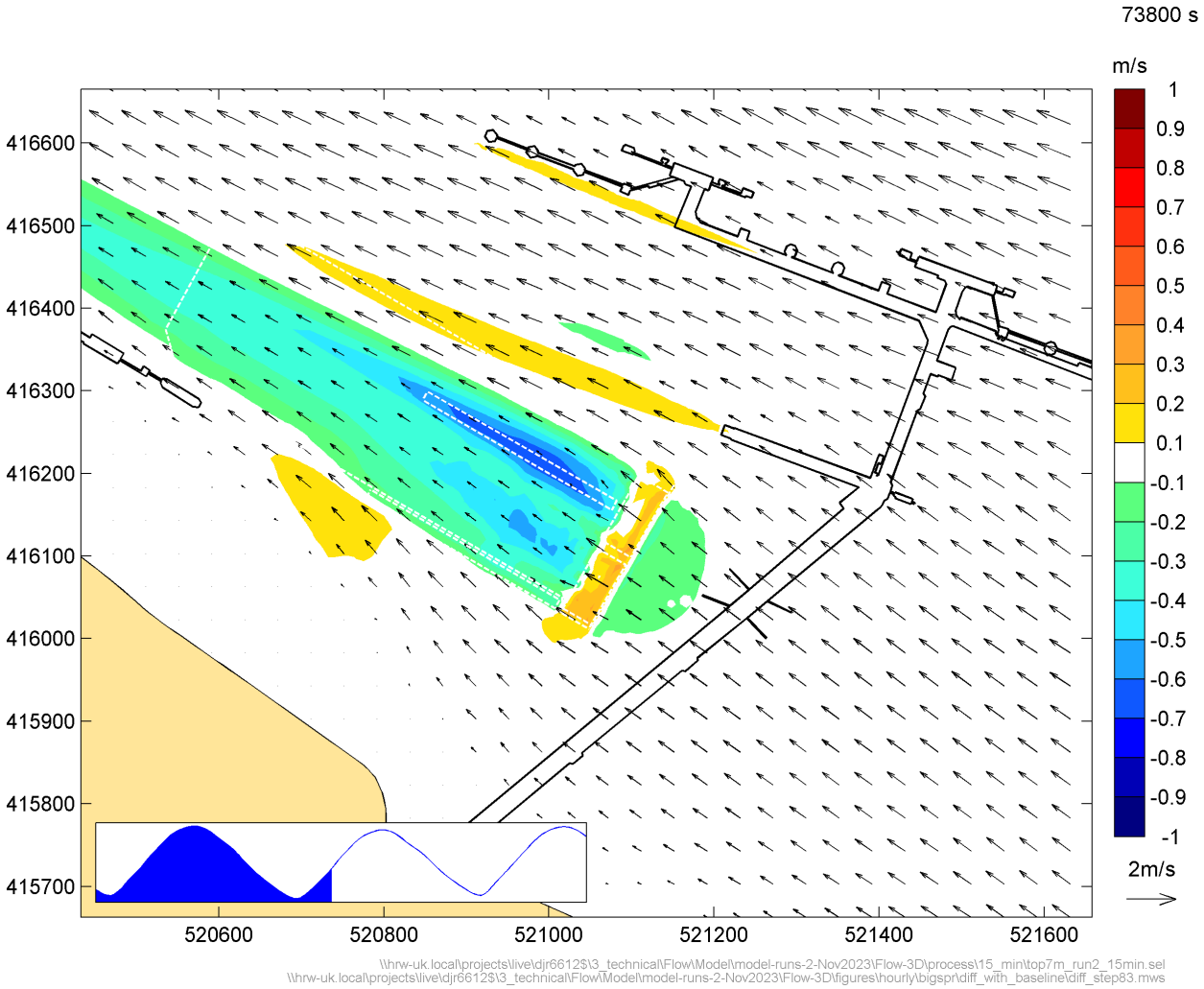

Figure B.3: Difference in current speed between revised IERRT and baseline conditions, LW+2, peak spring tide

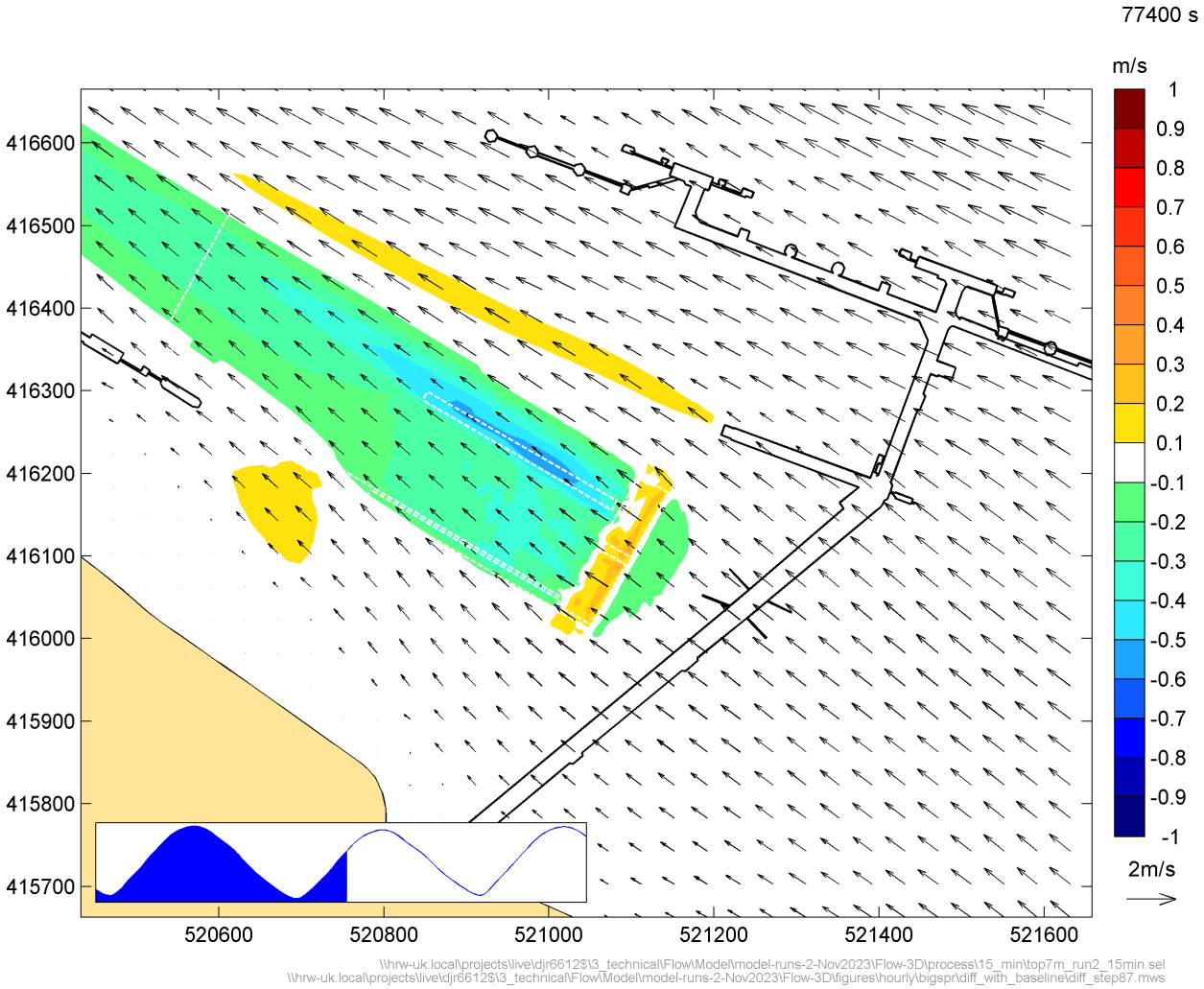

Figure B.4: Difference in current speed between revised IERRT and baseline conditions, LW+3, peak spring tide

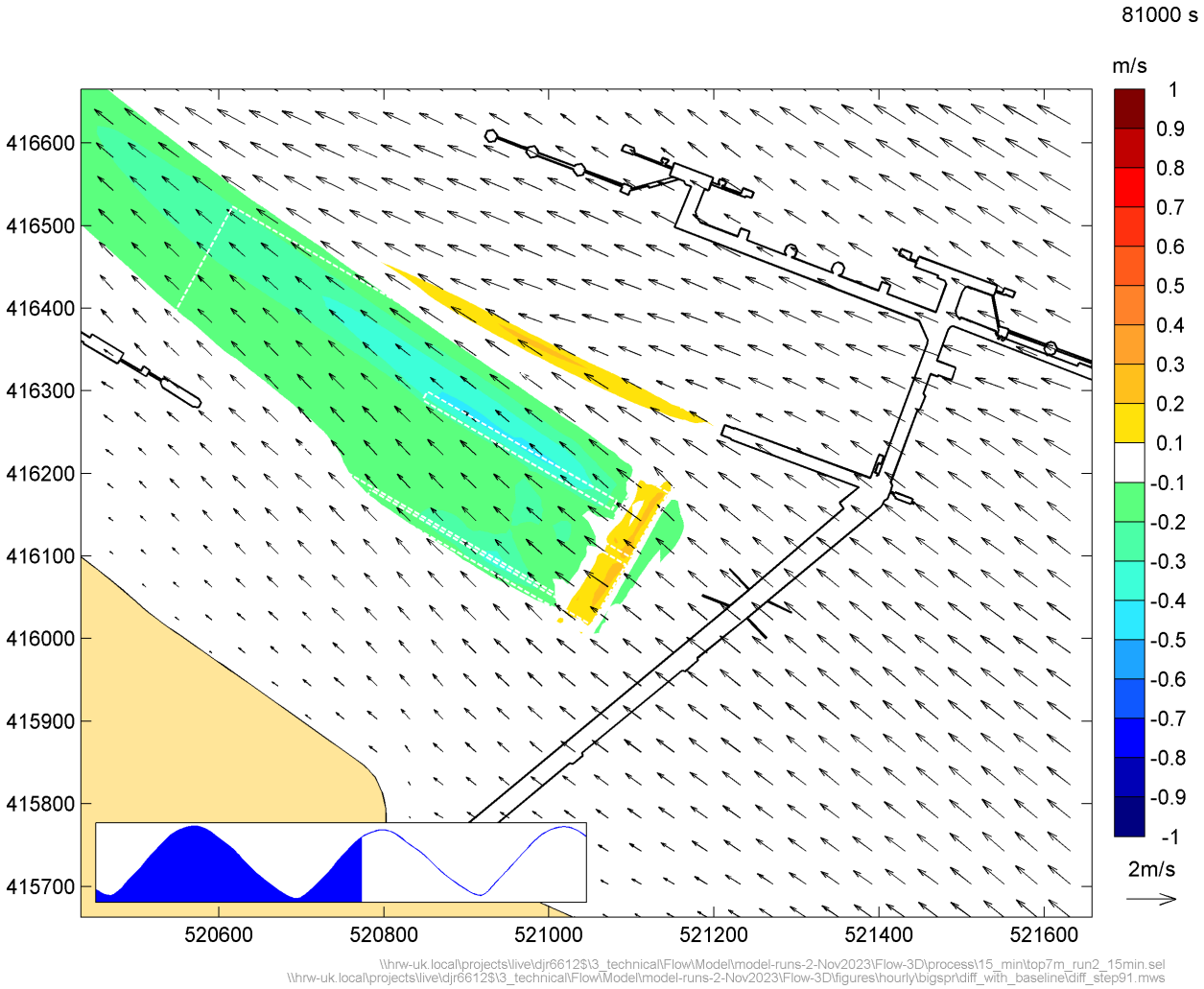

Figure B.5: Difference in current speed between revised IERRT and baseline conditions, LW+4, peak spring tide

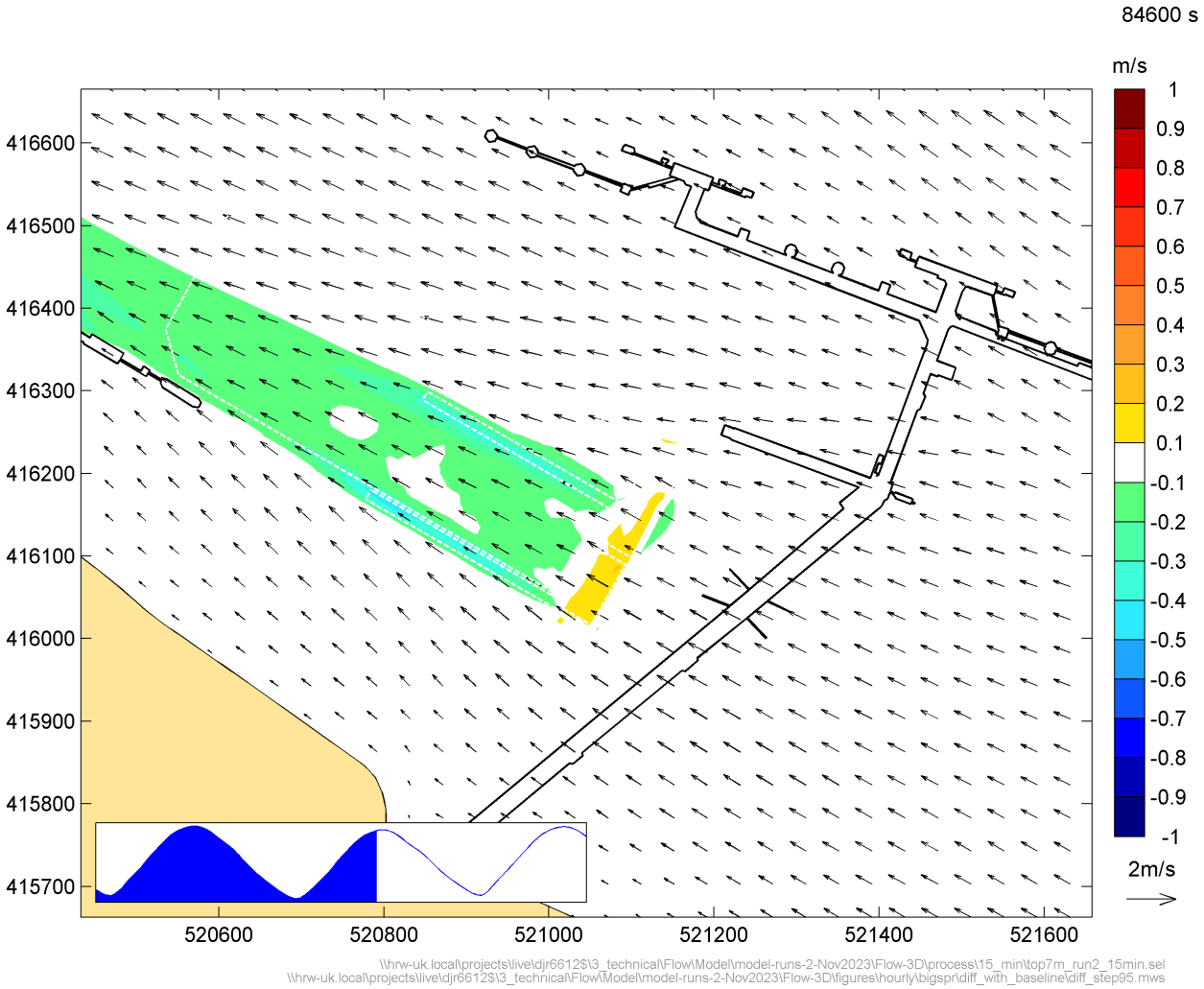

Figure B.6: Difference in current speed between revised IERRT and baseline conditions, LW+5, peak spring tide

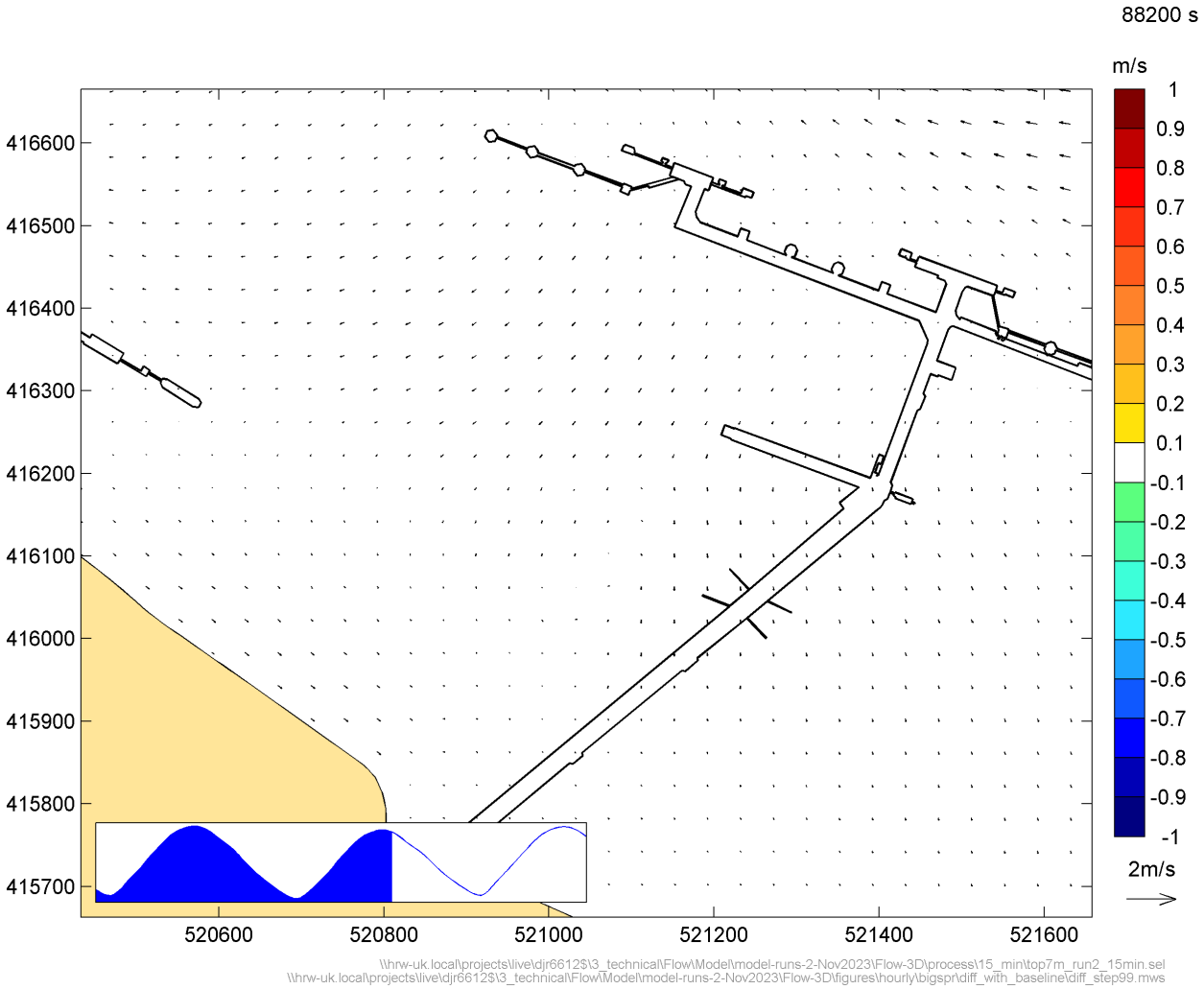

Figure B.7: Difference in current speed between revised IERRT and baseline conditions, LW+6, peak spring tide

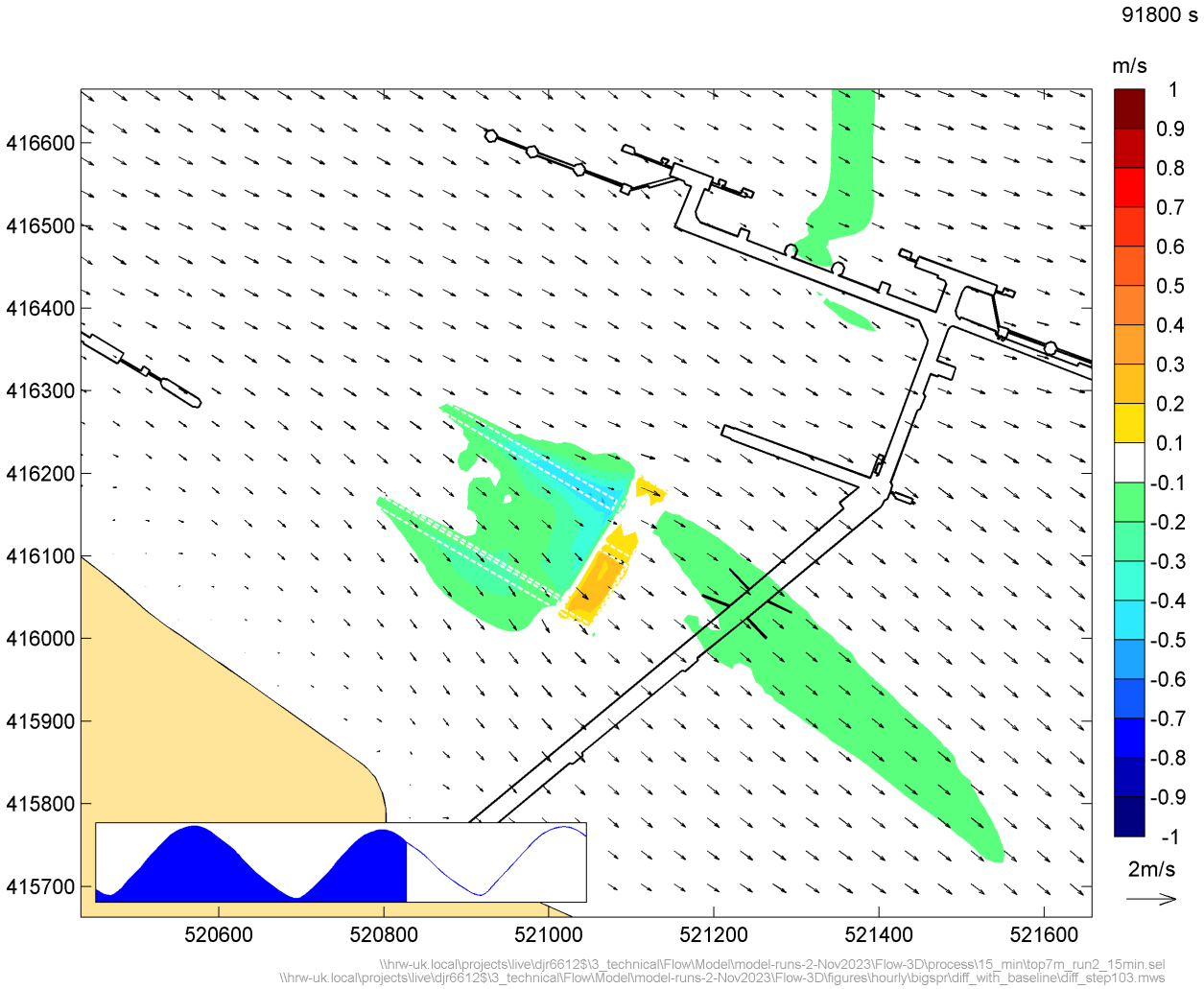

Figure B.8: Difference in current speed between revised IERRT and baseline conditions, LW+7, peak spring tide

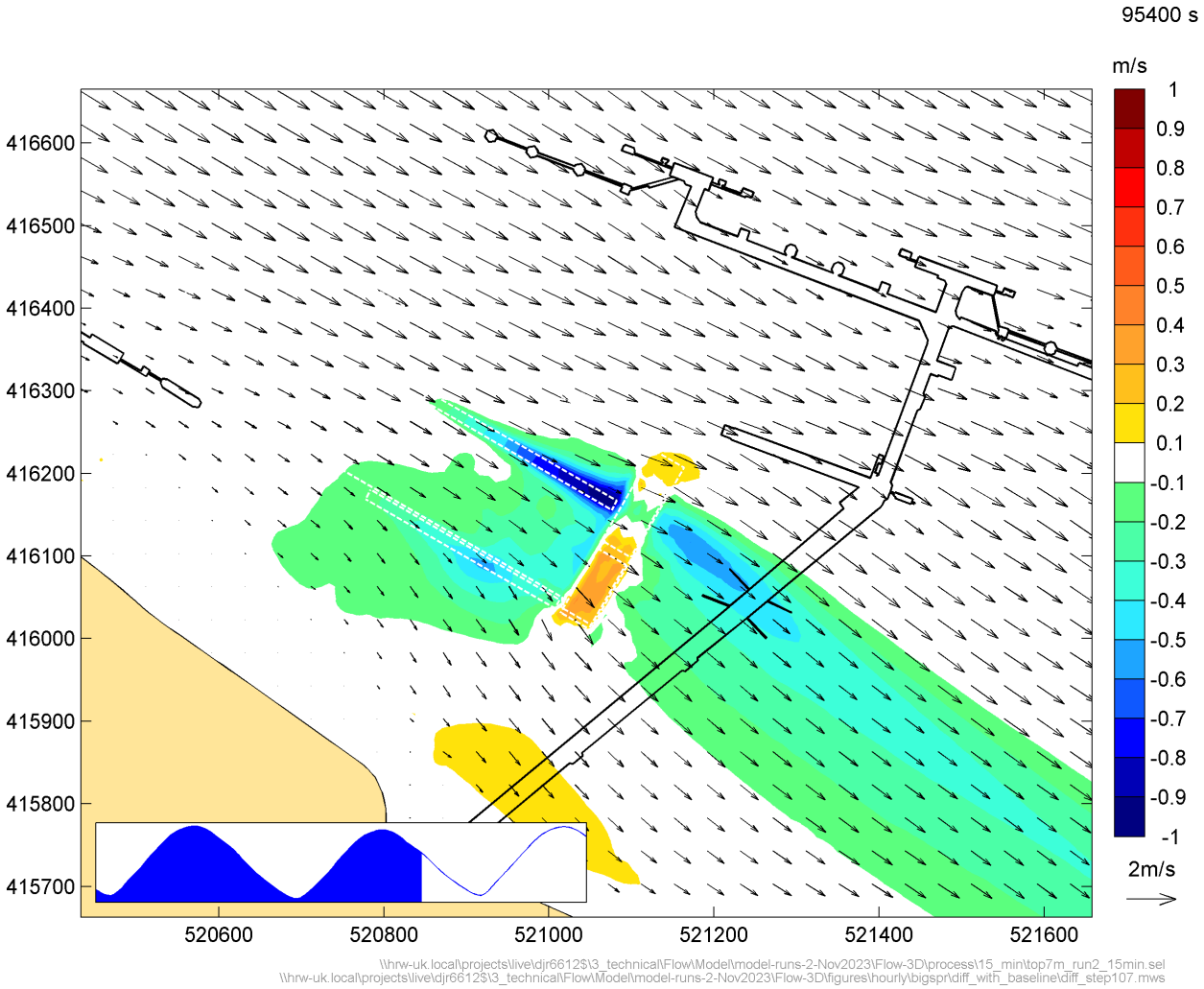

Figure B.9: Difference in current speed between revised IERRT and baseline conditions, LW+8, peak spring tide

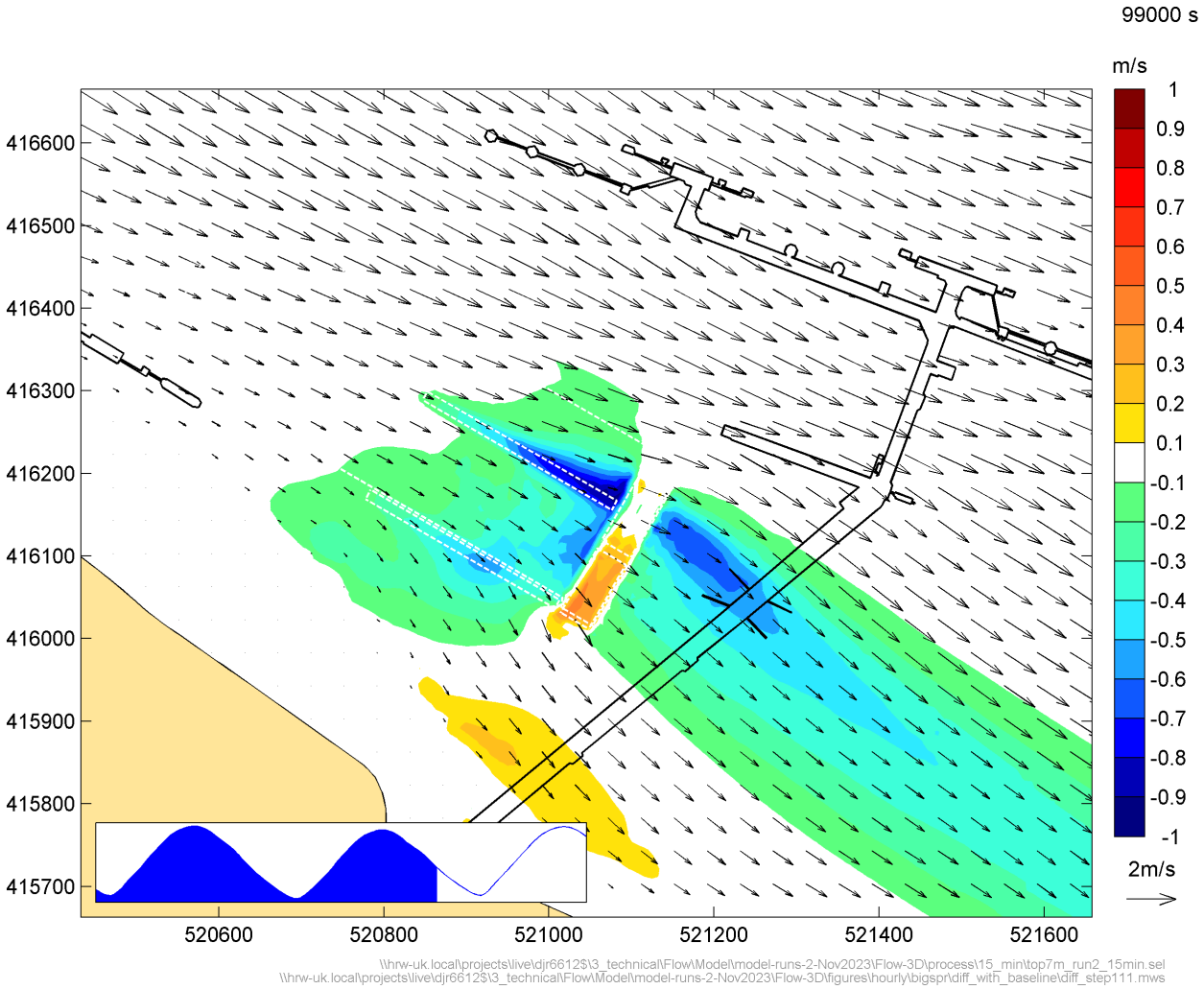

Figure B.10: Difference in current speed between revised IERRT and baseline conditions, LW+9, peak spring tide

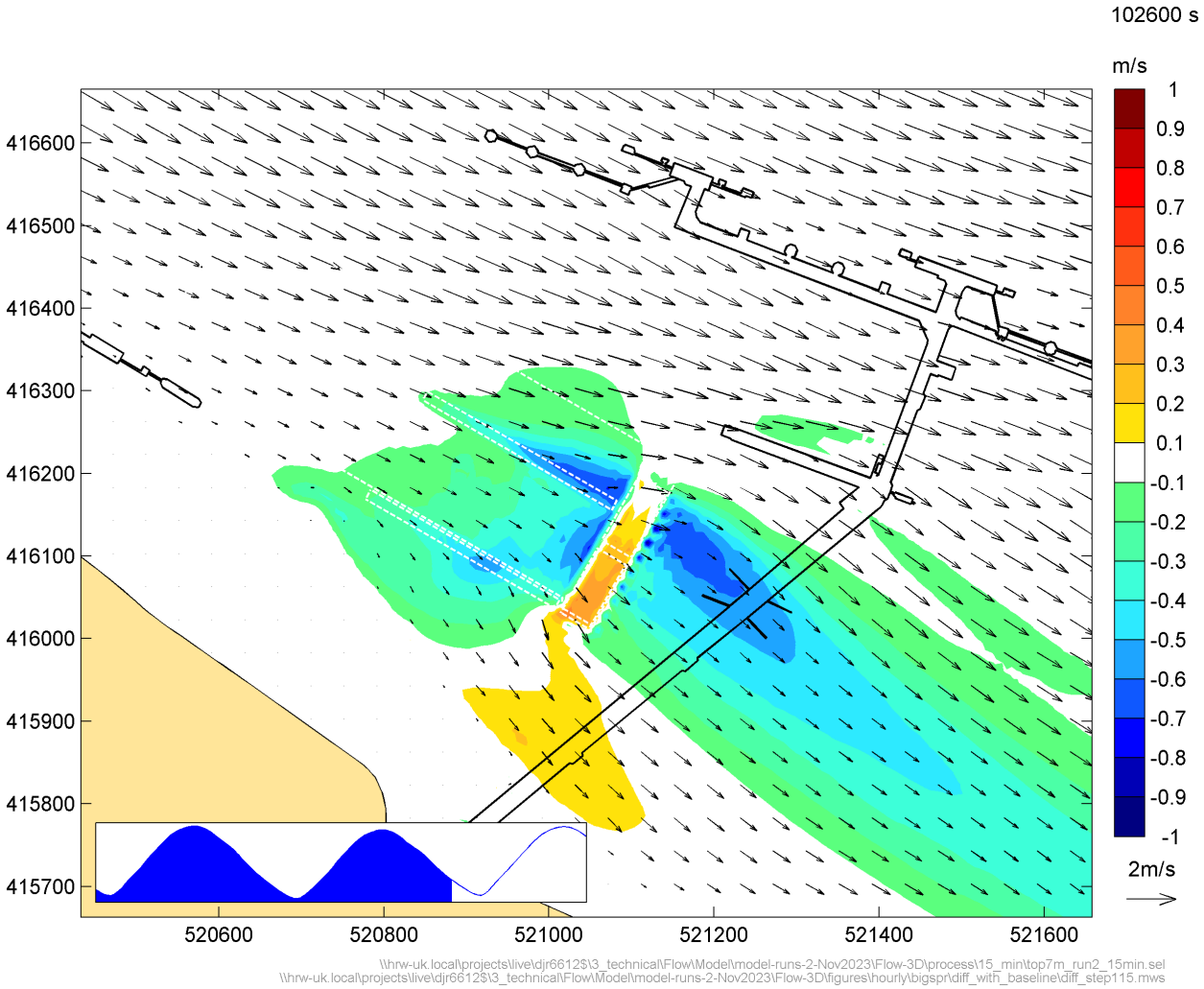

Figure B.11: Difference in current speed between revised IERRT and baseline conditions, LW+10, peak spring tide

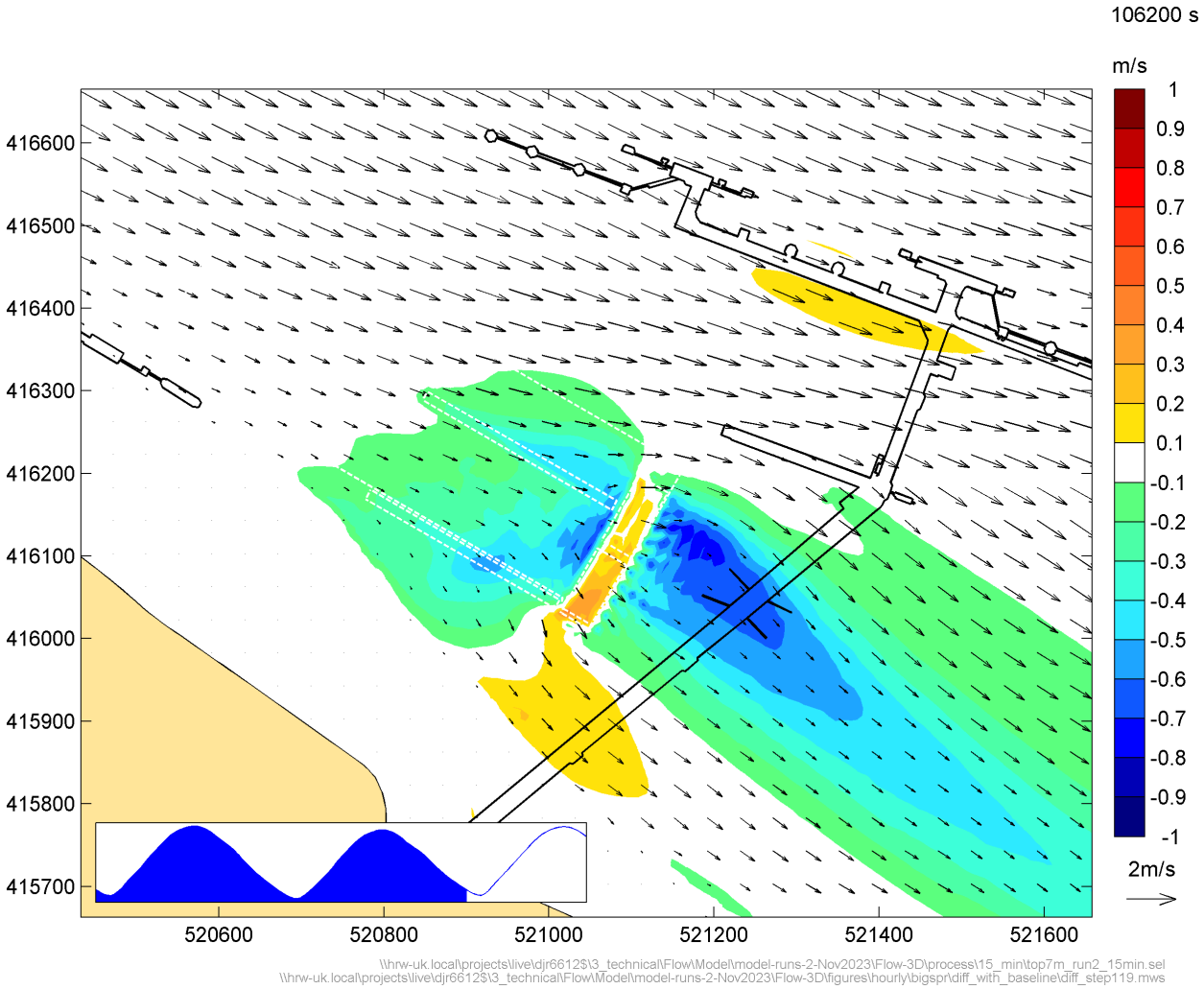

Figure B.12: Difference in current speed between revised IERRT and baseline conditions, LW+11, peak spring tide

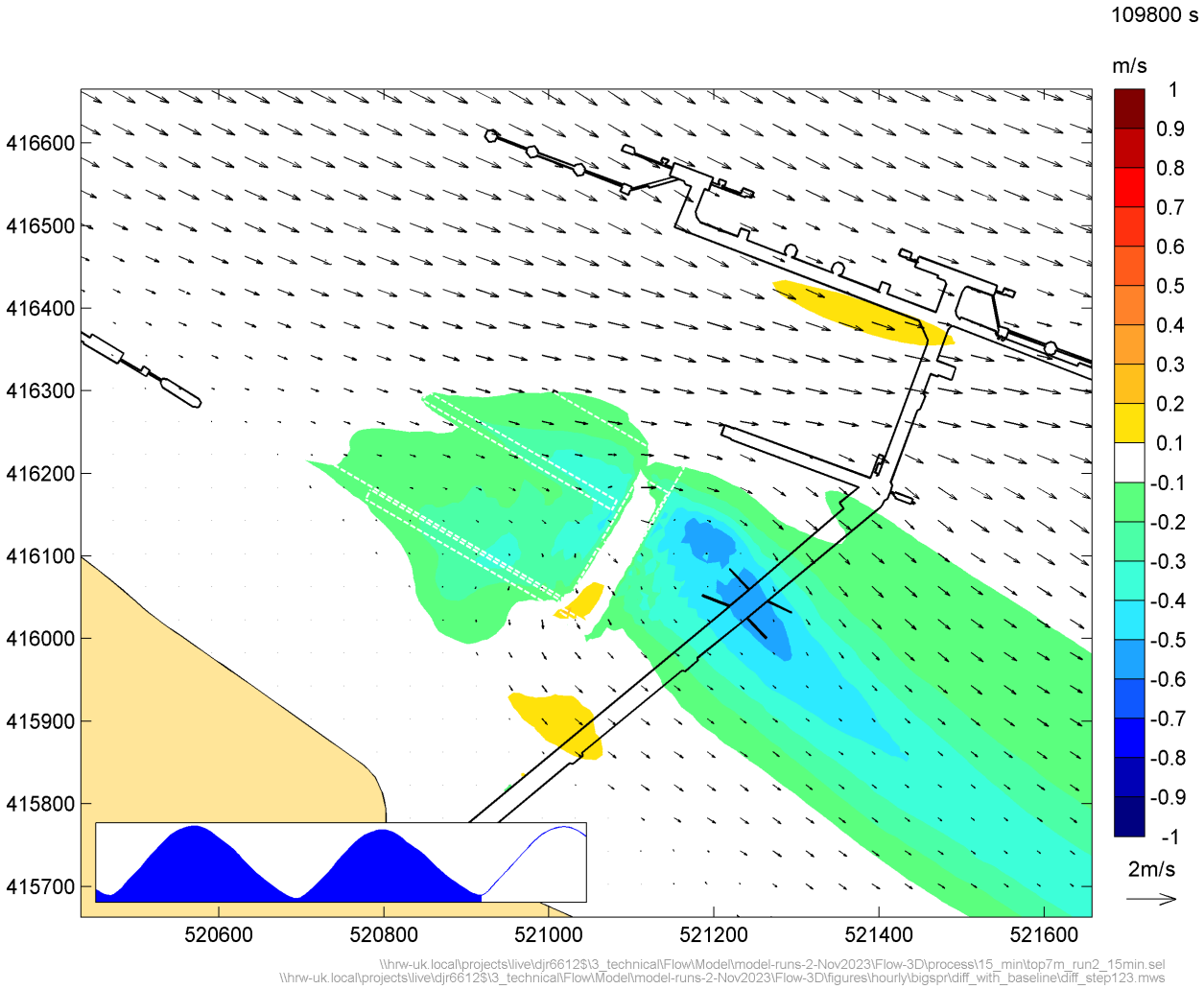

Figure B.13: Difference in current speed between revised IERRT and baseline conditions, LW+12, peak spring tide

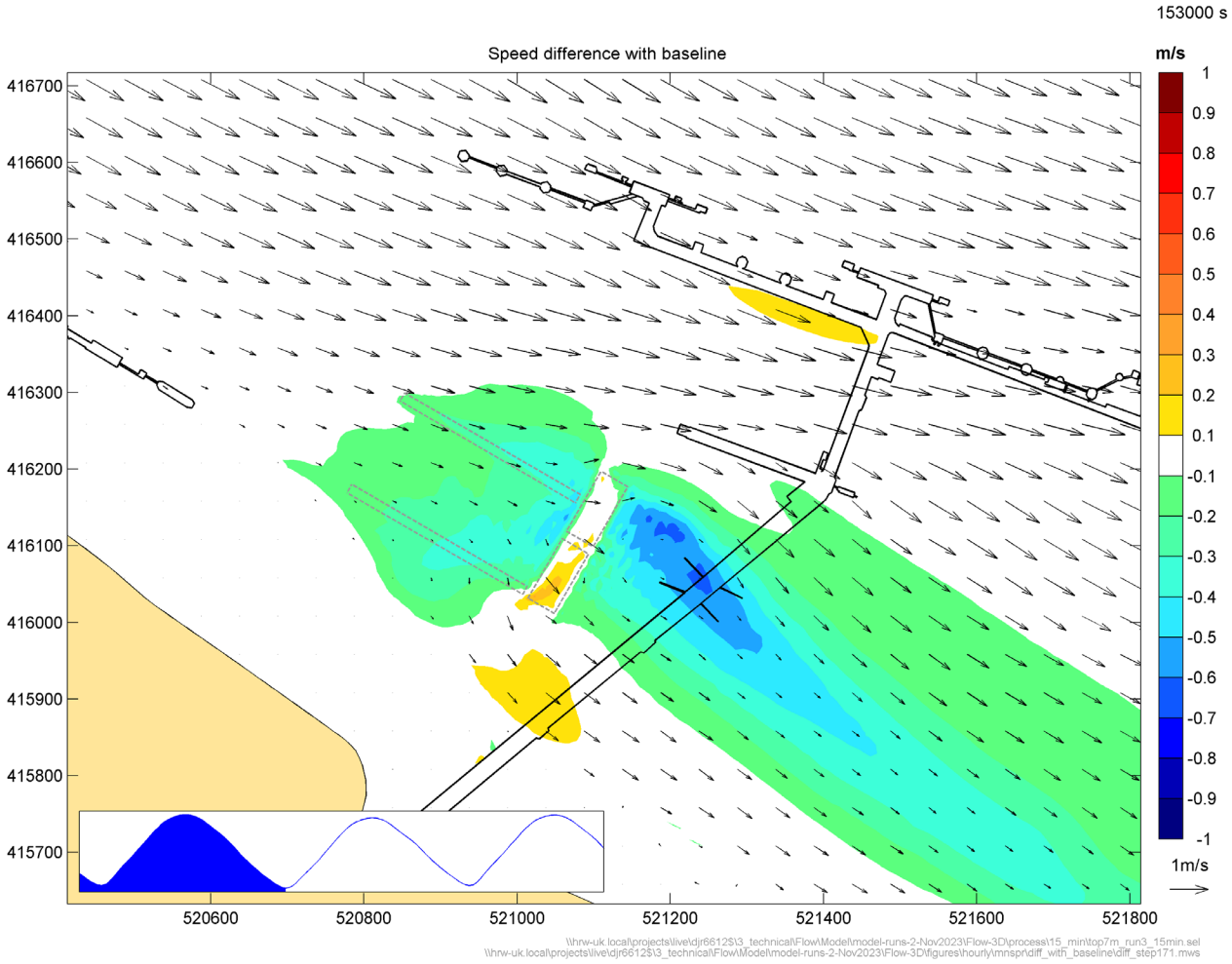

Figure B.14: Difference in current speed between revised IERRT and baseline conditions, LW+0, peak spring tide

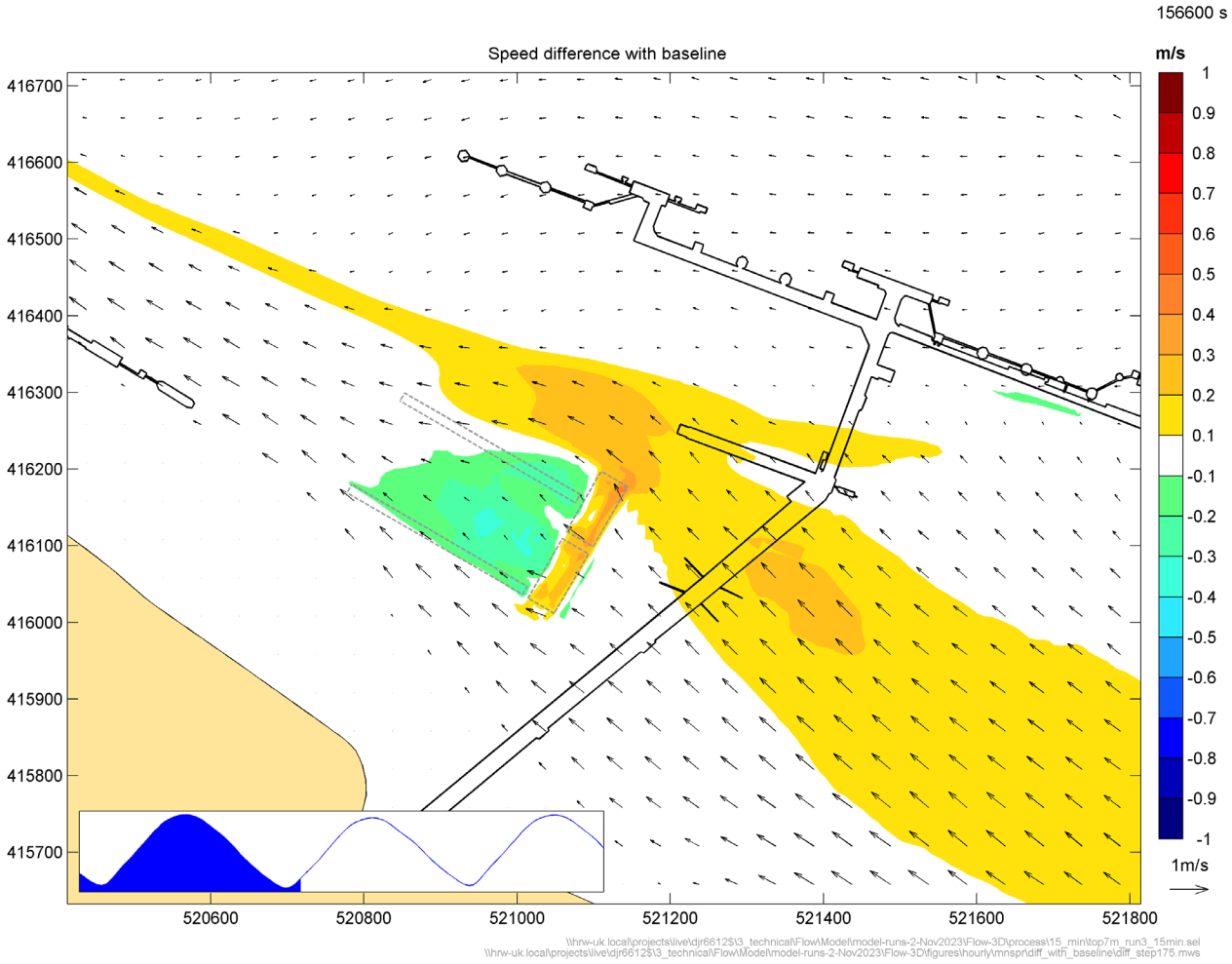

Figure B.15: Difference in current speed between revised IERRT and baseline conditions, LW+1, mean spring tide

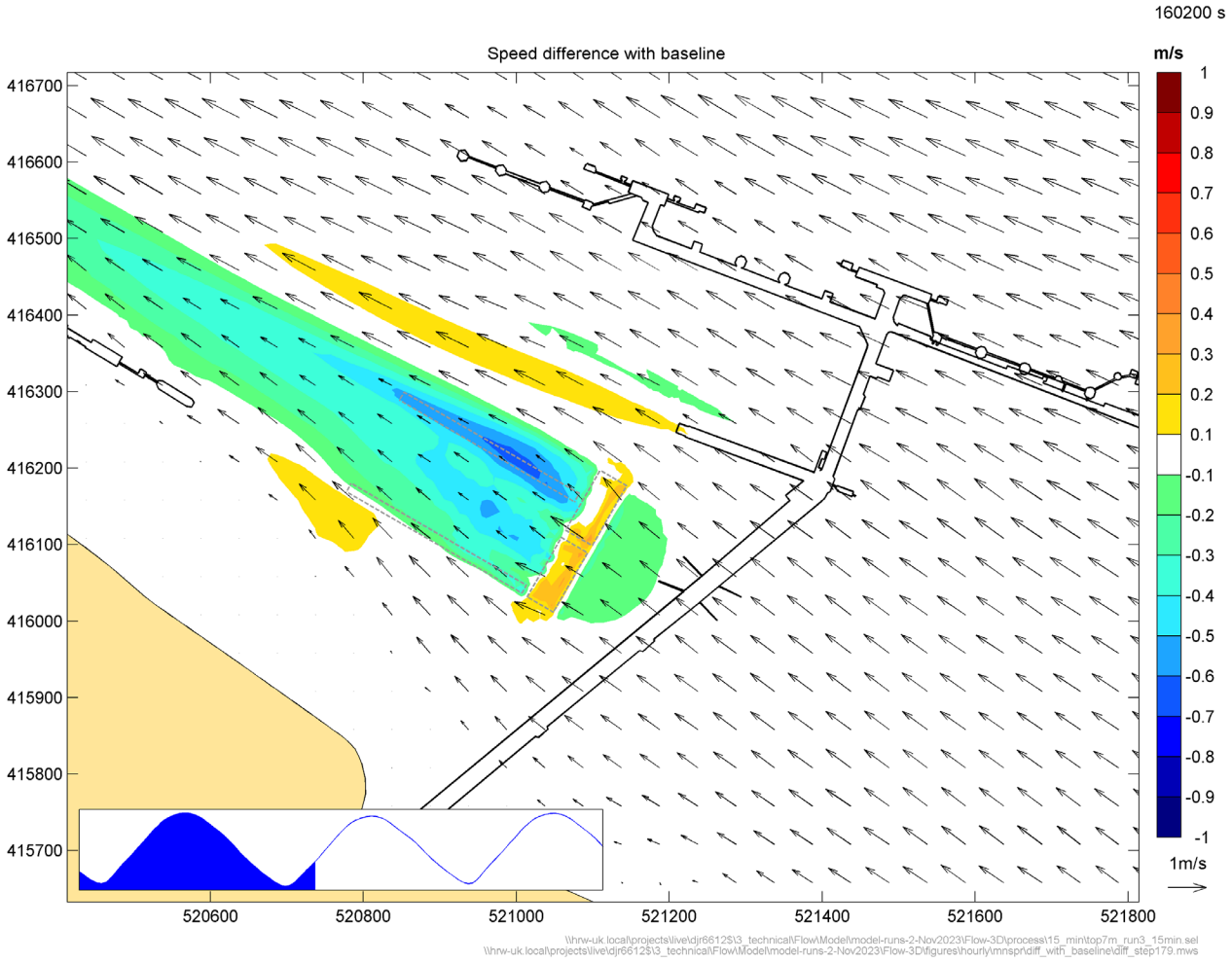

Figure B.16: Difference in current speed between revised IERRT and baseline conditions, LW+2, mean spring tide

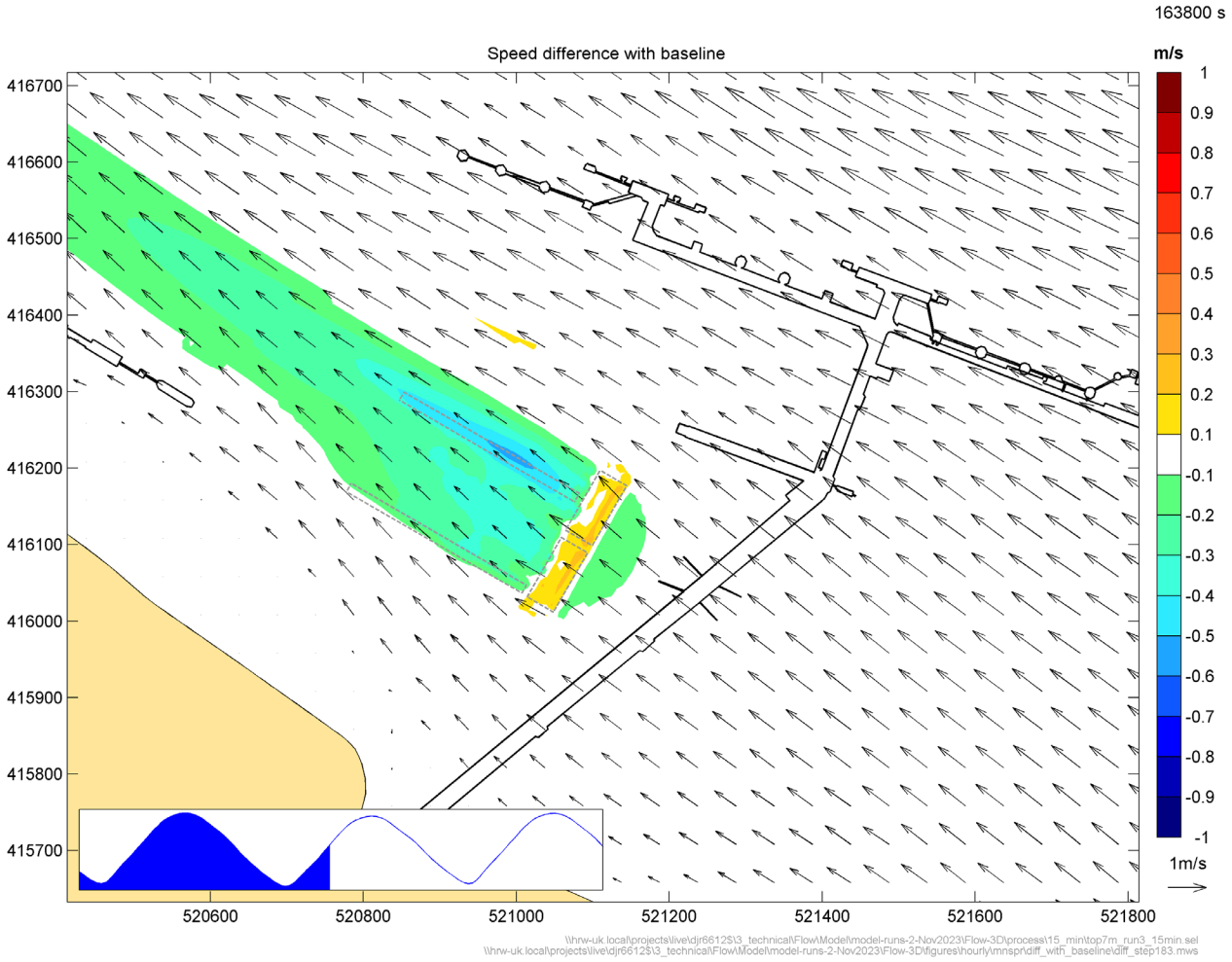

Figure B.17: Difference in current speed between revised IERRT and baseline conditions, LW+3, mean spring tide

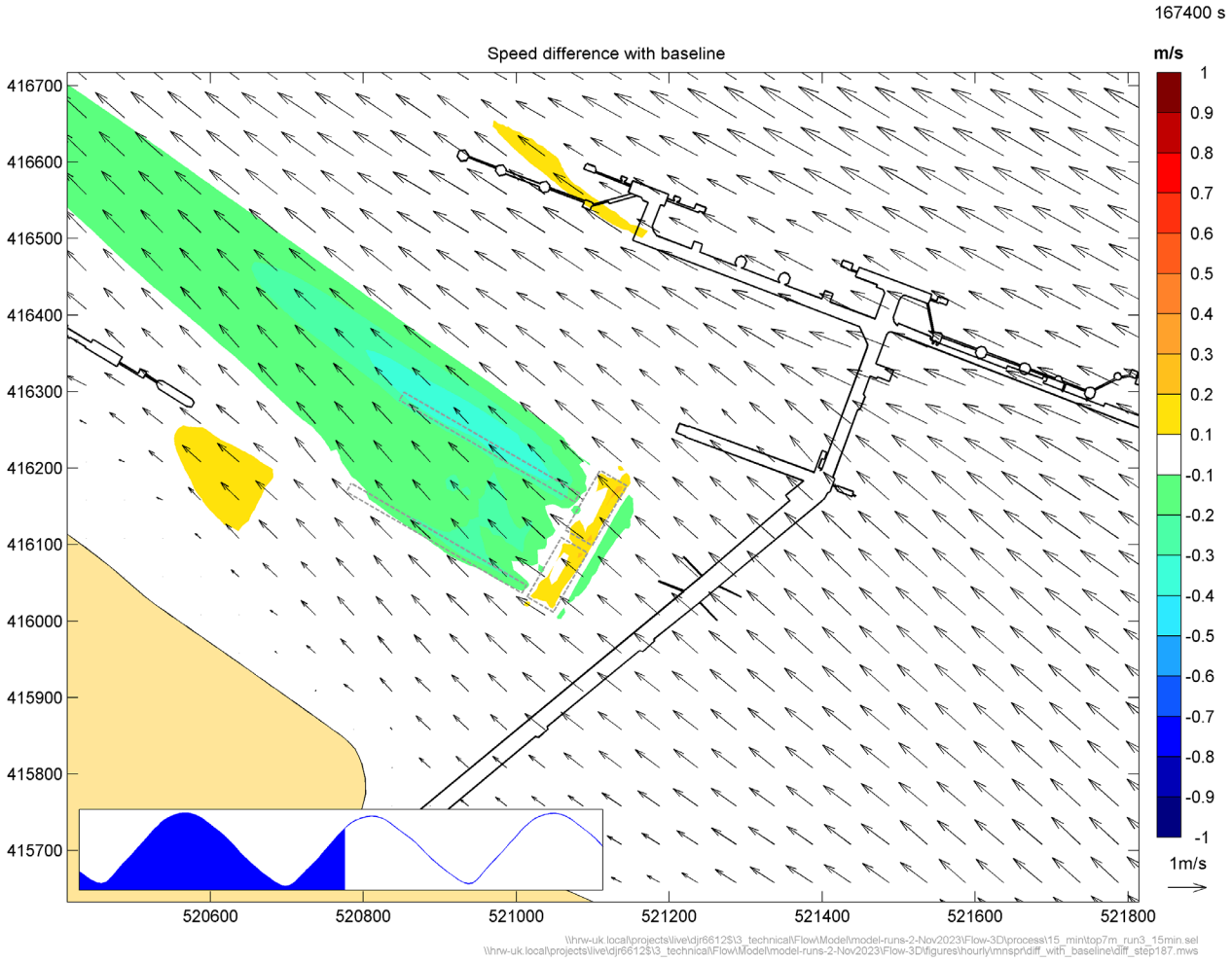

Figure B.18: Difference in current speed between revised IERRT and baseline conditions, LW+4, mean spring tide

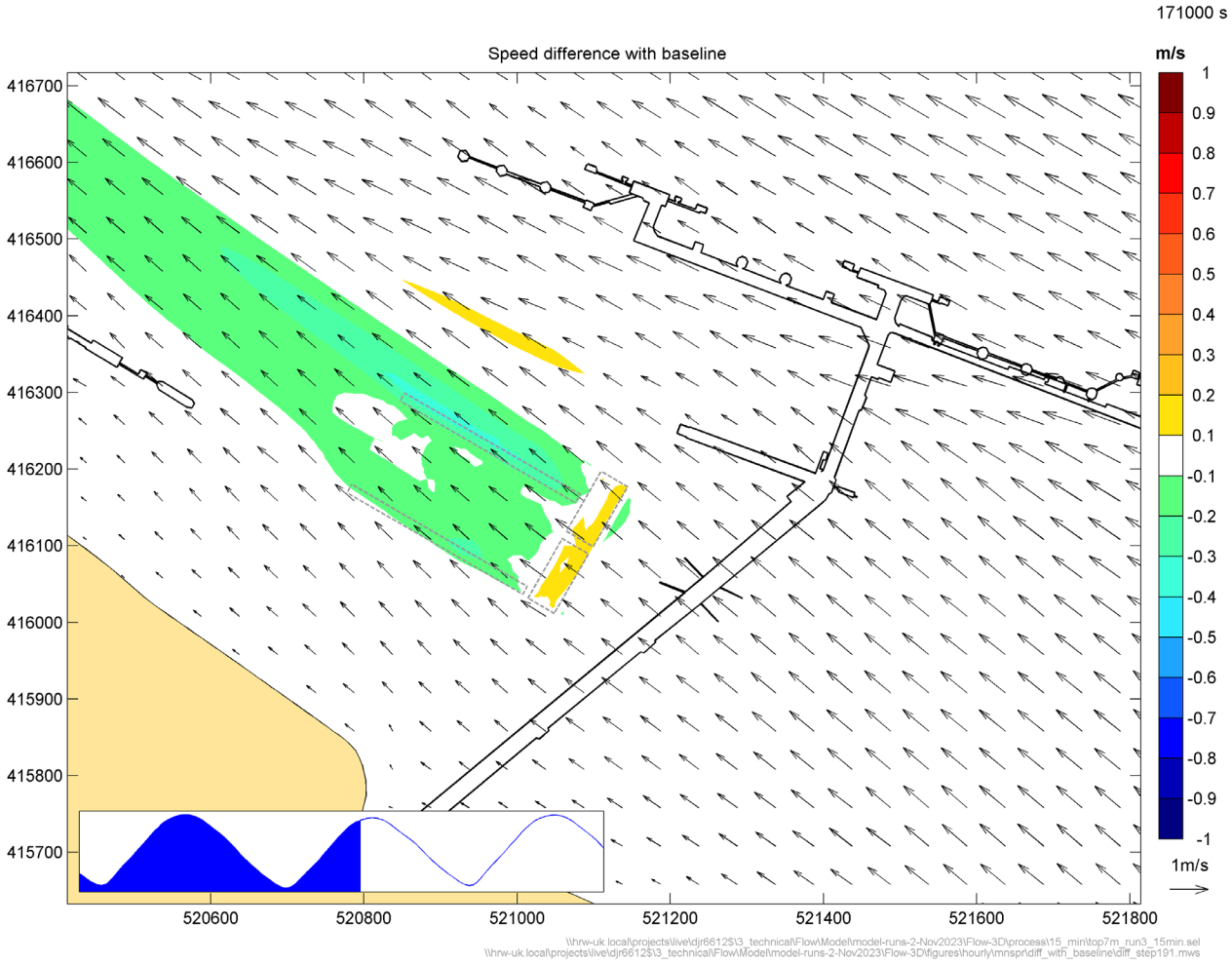

Figure B.19: Difference in current speed between revised IERRT and baseline conditions, LW+5, mean spring tide

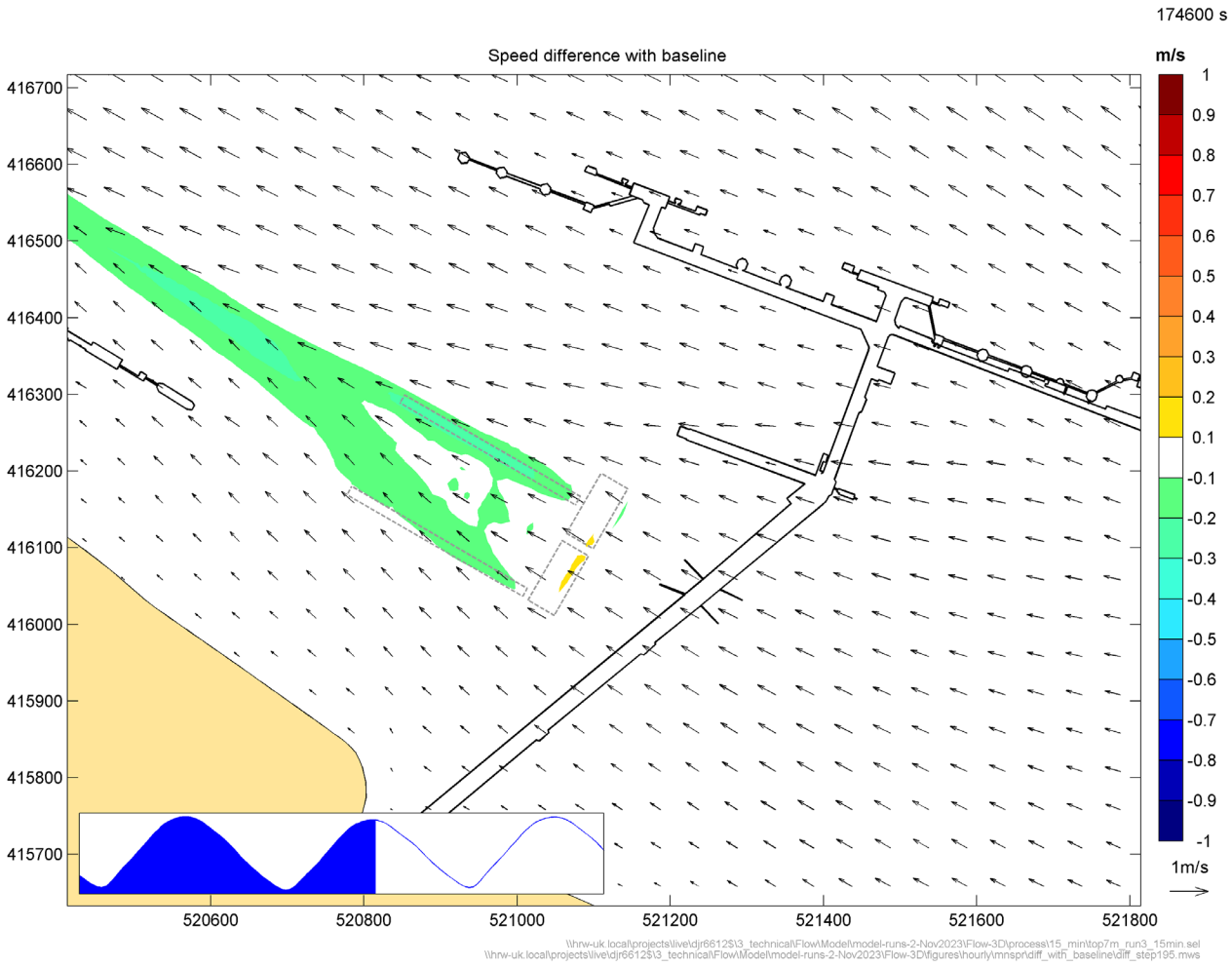

Figure B.20: Difference in current speed between revised IERRT and baseline conditions, LW+6, mean spring tide

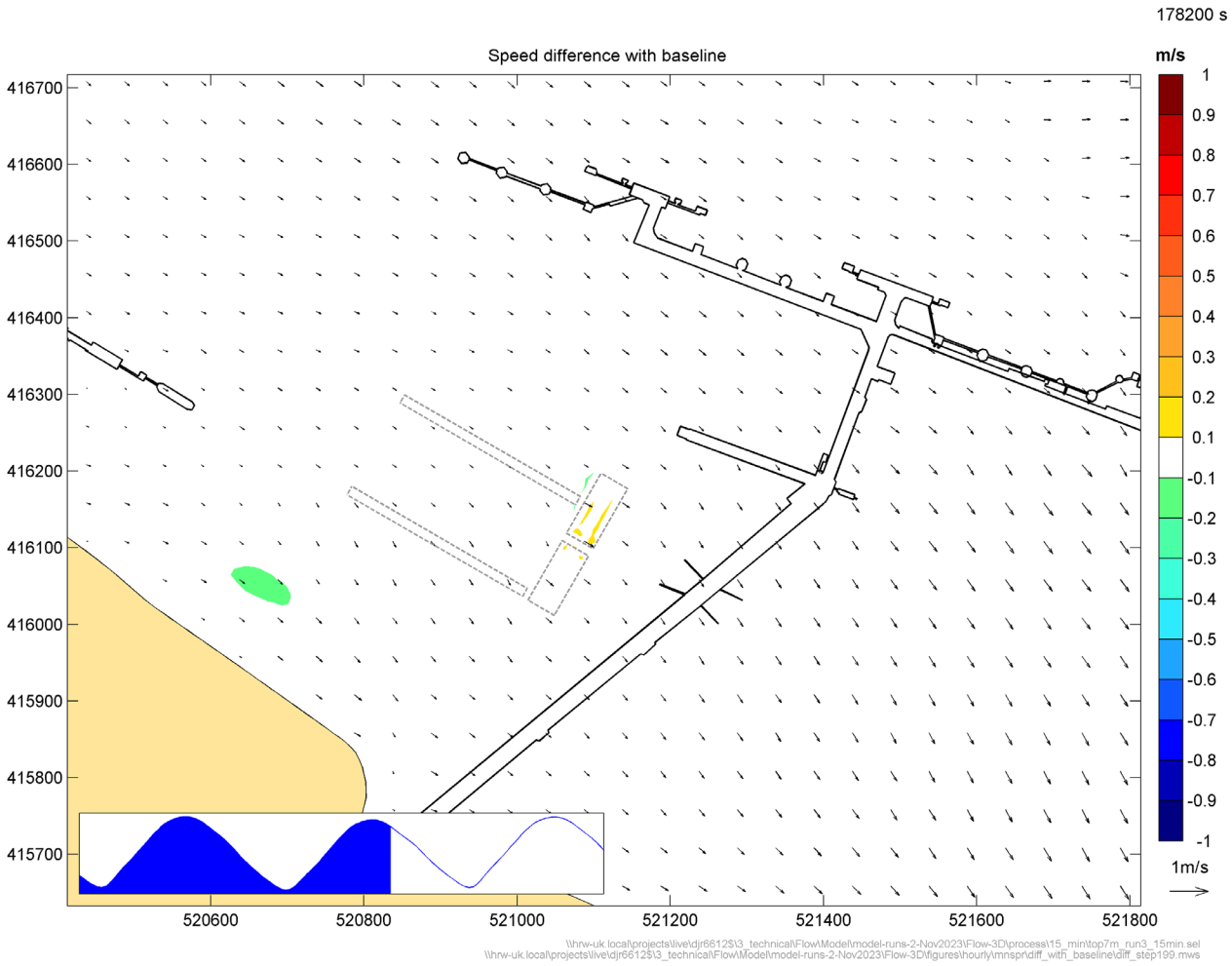

Figure B.21: Difference in current speed between revised IERRT and baseline conditions, LW+7, mean spring tide

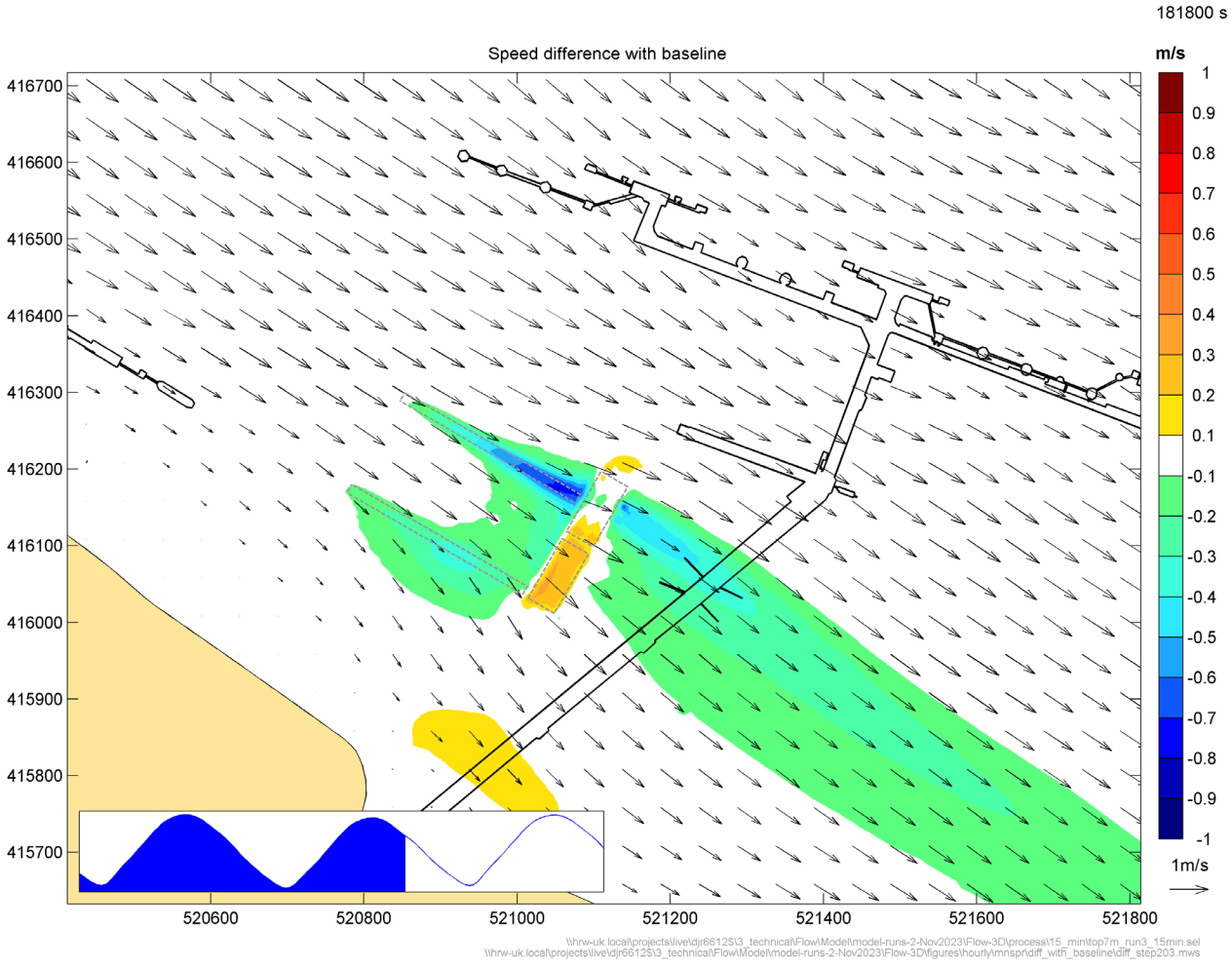

Figure B.22: Difference in current speed between revised IERRT and baseline conditions, LW+8, mean spring tide

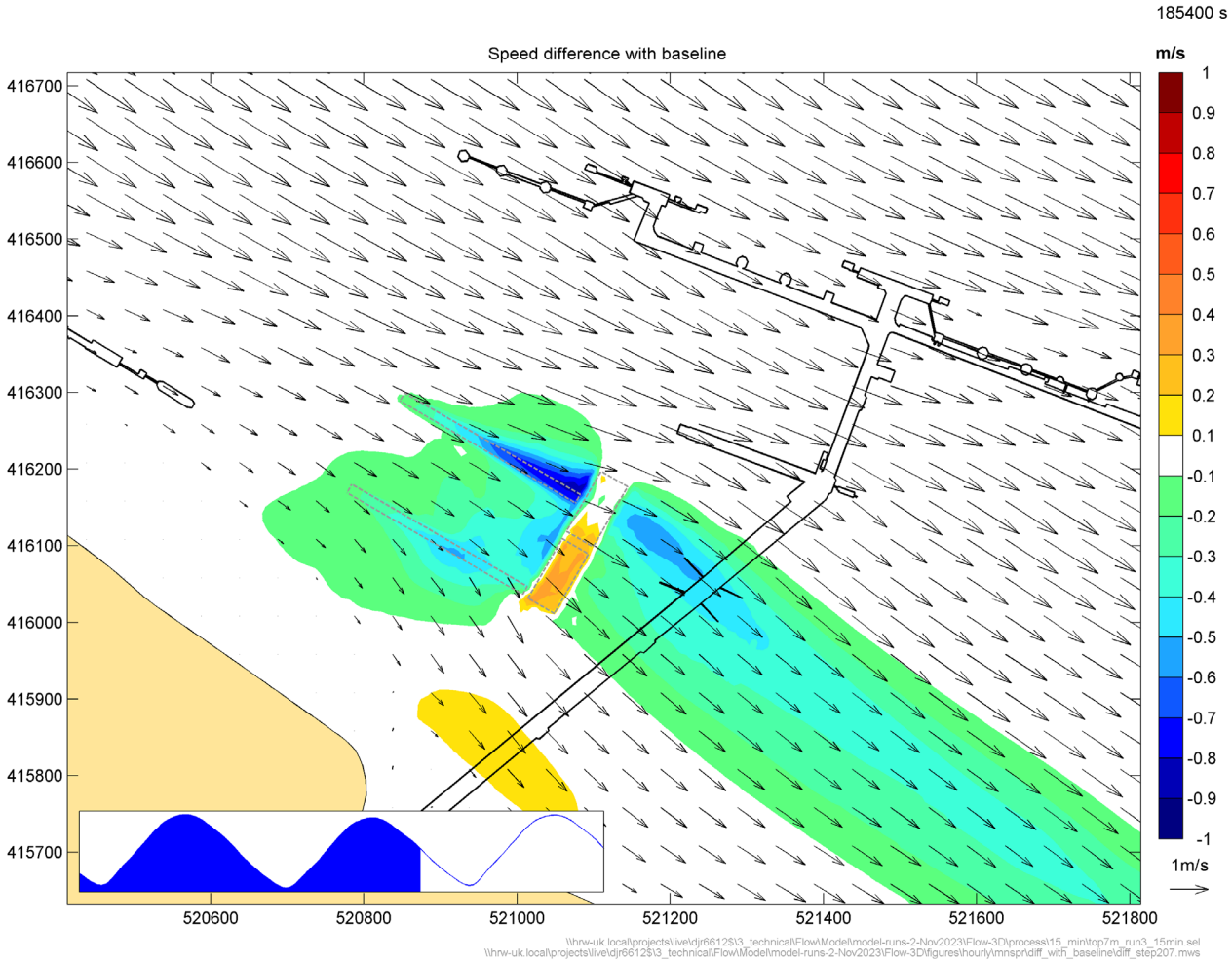

Figure B.23: Difference in current speed between revised IERRT and baseline conditions, LW+9, mean spring tide

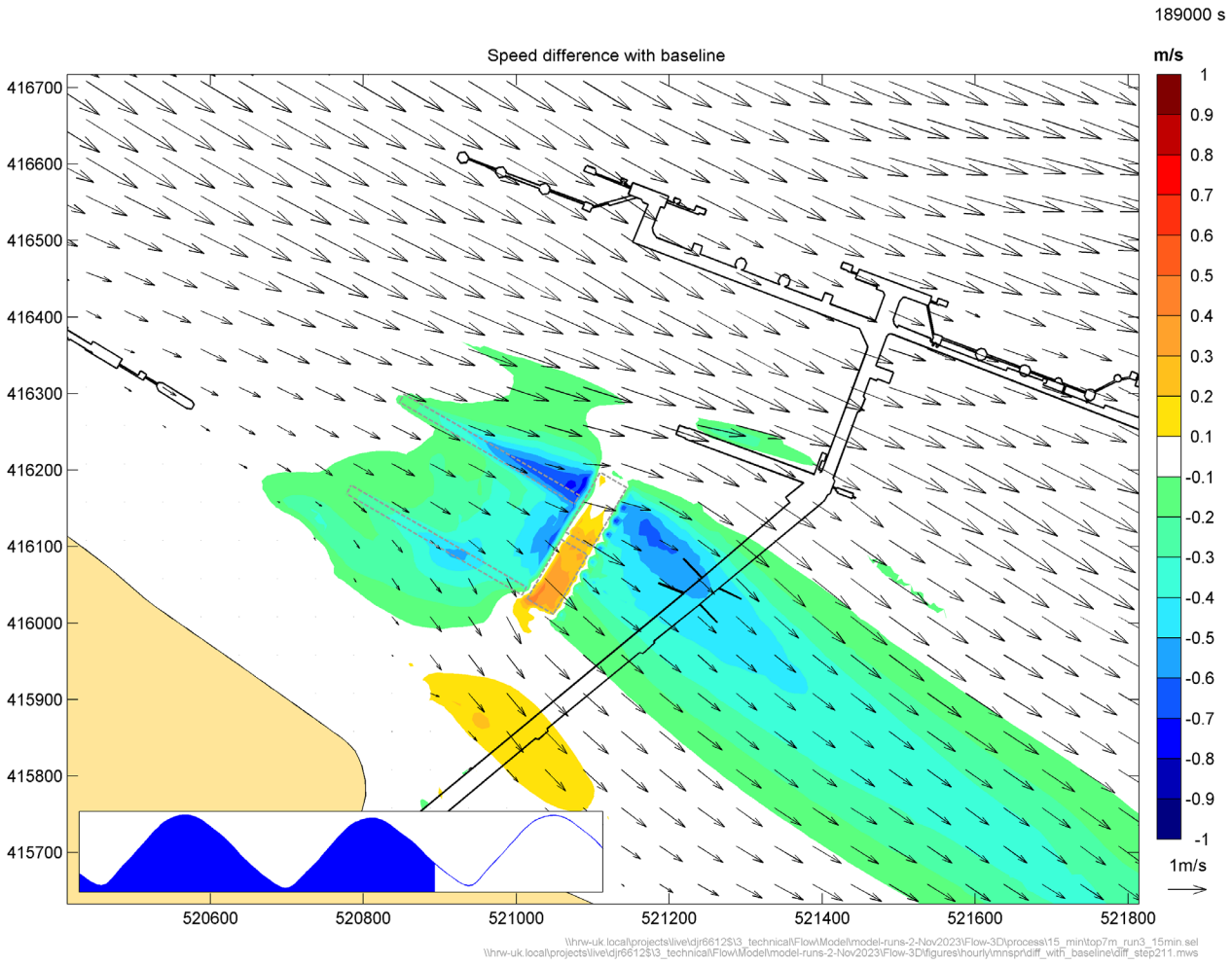

Figure B.24: Difference in current speed between revised IERRT and baseline conditions, LW+10, mean spring tide

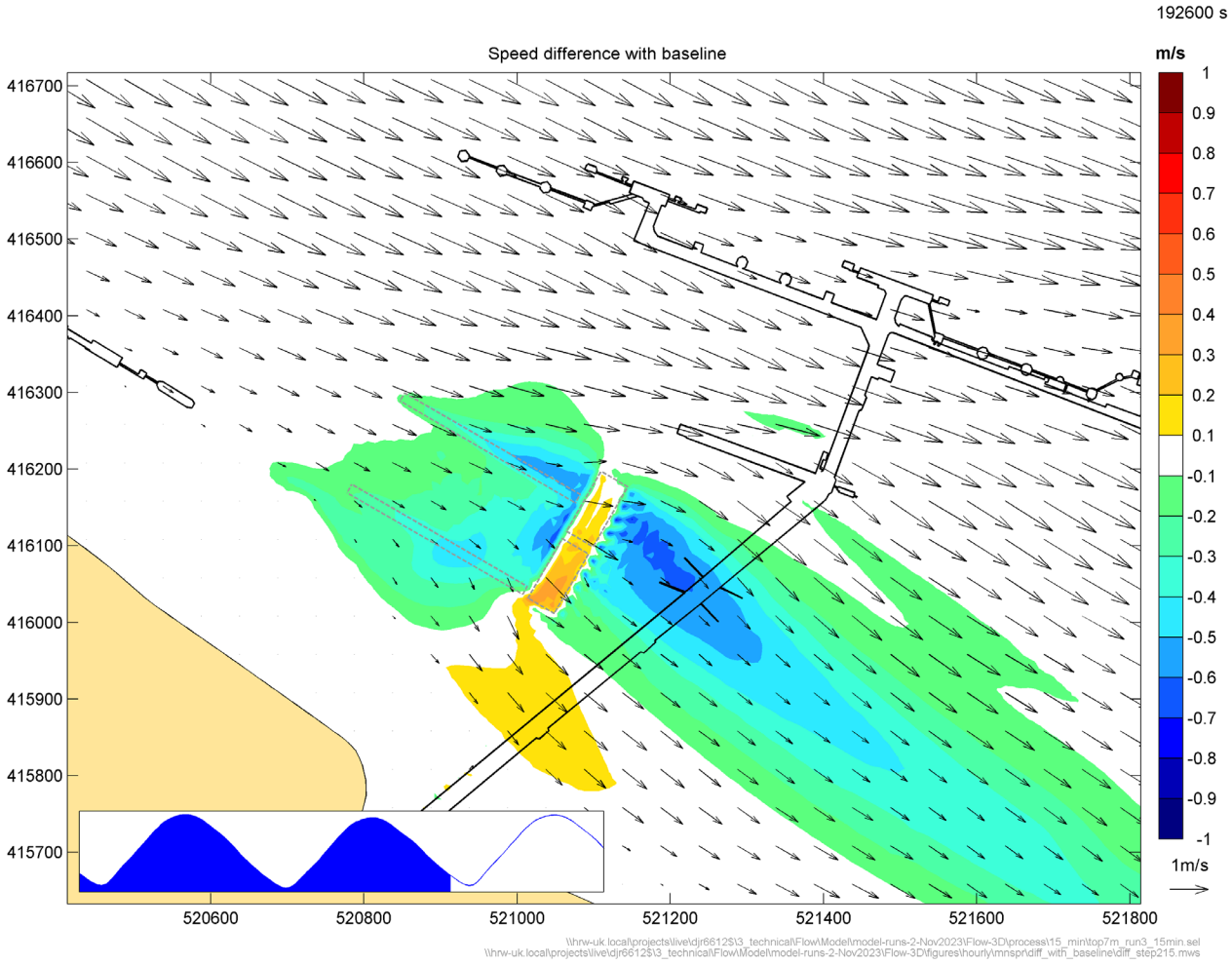

Figure B.25: Difference in current speed between revised IERRT and baseline conditions, LW+11, mean spring tide

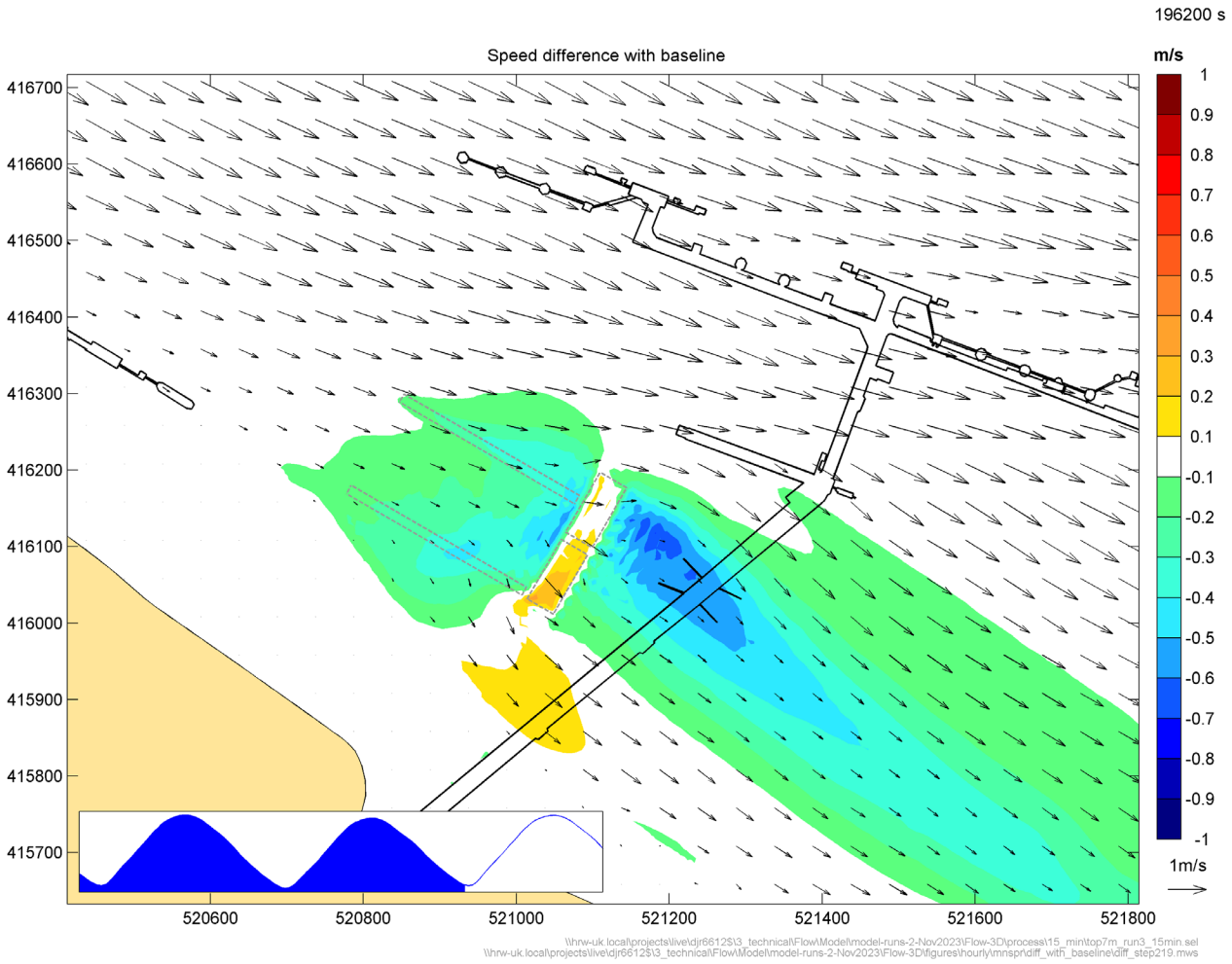

Figure B.26: Difference in current speed between revised IERRT and baseline conditions, LW+12, mean spring tide

C Detailed hourly patterns of currents between IERRT and IOT

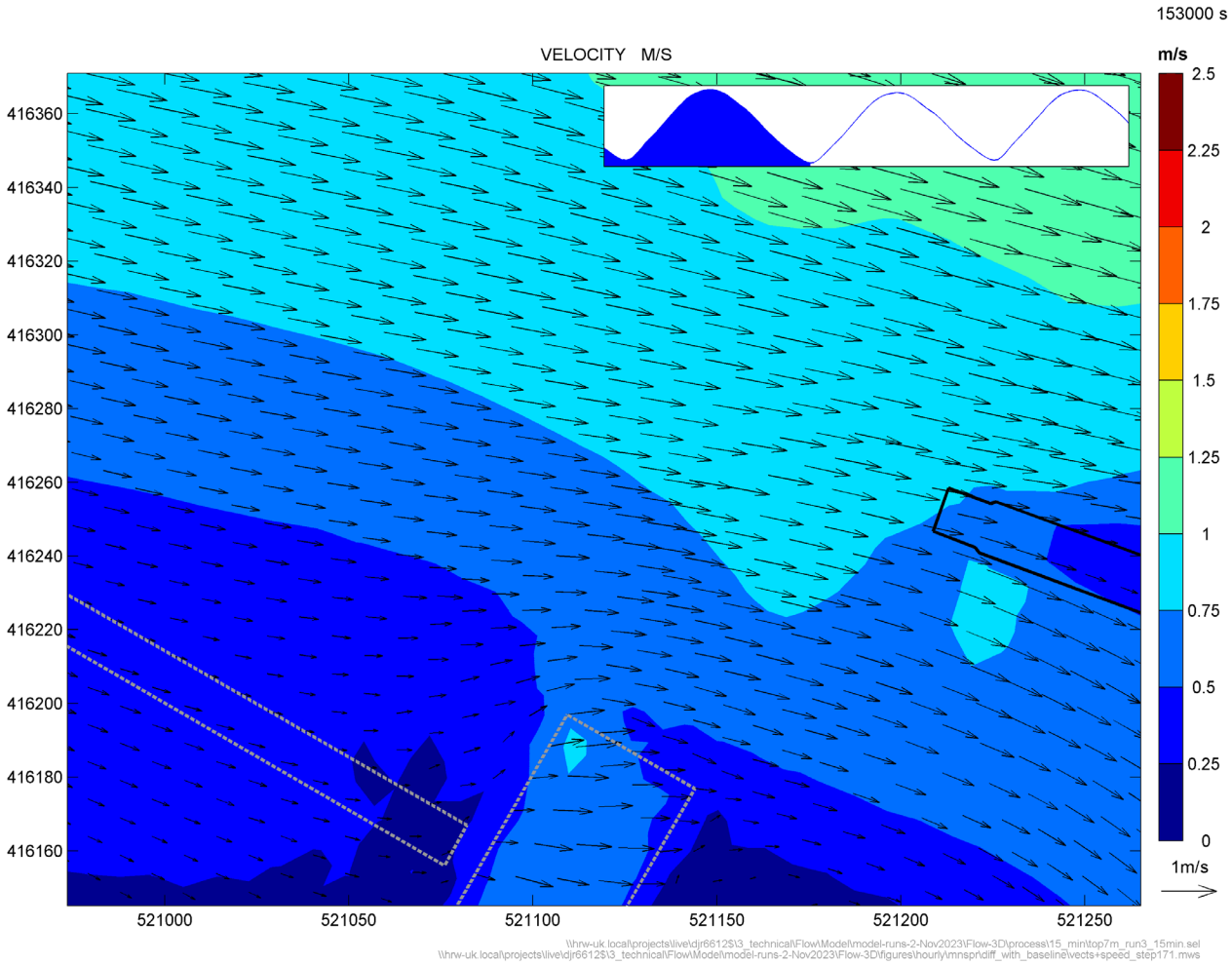

Figure C.1: Difference in current speed between revised and original IERRT layout, LW+0, mean spring tide

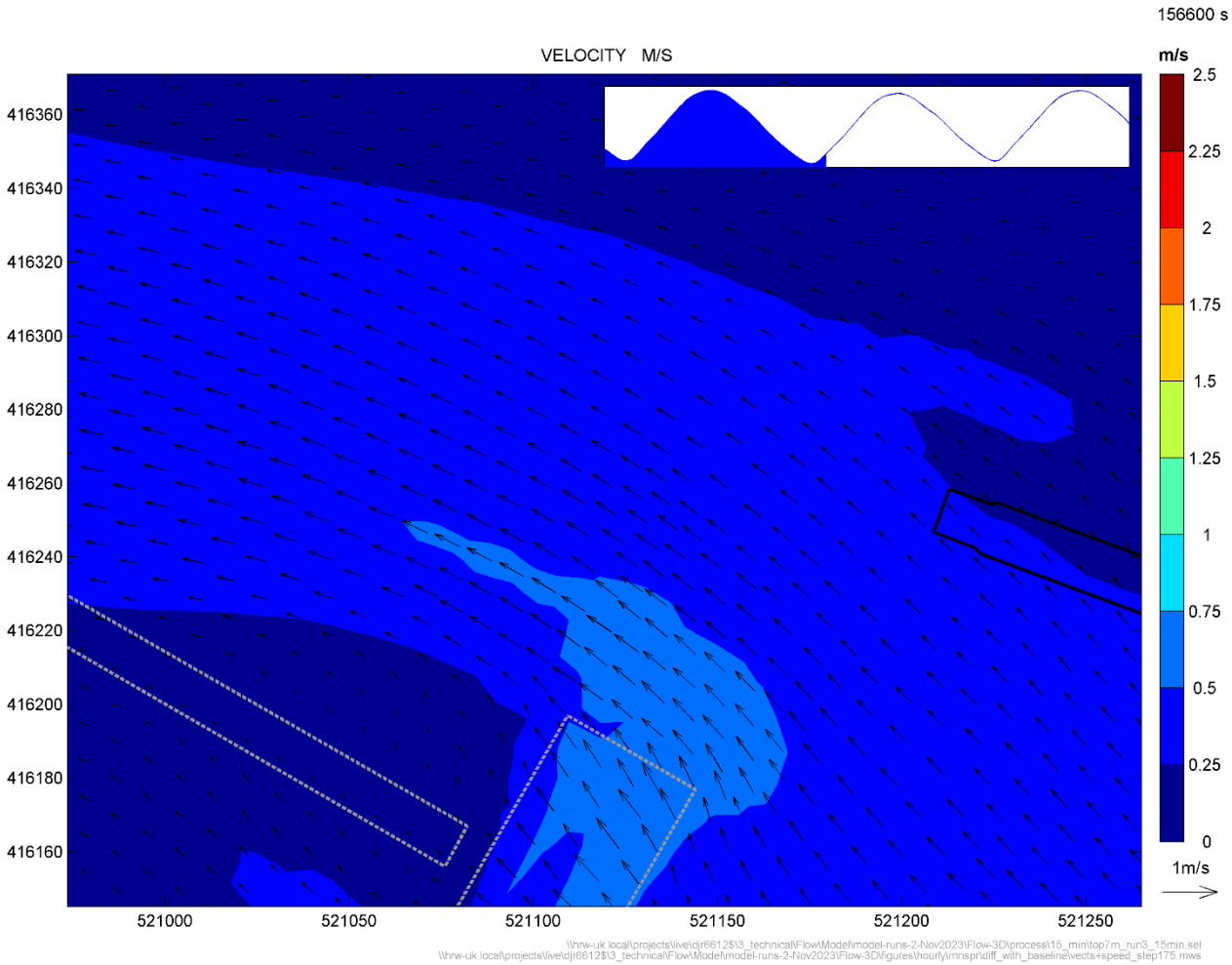

Figure C.2: Difference in current speed between revised and original IERRT layout, LW+1, mean spring tide

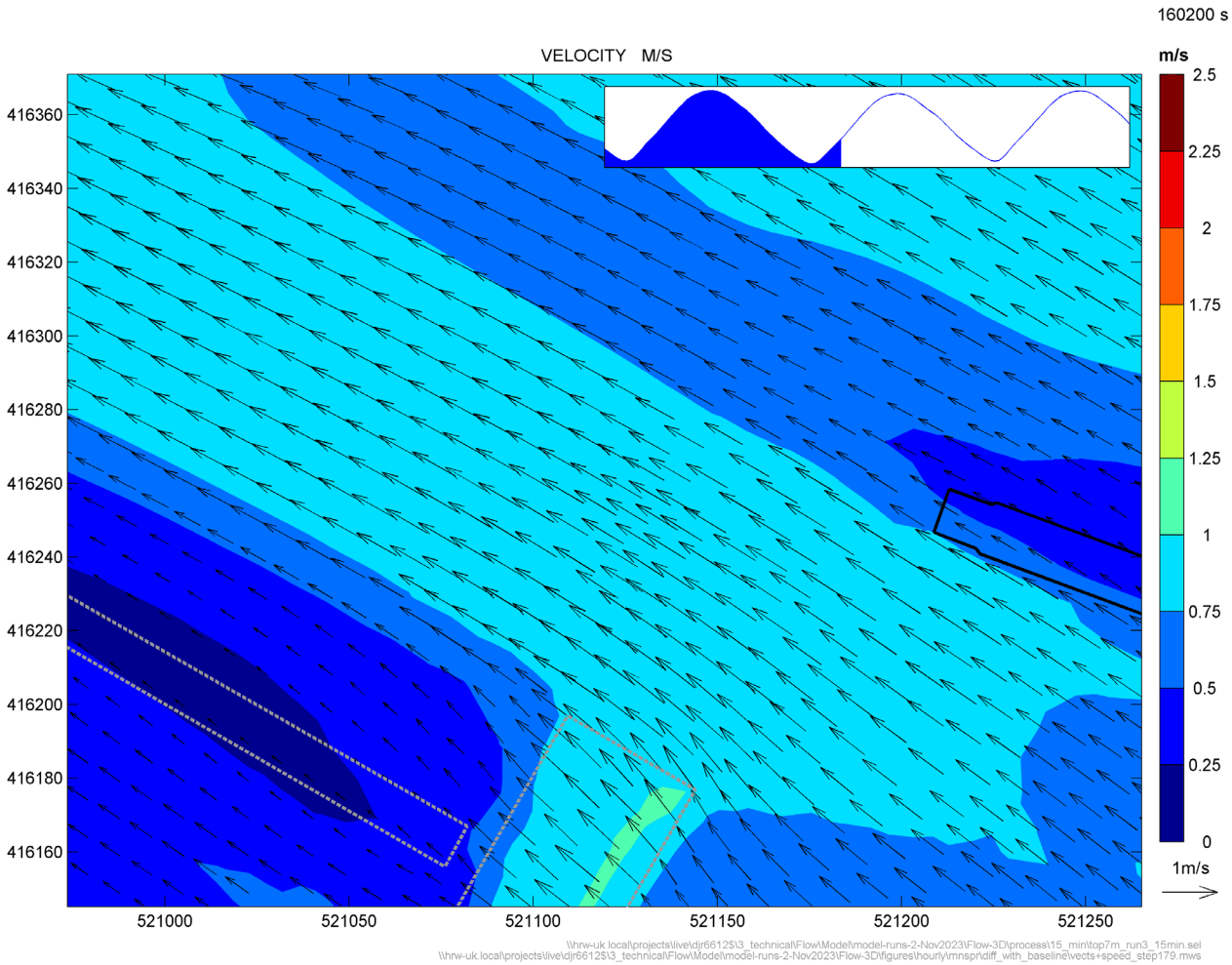

Figure C.3: Difference in current speed between revised and original IERRT layout, LW+2, mean spring tide

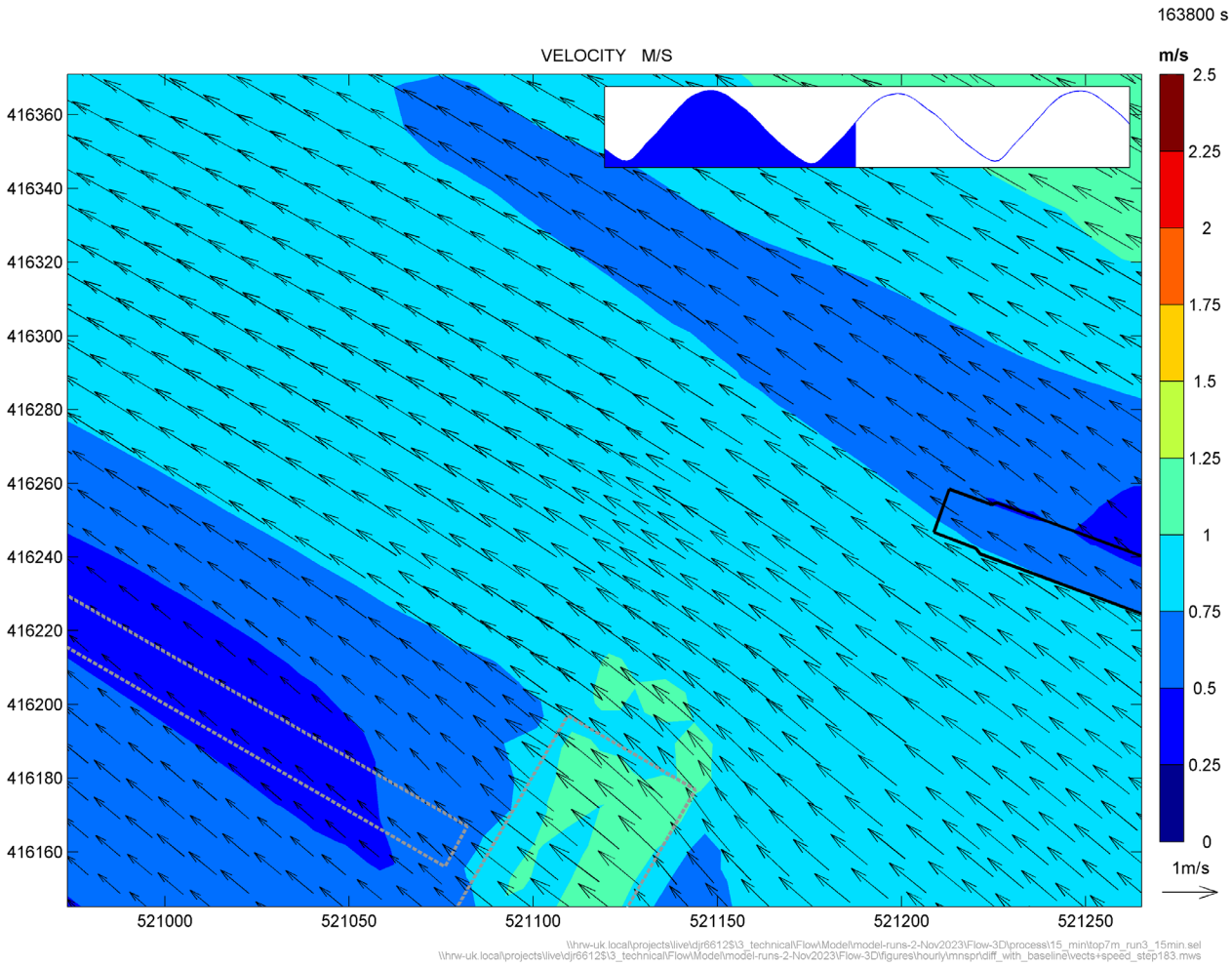

Figure C.4: Difference in current speed between revised and original IERRT layout, LW+3, mean spring tide

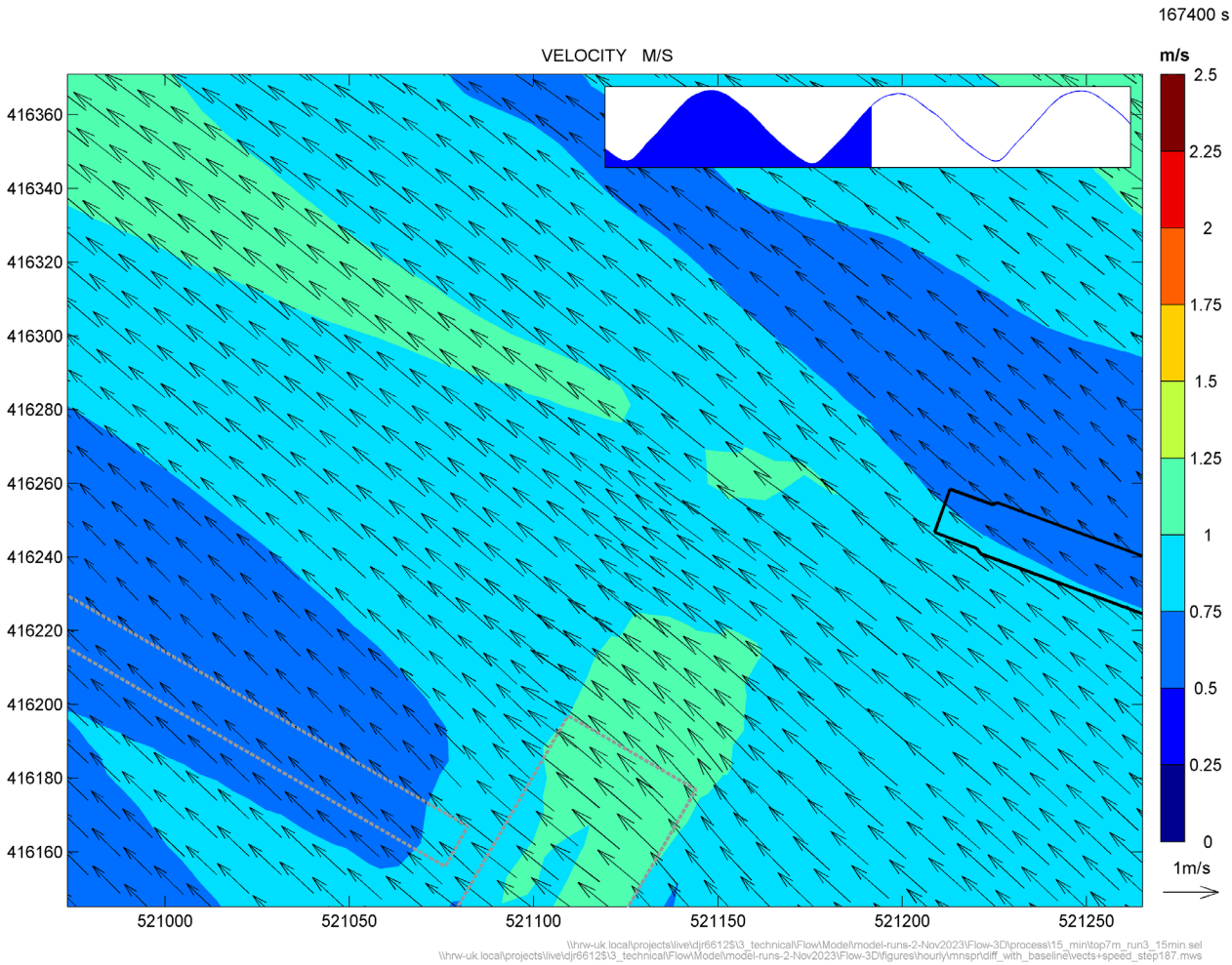

Figure C.5: Difference in current speed between revised and original IERRT layout, LW+4, mean spring tide

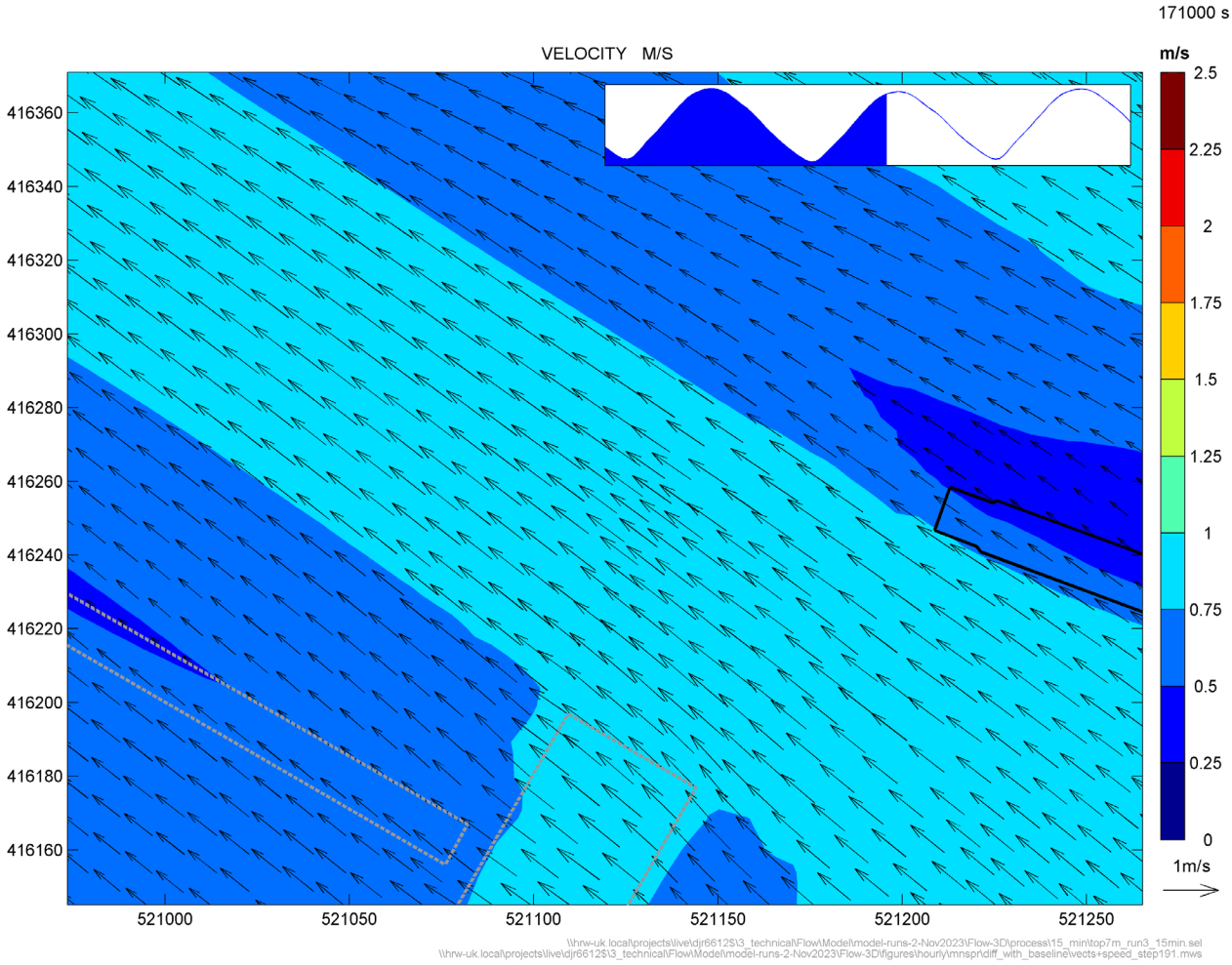

Figure C.6: Difference in current speed between revised and original IERRT layout, LW+5, mean spring tide

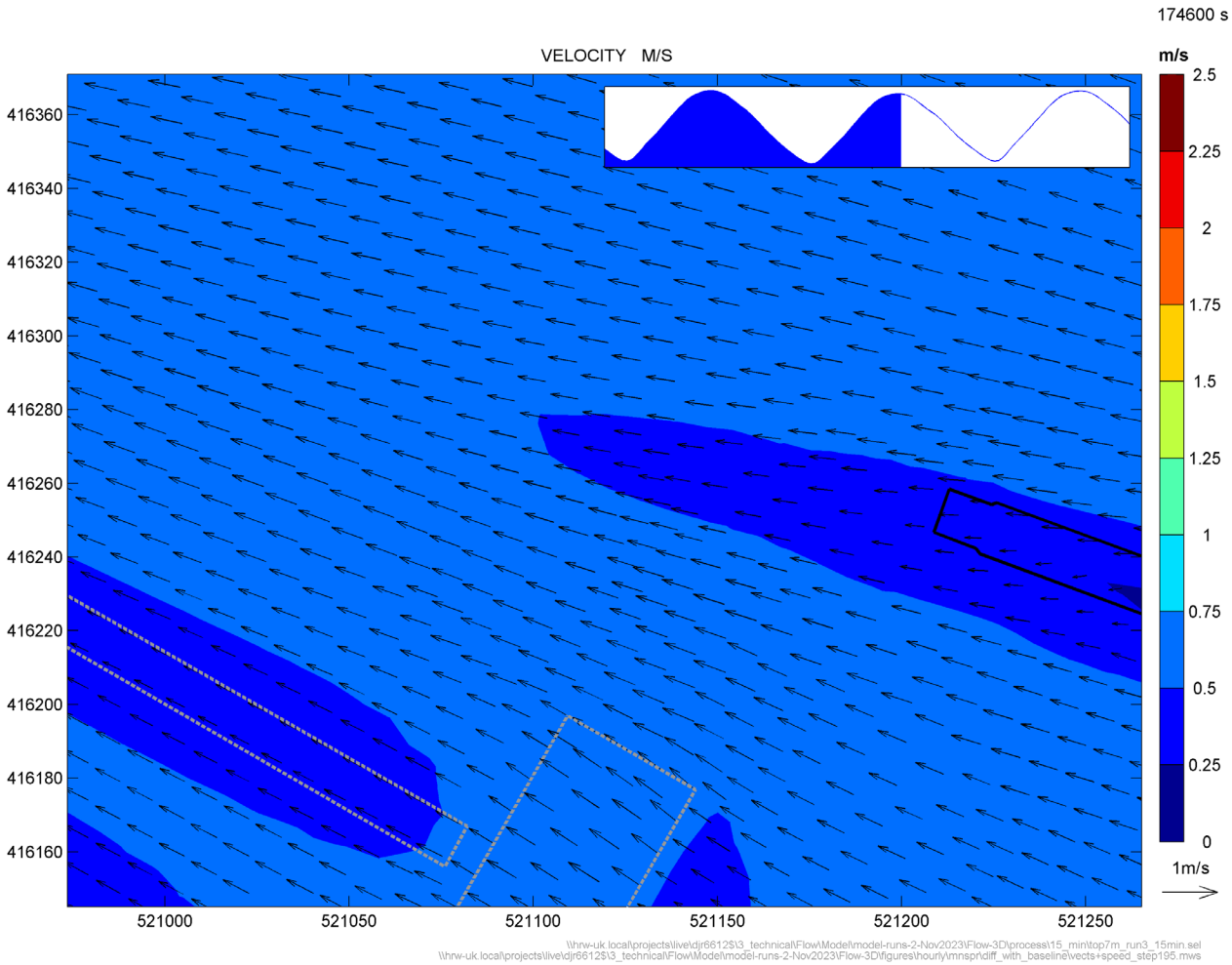

Figure C.7: Difference in current speed between revised and original IERRT layout, LW+6, mean spring tide

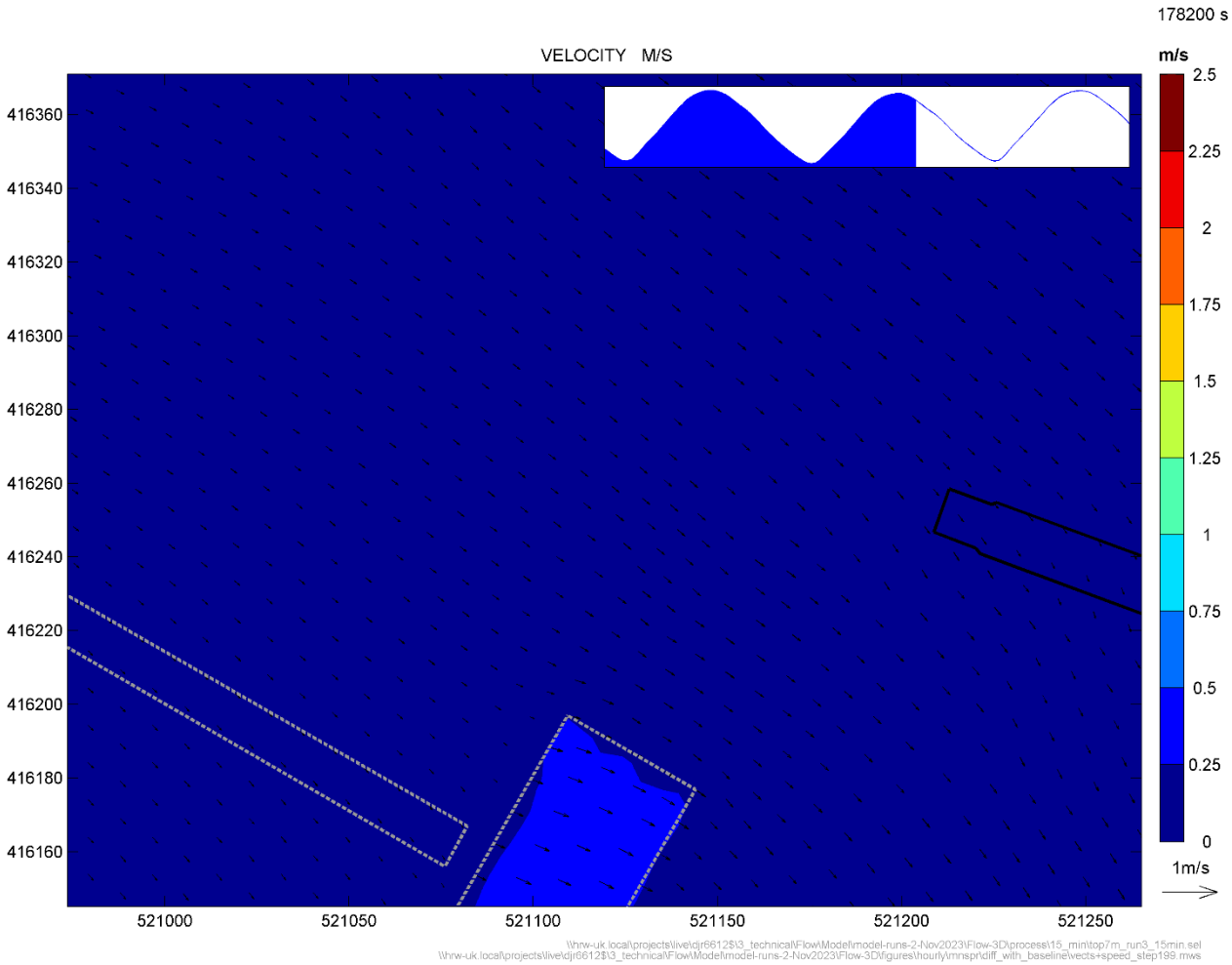

Figure C.8: Difference in current speed between revised and original IERRT layout, LW+7 mean spring tide

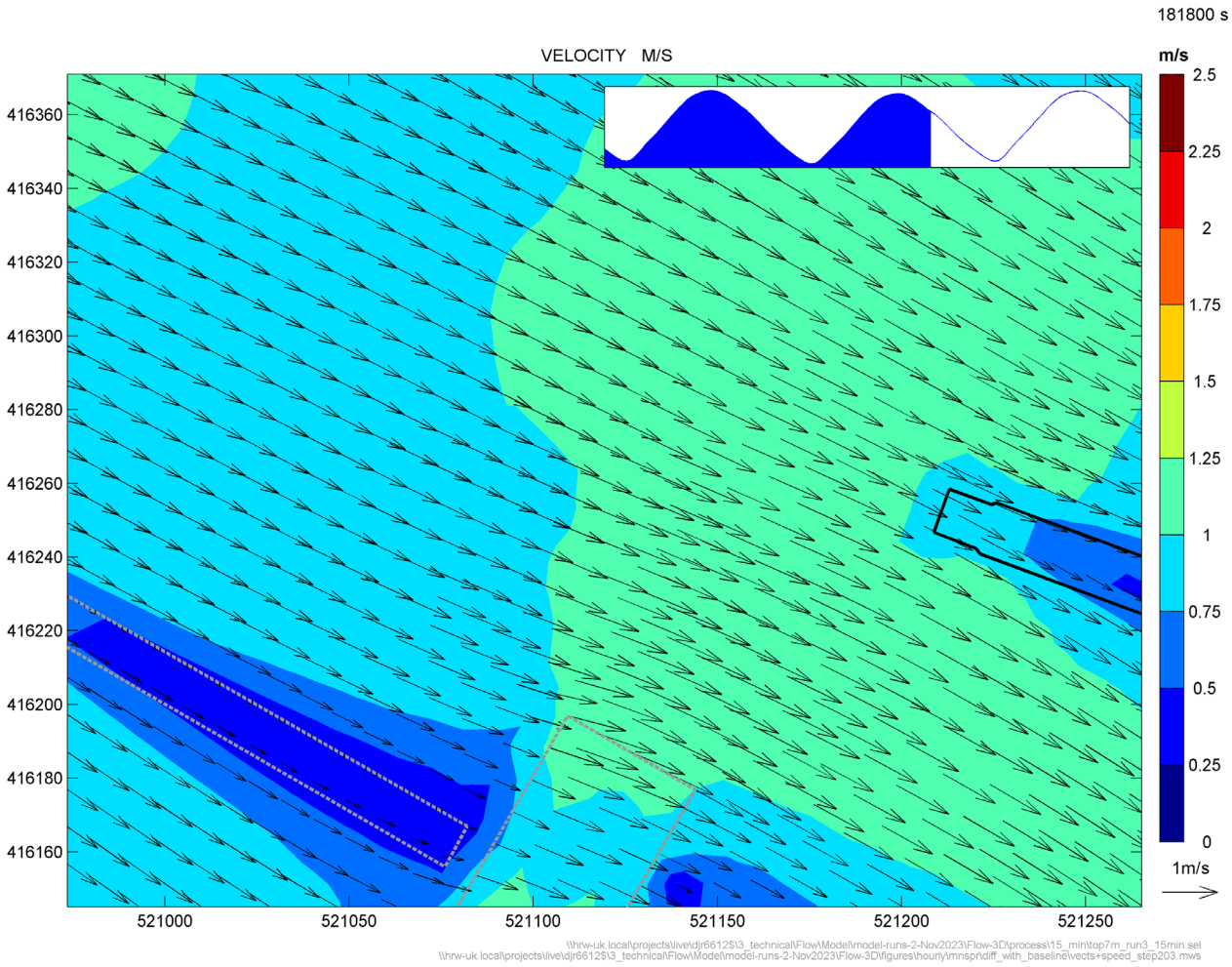

Figure C.9: Difference in current speed between revised and original IERRT layout, LW+8, mean spring tide

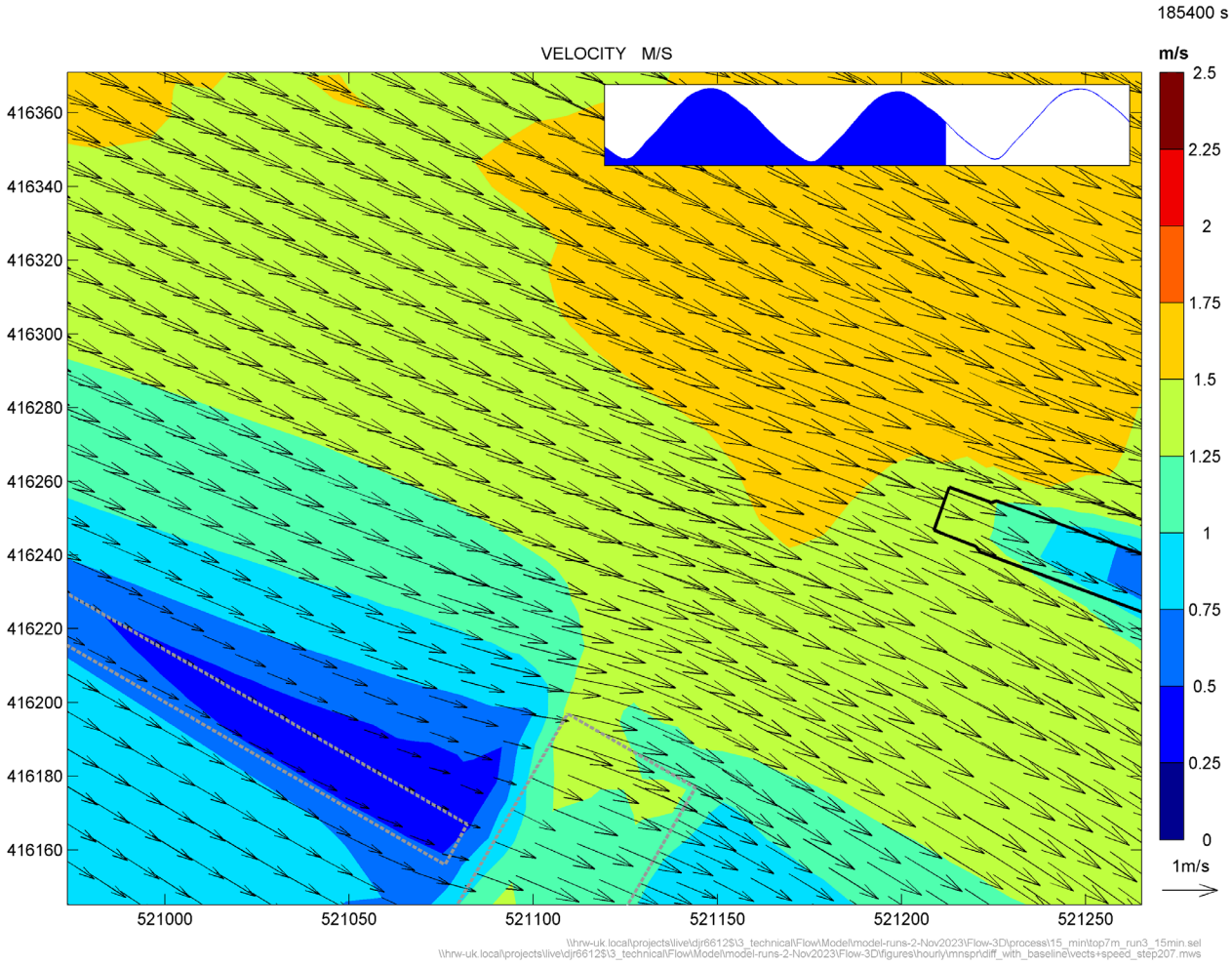

Figure C.10: Difference in current speed between revised and original IERRT layout, LW+9, mean spring tide

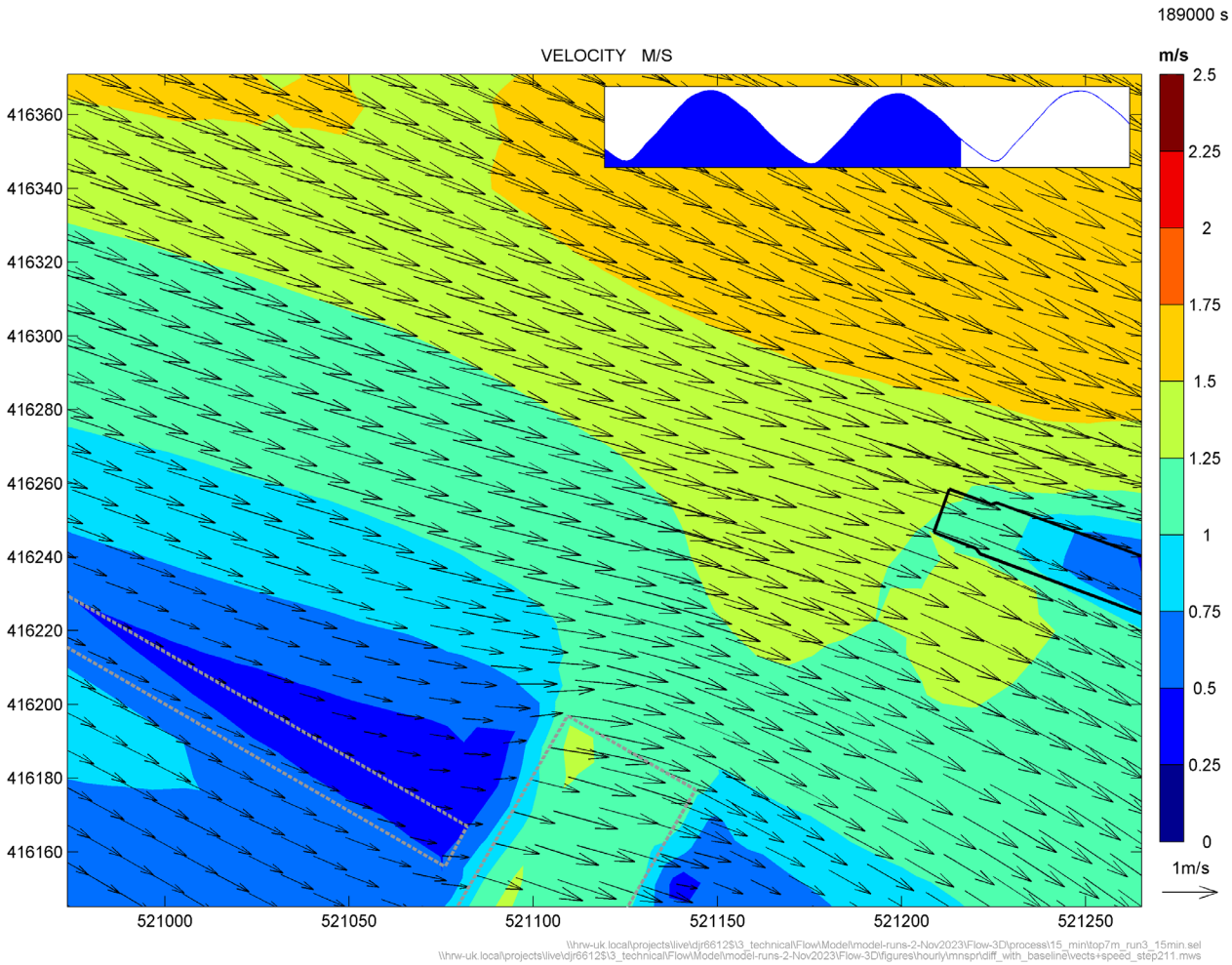

Figure C.11: Difference in current speed between revised and original IERRT layout, LW+10, mean spring tide

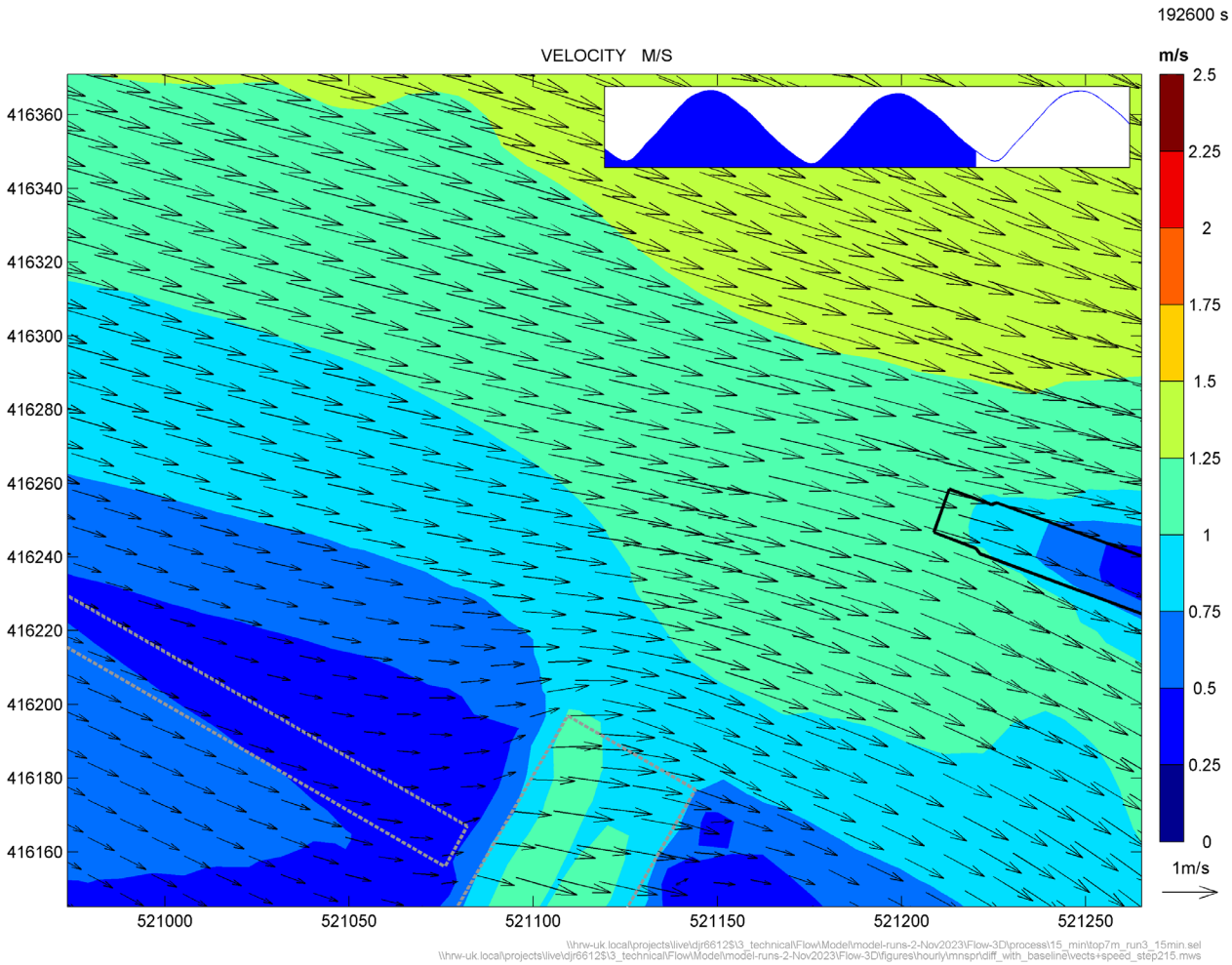

Figure C.12: Difference in current speed between revised and original IERRT layout, LW+11, mean spring tide

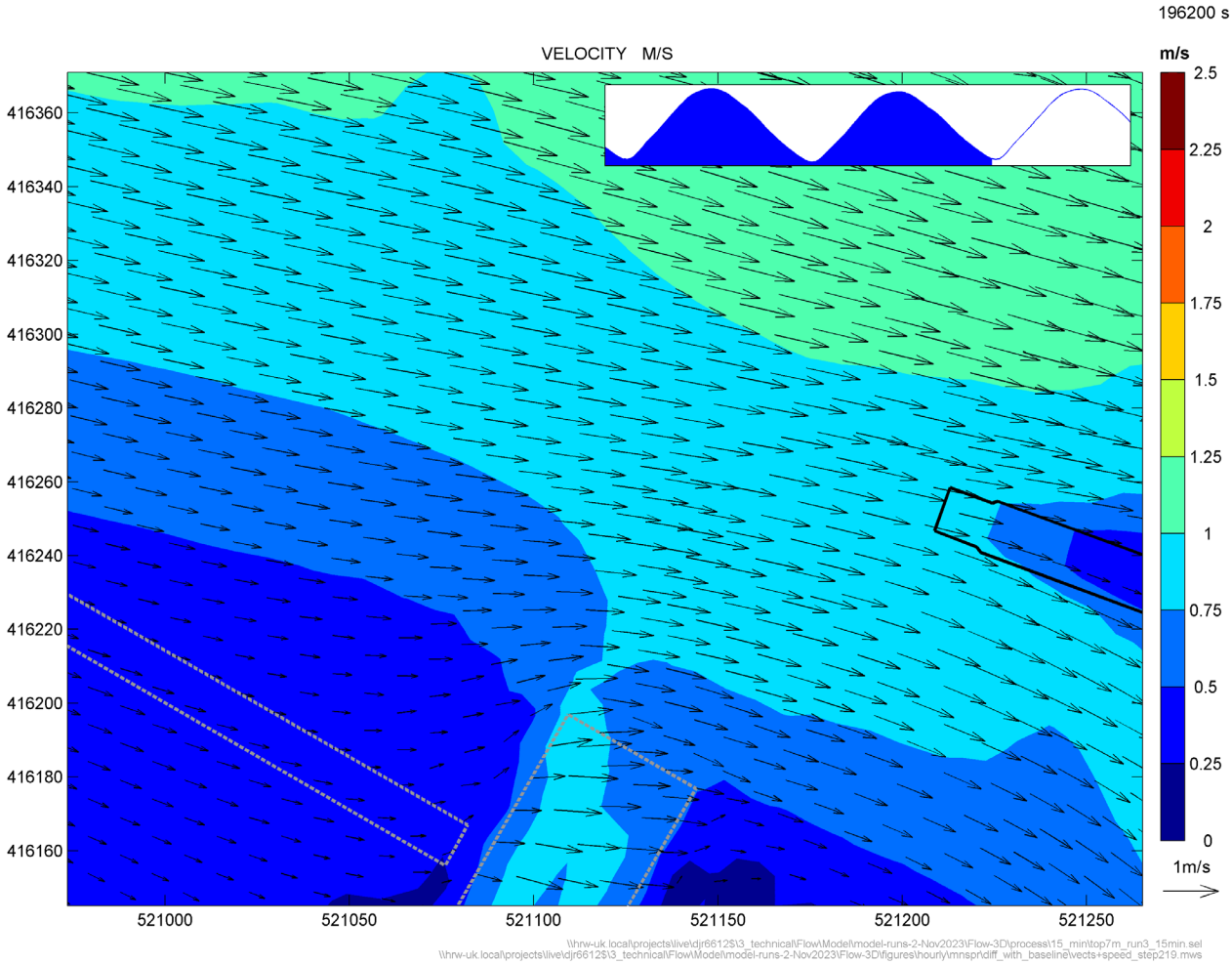

Figure C.13: Difference in current speed between revised and original IERRT layout, LW+12, mean spring tide

hrwallingford

We design smarter, more resilient solutions across both the natural and built environment to help everyone live and work more sustainably with water.

HR Wallingford
Howbery Park
Wallingford
Oxfordshire OX10 8BA
United Kingdom

+44 (0)1491 835381

info@hrwallingford.com

www.hrwallingford.com

bsi PAS 99 Integrated Management Systems CERTIFIED
IMR 719286

bsi ISO 9001 Quality Management Systems CERTIFIED
FS 516431

bsi ISO 45001 Occupational Health and Safety Management CERTIFIED
OHS 595357

bsi ISO 14001 Environmental Management CERTIFIED
EMS 558310